EFFECTS OF CHAIN LENGTH AND CHAIN LENGTH MISMATCH ON ORIENTATIONAL ORDER IN FLUID STATE LIPID BILAYER MEMBRANES

DALIAN LU

EFFECTS OF CHAIN LENGTH AND CHAIN LENGTH MISMATCH ON ORIENTATIONAL ORDER IN FLUID STATE LIPID BILAYER MEMBRANES

By

©Dalian Lu

A THESIS SUBMITTED TO THE SCHOOL OF GRADUATE STUDIES IN PARTIAL FULFILLMENT OF THE REQUIREMENTS FOR THE DEGREE OF DOCTOR OF PHILOSOPHY

DEPARTMENT OF PHYSICS
MEMORIAL UNIVERSITY OF NEWFOUNDLAND

JULY 1995

ST. JOHN'S NEWFOUNDLAND CANADA

ISBN 0-612-06132-9

Canada

Acknowledgements

It is my great pleasure to thank all those who have contributed to this dissertation. I am grateful to my supervisor, Dr. Michael R. Morrow, for his support and guidance over the whole stage of my research work and thesis writing.

I wish to thank Drs. J. P. Whitehead, Chris W. M. Grant and Dev Singh for their collaboration on my research projects. I have learned a lot from them. I also wish to thank Professor M. Bloom and Clare Morrison for providing a copy of the de-Paking program.

I express my appreciation to Drs. N. H. Rich and J. R. de Bruyn for their participation in my Supervisor's Committee and for their comments and careful reading of this thesis. I would also wish to thank Dr. Ron Beavis, who also served on the Supervisor's Committee.

I would like to thank Mrs. J. Barron and Mrs. D. Corbett for their efficient and kind service.

I gratefully acknowledge the financial assistance provided by the School of Graduate Studies and Department of Physics in the form of Graduate Fellowships and Teaching Assistantships. I also gratefully acknowledge the Women's Association of Memorial University for their awarding me a Graduate Student Scholarship for 1994.

Abstract

Deuterium NMR spectroscopy was used to study the effects of chain length and chain length mismatch on orientational order in fluid state lipid bilayer model membranes. Samples like diacyl phospholipids, glycolipids, binary mixtures of phospholipids, binary mixtures of glycolipids with phospholipids, and ternary mixtures containing cholesterol were used. Special attention was paid to examining how the line shape of the orientational order parameter profile and the temperature dependence of first moment near the gel/fluid phase transition were determined by a limited set of factors.

The shape of the smoothed order parameter profile has been found to be determined largely by the mean order parameter for the diacyl phospholipid bilayers if position along the chain is normalized. Even in the case of binary mixtures, the observed shapes of the smoothed order parameter profiles with the same mean order parameter were largely independent of the constituent's concentration within the membrane. These observations suggest that the mean order parameter is one of a few parameters which determine the shape of smoothed orientational order parameter profiles. It was also observed that with decreasing chain length, the amplitude of the discontinuity in M_1 decreases and the slope of M_1 versus T increases for the diacyl phospholipid bilayers at the transition temperature. It was found that the dependence of M_1 on T could be accounted for by a Landau theory and that the observed behaviour was sensitive to the chain length dependent differences between the spinodal temperature and the transition temperature.

In chain-length mismatched bilayers, the orientational order parameter profiles for very long chains were found to have a second plateau near the methyl end of the chain. The existence of such a second plateau in the order parameter profile suggests that the

mismatched part of the long chains and the methyl ends of the short chains from the opposite monolayers are mingled with each other, forming a very fluid central layer in the middle of the bilayer. This fluid central layer may link the two sides of the bilayer in the biological membranes. The existence of cholesterol in these chain mismatched systems has large influence on order parameter profiles of its neighboring chains but has a little influence on the second plateau for the very long chain in the bilayer mixture.

The phase diagrams for binary mixtures with either component deuterated can be different. It was found that the ^{2}H-NMR spectra which represent different labeled components at the same temperature simultaneously represent the states of the two components in a given mixture, whereas this is not the case for the profiles selected to have the same plateau value. This discovery may be helpful for interpreting ^{2}H-NMR experimental results for binary lipid bilayer mixtures.

Abbreviations

^{2}H-NMR: deuterium nuclear magnetic resonance.

DLPC: dilauroylphosphatidylcholine.

DMPC: dimyristoylphosphatidylcholine.

DPPC: dipalmitoylphosphatidylcholine.

DSPC: distearoylphosphatidylcholine.

SOPC: 1-stearoyl-2-oleoylphosphatidylcholine.

GSL: glycosphingolipid.

18:0 GalCer: *N*-stearol galactosyl ceramide.

24:0 GalCer: *N*-lignoceroyl galactosyl ceramide.

OOPP: orientational order parameter profile.

sn-1: "stereospecifically numbered" at position 1 of the glycerol backbone.

sn-2: "stereospecifically numbered" at position 2 of the glycerol backbone.

Table of Contents

List of Tables

List of Figures

Chapter 1

Introduction

Biomembranes are complicated systems. To understand their physiological roles one must understand their structure and physical properties. Technical innovations in the laboratory have led to the accumulation of a great deal of knowledge. A number of excellent books dealing with the properties of membranes and bilayers have recently been published [1-5] . In this Chapter, the membrane structure and research methods related to my Ph.D. project will be described briefly and my project will be outlined.

1.1 Structure of Lipid Bilayers

All biological membranes are assemblies of varieties of lipid and protein molecules held together by noncovalent interactions. A schematic view of a small section of cell membrane is shown in Fig. 1.1. As can be seen in this figure, lipids in the membrane are in a bilayer configuration. The lipid bilayer provides the basic structure of a membrane. Various protein molecules are embedded in the lipid bilayer and mediate some functions of the membrane.

In cell membranes there are three major types of lipids, namely phospholipids (the most abundant), cholesterol, and glycolipids. These lipids are amphiphilic molecules with one end hydrophilic (polar) and the other end hydrophobic (nonpolar). Fig. 1.2 shows a typical phospholipid molecule which has a polar headgroup and two hydrophobic tails. The tails may vary in length and degree of saturation. Differences in chain length and

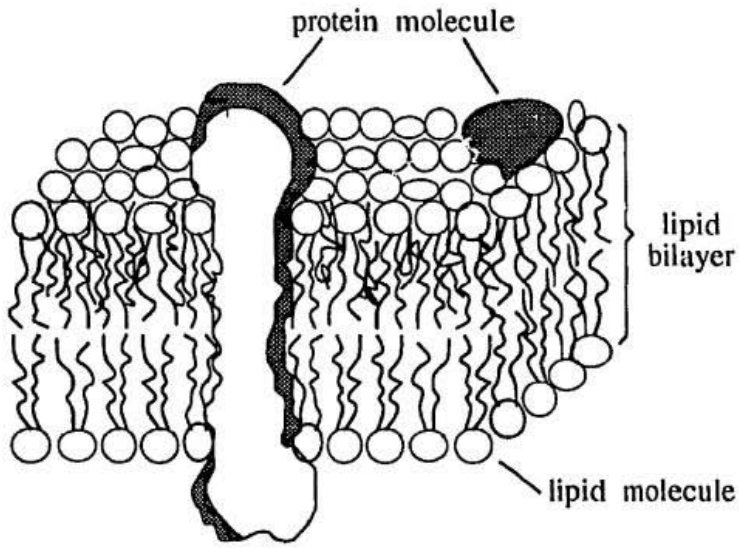

Figure 1.1: A schematic three dimensional view of a small section of biological membrane.

saturation influence membrane physical properties, such as fluidity, which determine the functioning of membranes.

Two-chain lipid molecules generally form bilayer vesicles spontaneously when dispersed in water. This is due to their amphiphilic nature. One of the very important features of lipid bilayers is their thermotropic phase behavior. Important phospholipid phases observed, in order of increasing temperature, include the crystalline phase (L_c), gel phase (L_β), an intermediate ripple phase ($P_{\beta'}$), and the fluid or liquid crystalline phase (L_α). The gel to liquid crystal transition at temperature T_m is called the main transition and is identified as a chain-melting transition. It has been demonstrated that the behavior of an artificial lipid bilayer (model membrane) is similar to that of the lipid

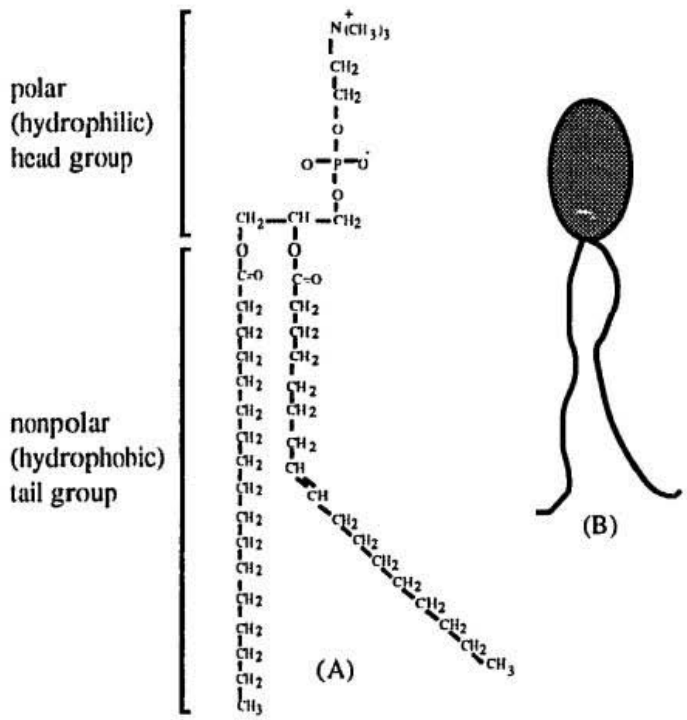

Figure 1.2: The parts of the phospholipid molecule phosphatidylcholine represented in formula (A) and as a symbol (B).

bilayer in cell membranes [6].

1.2 ^{2}H-NMR Study on Bilayer Structure

The possible motion of molecules in a membrane include diffusion and isomerization. It has been widely accepted that the headgroups of lipid molecules and water form an interface along which one end of molecule moves [2] and that the rotation about the C-C bonds of the lipid hydrocarbon chains contributes to the bilayer fluidity and determines many of the physical properties of the lipid bilayer [7]. The rotation of each methylene segment about a C-C bond creates a different conformation. There are three stable

conformations for a segment in a lipid acyl chain, namely *gauche*$^+$ (g^+), *trans* (t), and *gauche*$^-$ (g^-) as shown in Fig. 1.3. The conformation changes with an isomerization rate of about $10^9\ s^{-1}$ at room temperature [8].

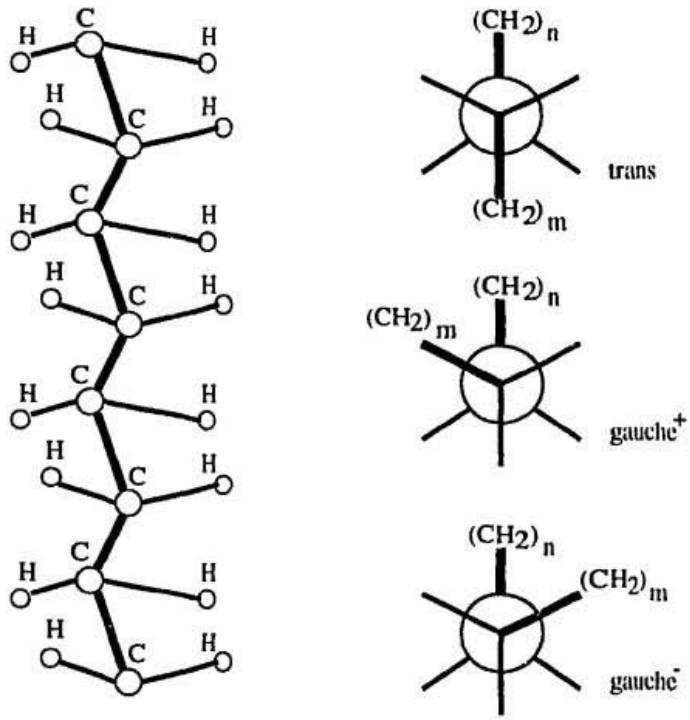

Figure 1.3: Lipid hydrocarbon chain and conformations about a single C-C bond. The three staggered conformations (shown in right column) are viewed along the C-C bond (see left column) and are related by 120° rotations about the bond axis. Steric interactions between the two chain segments, $(CH_2)_n$ and $(CH_2)_m$, cause the two gauche conformations to be of higher energy than the trans conformation.

The chain motion can be partially characterized by an orientational order parameter [2][9]. In the liquid crystalline state, on average, the constituent lipid molecules have motions characterized by cylindrical symmetry with the bilayer normal as the axis of motional averaging. For a given carbon deuterium bond on a lipid chain, the orientational

order parameter is defined as [6, 9, 10]:

$$S_{CD} = \frac{1}{2}(3\langle cos^2\theta_{CD}\rangle - 1), \tag{1.1}$$

where θ_{CD} is the angle between the C-D bond and the bilayer normal and the average is taken over conformations sampled on the time scale of the experiment. Because the chain is dominated by conformations for which $\theta_{CD} = 90°$, S_{CD} is generally negative [9]. For a C-D bond undergoing isotropic reorientation, $\langle \cos^2\theta_{CD}\rangle = \frac{1}{3}$ and S_{CD}=0. Thus a large absolute value of the order parameter implies small amplitude reorientation for the segment.

Because the tensor interactions of the spin system are not fully averaged by molecular motions in the bilayer, ^{2}H-NMR, as applied to bilayer membranes, is referred to as solid-state NMR. The ^{2}H-NMR spectrum of a deuteron on a lipid acyl chain is a Pake doublet in the liquid crystalline phase. It results from the superposition of doublets arising from randomly oriented domains and is also referred to as a powder pattern. Sharp edges corresponding to molecules reorienting about axes perpendicular to the applied magnetic field are separated by the quadrupole splitting, $\Delta\nu_Q$ [9]. The orientational order parameter can be measured via the nuclear quadrupole splitting through

$$\Delta\nu_Q = \frac{3}{4}\frac{e^2qQ}{h}S_{CD}, \tag{1.2}$$

where $\frac{3}{4}\frac{e^2qQ}{h} \simeq 125$kHz. S_{CD} reflects the time averaged angular amplitude of motion of the chain segment on the ^{2}H-NMR time scale of 10^{-6} to $10^{-5}s$ and is thus sensitive to the average environment sampled as molecules diffuse through the bilayer. Fig. 1.4 shows a typical ^{2}H-NMR spectrum for a perdeuterated (i.e. with all hydrogen atoms on an acyl chain replaced by deuteriums) sample in the liquid crystalline phase. It consists of a superposition of Pake doublets arising from deuterons along the chain with a range of orientational order parameters.

After the pioneering ^{2}H-NMR work done on soap molecules by Oldfield et al. (1971) [11], the ^{2}H-NMR method was soon applied to diacyl lipid bilayer membranes. Through a series of studies, Seelig and co-workers [9, 12-19] have addressed various basic issues, such as : (1) hydrocarbon chain orientation at various positions in the bilayer, (2) motions of the chain segments, (3) the determination of chain extension (the chain length projected on the bilayer normal) or bilayer thickness in terms of the measured segmental order parameters, (4) magnetic ordering of phospholipid membranes [18], and (5) conformational changes of the headgroup due to membrane dehydration [19].

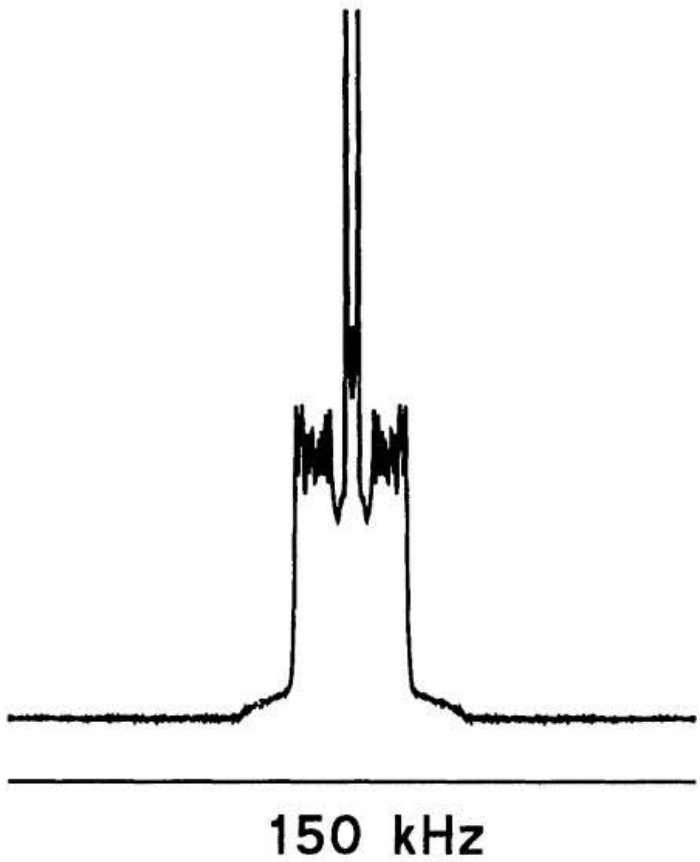

Figure 1.4: Powder spectrum for DMPC[d_{54}] at 44 °C.

To list all contributors in this field is difficult because of the diversity of membranes and their physical properties. Here I will specifically mention two more groups, not only because they have contributed significantly in this field, but also because the techniques developed by them have been heavily used in this project. Bloom and co-workers [20-25] have made important contributions to the understanding of the physical information contained in ^{2}H-NMR spectra. One of their contributions is spectral "de-Pakeing" [21][22], which is a procedure for obtaining the spectrum of an oriented system from that of the powder spectrum for a perdeuterated system (see Fig. 1.5. There the total width of the spectrum (150 kHz) is indicated by the bottom line. This practice will be followed in this thesis.). This procedure improves the definition between the peaks in a spectrum and is widely used at present in the analysis of spectra. Davis and co-workers [6, 26-31] have also made many contributions to the field of membrane studies by use of ^{2}H-NMR, including techniques to construct binary phase diagrams by spectral subtraction. Other important contributions related to my project will be cited in the later chapters in this thesis.

1.3 Analysis of ^{2}H-NMR Spectra

Information about acyl chain ordering, obtained from ^{2}H-NMR, can be variously expressed as an orientational order parameter profile, a mean order parameter, and a spectral first moment. The significance of these properties in the description of bilayer structure and bilayer phase behaviour is briefly discussed in this section. The technique for extracting the orientational order parameter profile from the NMR spectrum is also discussed. The theory of ^{2}H-NMR as applied to bilayer systems is reviewed in the next chapter.

1.3.1 Order Parameter Profile

The orientational order parameter profile of a lipid acyl chain is obtained by plotting order parameter versus carbon number. Usually, values of the order parameters for the upper half chain, near the headgroup, change slowly with position along the chain. Along the lower half of the chain, the order parameters in magnitude decrease more or less exponentially toward the methyl end. The region where the values of the order parameter change slowly is called the plateau.

The orientational order parameter reflects the time-averaged orientation of a chain segment. It is not directly related to the rate of the segmental motion, which is better studied by relaxation time experiments. However, a smaller value of the order parameter generally means a larger angular amplitude of motion of the chain segment. Thus the shape of the order parameter profile indicates that segments in the plateau area of a chain are more ordered than the rest of the chain and that the ordering of segments in a chain decreases along the lower half of the chain resulting in a more fluid state in the bilayer middle region.

The term flux is sometimes used to describe the extension of the chains passing per unit area toward the bilayer middle region. The shape of the order parameter profile also suggests that the molecular chain flux corresponding to the plateau region is a constant and that the flux decreases more or less exponentially towards the methyl group [32]. Theoretical consideration of experimentally determined order parameter profiles [15][33] has suggested that the molecular chains lie basically parallel to the bilayer normal. The probability of the acyl chain segments folding back may be negligible in the plateau area and increase along the lower half chain to a maximum value about 0.14 for the methyl in a chain with 14 carbons [34].

Knowing the order parameter profile, one can estimate mean chain extension [15][35].

If additional assumptions are made, information about the area per chain for the bilayer in the fluid state can be obtained from the mean order parameter,

$$\langle S_{CD} \rangle = \frac{\sum_{i=2}^{N} S_{CD}^{i}}{(N-1)}, \tag{1.3}$$

where N is the total carbon number of the chain. The area per chain then has a simple empirical relationship with $\langle S_{CD} \rangle$, as demonstrated by Boden et al. [36].

Thus the order parameter and its profile provide structural information about chain segment position, orientation, and conformation in a lipid bilayer, from which physical quantities like the bilayer thickness, the area per lipid molecule, and the coefficient of thermal expansion of the acyl chain length can be obtained.

1.3.2 Spectral First Moment and Phase Transitions

The first moment of the half spectrum is given by

$$M_1 = \frac{\int_0^\infty f(w) w dw}{\int_0^\infty f(w) dw}, \tag{1.4}$$

where $f(w)$ is the spectrum. The relationship between M_1 and the mean orientational order parameter of a perdeuterated chain $\langle S_{CD} \rangle$ is given by [6]

$$M_1 = \frac{\pi}{\sqrt{3}} \frac{e^2 q Q}{h} \langle S_{CD} \rangle.$$

The phase transition behavior of a bilayer is reflected in the dependence of M_1 on temperature T. For a single component bilayer, M_1 changes dramatically at the temperature of the main phase transition. Using the model of Schindler and Seelig [15] the mean extension in $\mathring{A}$ per segment of the acyl chain in a bilayer can be related to the first moment in kHz through [6, 13, 15, 37],

$$\langle l \rangle = 1.25[\frac{1}{2} + \frac{\sqrt{3}}{\pi 167} M_1]. \tag{1.5}$$

If the bilayer volume is treated as being constant, the area per lipid may then be taken to be approximately proportional to $\langle l \rangle^{-1}$ [37]. This quantity also changes greatly during the phase transition. We thus see that M_1 is closely related to the structural parameters of the bilayer.

Some features of the bilayer phase transition can be modeled by using a phenomenological Landau theory [38]. In this model, the free energy $f(s)$ is expanded as a power series in an order parameter s around $s = 0$. When $f(s)$ is a global minimum $f_m(s_m)$ at s_m, then $f_m(s_m)$ is equal to the Gibbs free energy of the system. The Landau order parameter is defined as a scalar order parameter [39], satisfying

$$s = 0, \quad T \geq T_c;$$

$$s \neq 0, \quad T < T_c.$$

where T_c is critical temperature for the system. The Landau free energy generally has the form:

$$f(s) = a_0 + a_1 s + \frac{1}{2} a_2 s^2 + \frac{1}{3} a_3 s^3 + \frac{1}{4} a_4 s^4 + \cdots, \tag{1.6}$$

where a_0 is a constant, and $a_1, a_2, \cdots$ are functions of temperature T. In Chapter 4 the determination of a thermodynamic Landau order parameter from the acyl chain mean orientational order parameter for a diacyl phospholipid family will be discussed.

The phase behavior of a two-component lipid bilayer is generally more complicated. As temperature is increased, the system usually goes from the gel phase, via a region of two-phase coexistence, to liquid crystalline phase. The corresponding first moment does not change as abruptly as in single component bilayer. In general, the shape of the two-phase region in the binary phase diagram will depend on which component is deuterated [40][41]. In some cases, acyl chain ^{2}H-NMR spectra for a binary mixture can be used to construct the phase diagram. Phase boundaries can be determined by inspection of the

spectra combined with the use of spectral subtraction [41-43] . This approach is used in Chapter 5.

1.3.3 Techniques Used to Extract Order Parameter Profiles

The first order perturbation Hamiltonian (see next chapter for detail) describing axially symmetric second-rank tensor interactions is scaled by an orientational factor, $P_2(\cos\phi) = (3\cos^2\phi - 1)/2$, where ϕ is the angle between the externally applied magnetic field and the motional symmetry axis (bilayer normal in lipid membranes) [9][24] (see Fig. 2.2). In the case of crystalline powders containing a large number of randomly oriented domains, this scaling results in a characteristic powder line shape ("powder pattern") due to the superposition of contributions from each such domain. In a spin 1 system, the powder pattern has a characteristic line shape dominated by a pair of peaks associated with $\phi = \pi/2$, the most probable value of ϕ. This line shape is called a "Pake doublet," after G. E. Pake who was the first to study such systems in detail [44][45].

Well resolved powder patterns can be obtained from samples with a few sites specifically deuterated. In these cases, the corresponding order parameters can be measured unambiguously. However, in more complex system, with a large number of deuteration sites per molecule involved, it is difficult to get accurate order parameters directly from powder spectra. Bloom and co-workers [21][22] have demonstrated that the powder pattern produced by a polycrystalline sample can be deconvoluted to a "oriented spectrum" which would arise from a single crystal with an orientation parallel to the external magnetic field (i.e. ϕ=0°). For a perdeuterated lipid membrane, the oriented spectrum can be used to obtain a smoothed order parameter profile, which reflects the physical information required to characterize the anisotropic order of membranes, by assuming that the order parameter decreases monotonically along the chain from the interface towards the bilayer middle region [46]. Fig. 1.5 shows the depaked oriented spectrum of the powder

spectrum shown in Fig. 1.4 for DMPC at 44 °*C*. The method of peak assignment for the chain segments in DMPC will be discussed in Chapter 3. In this work, smoothed order parameter profiles obtained from such oriented spectra were used to obtain structural and thermodynamic information for lipid bilayer systems.

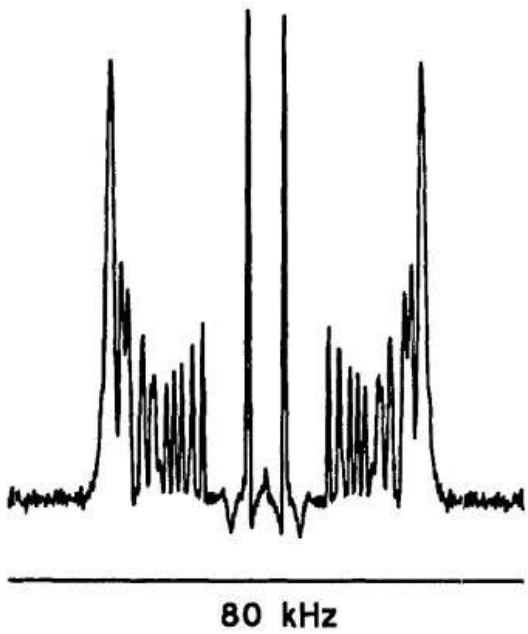

Figure 1.5: The de-Paked spectrum for DMPC at 44 °*C* (deconvoluted from Fig. 1.4). The doublet with the smallest splitting corresponds to the methyl group in the acyl chains. The next doublet corresponds to the methylene group next to the methyl group. The remaining doublets may be assigned to the other methylene groups (see Chapter 3 for details).

1.4 About This Work

The orientational order parameter profile and the mean orientational order are important properties of a bilayer system. The goal of this work is to examine the extent to which these properties are determined by a limited set of factors in a series of model membranes with increasing degrees of complexity. Among the issues addressed are :

1) the relationships between orientational order parameter profiles for bilayer lipids with a given headgroup and different chain lengths;

2) the dependence of the mean chain order parameter on temperature near the chain melting transition;

3) order parameter profile behavior in mixed lipid bilayer systems with mismatched chain lengths; and

4) the relationship between binary mixture miscibility and the chain length difference between components.

Factors which influence chain order were examined in a systematic way in some selected bilayer systems. Three classes of lipid which are important in biological membranes were used. These are phospholipids, glycosphingolipids,and cholesterol. Their structures are shown in Fig. 1.6. The kinds of bilayer examined were (1) single component phospholipid bilayers with the same head group but with chain lengths of 12, 14, 16, and 18 carbons (DLPC, DMPC, DPPC, and DSPC respectively)[1]; (2) binary mixtures of phospholipids with the same head group but different chain lengths (DMPC/DSPC); (3) the single glycolipid 24:0 GalCer [2]; (4) binary mixtures of a glycosphingolipid and phospholipid with small chain length mismatch (18:0 GalCer/SOPC) [3] and with significant chain length mismatch (24:0 GalCer/SOPC); (5) ternary systems containing cholesterol

[1] DLPC: dilauroylphosphatidylcholine; DMPC: dimyristoylphosphatidylcholine; DPPC: dipalmitoylphosphatidylcholine; DSPC: distearoylphosphatidylcholine.

[2] 24:0 GalCer: *N*-lignoceroyl galactosyl ceramide.

[3] 18:0 GalCer: *N*-stearol galactosyl ceramide; SOPC: 1-stearoyl-2-oleoylphosphatidylcholine.

and either 18:0 GalCer/SOPC or 24:0 GalCer/SOPC. These systems are represented schematically in Fig. 1.7. All samples were prepared as multilamellar vesicle dispersions in order to avoid the effects of vesicle tumbling and highly curved bilayer surfaces.

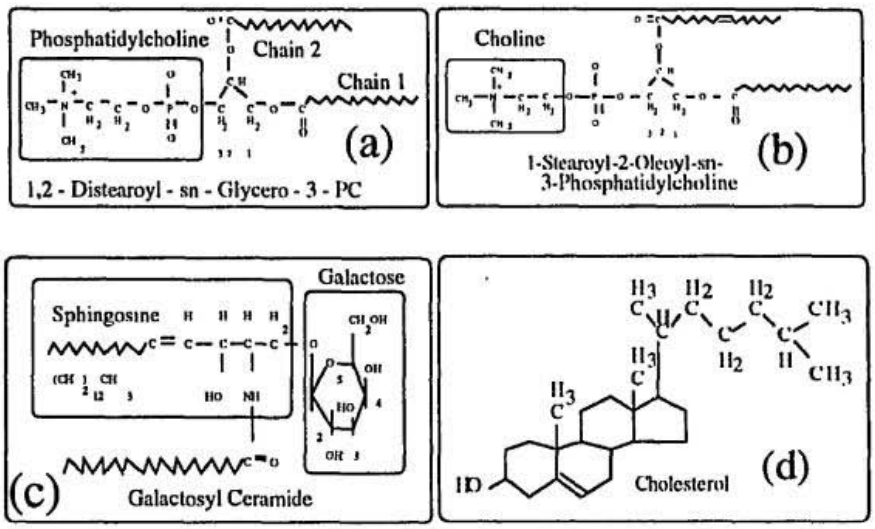

Figure 1.6: Chemical formula for lipid molecules used in this work: DSPC (a), SOPC (b), Galactosyl Ceramide (c), and cholesterol (d).

Glycosphingolipids were used as examples of a long chain membrane component in this work. An important reason for use of the glycosphingolipids in this research is that glycolipids have some receptor function in membranes and that this receptor function is known to depend on acyl chain length [47]. In glycosphingolipids, the sphingosine portion of the ceramide backbone does not generally vary. The fatty acid, which commonly ranges from 18 to 26 carbon atoms, may determine receptor function. It has been found that glycolipid fatty acid chain length has an effect on antibody binding to galactosylceramide in phosphatidylcholine liposomes [47][48]. It has been suggested that the stronger immune

response with longer chain species is due to relatively greater carbohydrate headgroup protrusion from the membranes, resulting from mismatch of the long fatty acid chain with the host matrix [47]. Cholesterol was used in some studies to examine the effect of

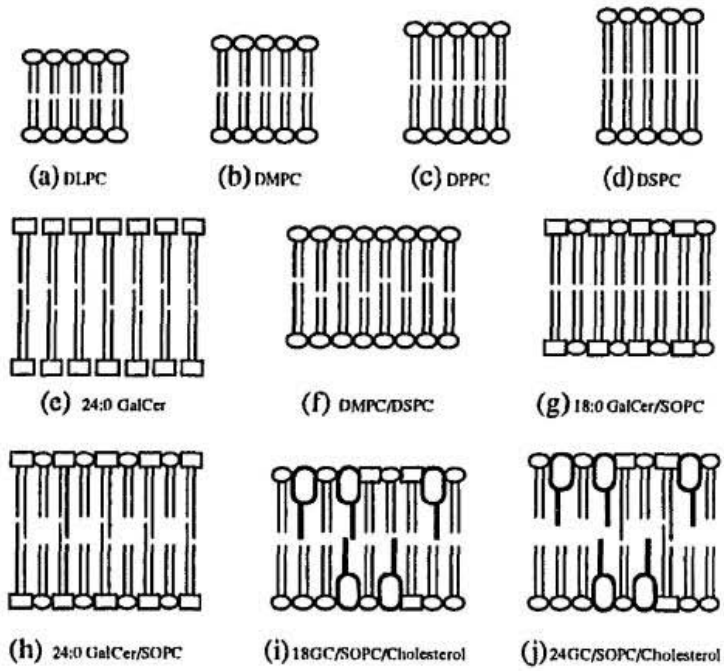

Figure 1.7: Lipids used in this work are represented schematically. Their chemical formulae are shown in Fig. 1.6. Bilayers (a) to (d) are single molecule bilayers. They differ only in chain length of the lipid component. Bilayer (e) is also a single molecule bilayer but its two moieties differ in length by six carbons (see Fig. 1.6(c)). Bilayers (f) to (h) are binary lipid mixtures. They may vary either in component chain length (f) or head group (g), or both (h). Bilayer (i) is the mixture of bilayer (g) and cholesterol. Bilayer (j) is the mixture of bilayer (h) and cholesterol.

steric constraint on glycosphingolipid fatty acid arrangement in bilayers. Samples of 23 mol% cholesterol with 10 mol% 24:0 GalCer in SOPC and with 10 mol% 18:0 GalCer in SOPC were used. All samples containing glycolipids were made by Dr. Chris W.M. Grant and Mr. Dev Singh of the Biochemistry Department, University of Western Ontario.

A common theme in this work is the way in which the shape of the smoothed orientational order parameter profile changes as the complexity of the system increases from a bilayer with a single type of chain and headgroup, through bilayers with a single headgroup but two chain lengths, to bilayers containing different classes of lipids with different chain lengths. One goal is to study how the orientational order parameter profile and the temperature dependence of the mean order parameter change with chain length within a family of single component phospholipid bilayers. Another goal is to learn how the profile reflects changes in chain packing in cases of chain-length mismatch.

For the single component diacyl phospholipid bilayers, the effect of chain length on the orientational order parameter profile (OOPP) was examined. It was found that the OOPP for phospholipids having different chain lengths is determined by the plateau value of the orientational order parameter if position along the chain is scaled [49]. The temperature dependence of the mean order parameter for a chain near the melting transition and the jump in mean order parameter at the transition were obtained for phospholipids having different chain lengths. These observations were fitted using a Landau model for free energy [37].

For the chain mismatched systems, including a single component mixed-chain system, a number of binary systems, and a ternary system, the effect of chain length mismatch on the order parameter profile was examined in some detail [50-54] . It was first found that the orientational order parameter profile for a very long chain in a chain mismatched lipid bilayer has a second plateau near the methyl group end of the chain which corresponds to the bilayer middle region [51-54] . The same may also be true for binary lipid bilayers of DMPC/DSPC containing small concentrations of DSPC. Cholesterol has little influence on the appearance of the second plateau in the PC-glycolipid system studied [53]. The experimental results suggest that when a second plateau appears in an orientational order parameter profile, the tails of the long chain from the opposite monolayers of the lipid

bilayer are mostly mingled with each other, forming a very fluid central layer in the center of the bilayer.

The effect of chain mismatch on a binary phase diagram was also examined. Gel phase immiscibility was found in a lipid bilayer with chains significantly mismatched (24:0 GalCer/SOPC), but not in a related lipid bilayer with chains effectively matched (18:0 GalCer/SOPC) [50][51].

In the binary system DMPC/DSPC, phase diagrams constructed from the spectra for one or the other component deuterated differ slightly [40]. However, it is useful to make the comparison between spectra (or OOPPs) for the two components. It is thus necessary to determine an appropriate way to select a pair of corresponding spectra for one or the other component deuterated, which can represent the states of the two components in a given mixture simultaneously. Work in Chapter 5 will demonstrate that a pair of orientational order parameter profiles which represent one or the other component deuterated, at the same temperature, simultaneously represent the states of the two components in a given mixture. This is not the case for a pair of profiles, for the two labeled components, selected to have the same area per lipid. This result confirms an earlier suggestion that the area per lipid cannot be assumed to be "locked-in" in a binary lipid bilayer [40].

The rest of this thesis is arranged as follows: Chapter 2 includes the review of ^{2}H-NMR theory and the wide line ^{2}H-NMR experiment; Chapter 3 discusses the extraction of information from model membrane acyl chain spectra; Chapter 4 presents the experimental results and discussions for single component lipid bilayers; Chapter 5 holds the experimental results and discussions for binary mixtures. The experimental results for the single mixed-chain lipid membrane 24:0 GalCer and on the effects of cholesterol on the GalCer chain arrangement in SOPC are also included in the Chapter 5. The last chapter, Chapter 6, is a summary and some concluding remarks.

Chapter 2

Review of ^{2}H-NMR Theory, The Wide Line Experiment, and Materials

NMR theory related to this project and some details of the wide line ^{2}H-NMR measurements performed in this project are reviewed in this chapter. The theory discussed here is basically a quantum mechanical description of deuterium NMR, although classical pictures for NMR are included for clarification. The first section discusses the Hamiltonian in a spin 1 system and introduces quadrupole splittings. The second section describes the formation of the quadrupole echo by using the spin density operator formalism. The third section presents the parameters for the quadrupole echo pulse sequence. The fourth section describes the spectrometer.

2.1 Hamiltonians and Quadrupole Splitting for Spin 1 System

Following Grimmer and Blumich [55], the energy of a deuterium nucleus in a high external magnetic field (B_0) is composed of the Zeeman energy (Z), quadrupole energy (Q), dipolar interaction energy (D), and chemical shift energy (C). The total Hamiltonian $\mathcal{H}$ may be written as the sum of the Hamiltonians for each individual interaction:

$$\mathcal{H} = \mathcal{H}^Z + \mathcal{H}^Q + \mathcal{H}^D + \mathcal{H}^C. \tag{2.1}$$

The order of magnitude (in the frequency units, rad/s) of the individual interactions are 10^8, 10^6, $5\text{x}10^4$, $2\text{x}10^4$ for $\mathcal{H}^Z, \mathcal{H}^Q, \mathcal{H}^D$, and $\mathcal{H}^C$, respectively [55]. Thus in an ^{2}H-NMR experiment, dipolar and chemical shift interactions may be neglected, deuterium may be treated as an isolated spin 1 nucleus, and the quadrupole interaction may be treated as

a first-order perturbation on the Zeeman interaction [30][55].

The Hamiltonian for the Zeeman interaction is [56]

$$\mathcal{H}^Z = -\gamma h\vec{B}_0 \cdot \vec{I} = h\omega_0 I_Z, \tag{2.2}$$

where $h = h/2\pi$ denotes Planck's constant, γ and $\vec{I}$ are the gyromagnetic ratio and nuclear spin operator for the deuteron, $\omega_0 = 2\pi\nu = -\gamma B_0$ is the Larmor frequency, and the direction of the Z-axis of the laboratory coordinate system (X, Y, Z) is defined by the magnetic field $\vec{B}_0$. The eigenvalues of the Zeeman Hamiltonian (see Fig. 2.1) are

$$E_m = h\omega_0 m; \qquad m = 1, 0, -1.$$

The Hamiltonian for the quadrupole interaction arises from the interaction between the nuclear quadrupole moment of the deuteron and the electric field gradient (EFG) at the position of the deuteron. Following Slichter [57], it has the form

$$\mathcal{H}^Q = \frac{eQ}{6I(2I-1)} \sum_{\alpha\beta} V_{\alpha\beta}[\frac{3}{2}(I_\alpha I_\beta + I_\beta I_\alpha) - \delta_{\alpha\beta} I^2], \tag{2.3}$$

where e is the elementary charge, eQ is the electric quadrupole moment of the deuteron, $V_{\alpha\beta}$ is the electric field gradient operator, and α and β stand for any three orthogonal axes. The quadrupole interaction can be regarded as a scalar product of two irreducible tensor operators of rank two [56][58].

$$\mathcal{H}^Q = C_Q \sum_{\alpha=-2}^{+2} (-1)^\alpha T_\alpha^{(2)} V_{-\alpha}^{(2)}, \tag{2.4}$$

where $T_\alpha^{(2)}$ is usually defined in the laboratory coordinate system

$$T_0^{(2)} = \frac{1}{\sqrt{6}}(3I_Z^2 - I(I+1)), \quad T_{\pm 1}^{(2)} = \frac{1}{\sqrt{2}}(I_{\pm 1} I_Z + I_Z I_{\pm 1}),$$

$$T_{\pm 2}^{(2)} = (I_{\pm 1})^2, \quad C_Q = \frac{eQ}{2I(2I-1)}, \quad I_{\pm 1} = \mp\frac{I_\pm}{\sqrt{2}};$$

I_Z and $I_\pm = I_X \pm iI_Y$ are deuteron spin operators. The electric field gradient (EFG) tensor has its simplest expression in the principal axis system (x', y', z'). In this system, the irreducible EFG tensor elements $V^{(2)}_{P,\alpha}$ are given by [9]:

$$\begin{aligned} V^{(2)}_{P,0} &= V_{z'z'} = eq, \\ V^{(2)}_{P,\pm 1} &= 0, \\ V^{(2)}_{P,\pm 2} &= \frac{1}{\sqrt{6}}(V_{x'x'} - V_{y'y'}) = \frac{1}{\sqrt{6}}\eta eq, \end{aligned} \tag{2.5}$$

where $V_{x'x'}, V_{y'y'}$, and $V_{z'z'}$ (or eq) are electric field gradients along the three cartesian axes. η is called the asymmetry parameter and defined as

$$\eta = \frac{V_{x'x'} - V_{y'y'}}{V_{z'z'}}, \tag{2.6}$$

where it is assumed that $V_{z'z'} \geq V_{x'x'} \geq V_{y'y'}$. Because the spin tensor operator $T^{(2)}_\alpha$ is expressed in the laboratory frame, the electric field gradient tensor in Eq. (2.4), $V^{(2)}_\alpha$, must be expressed in the laboratory system as well. This can be achieved through the transformation.

$$V^{(2)}_\alpha = \sum_{\alpha'=-2}^{+2} D^{(2)}_{\alpha',\alpha} V^{(2)}_{P,\alpha'}, \tag{2.7}$$

where $D^{(2)}_{\alpha',\alpha}$ are the Wigner rotation matrixes [9] which transform the electric field gradient tensor from the principal coordinate system ($V^{(2)}_{P,\alpha'}$) to the laboratory system ($V^{(2)}_\alpha$).

To first order approximation, among the $T^{(2)}_q$ in Eq. (2.4), only $T^{(2)}_0$ needs to be considered [58]. Therefore only $V^{(2)}_0$ in Eq. (2.7) needs to be considered. Eq. (2.4) then becomes

$$\begin{aligned} \mathcal{H}^Q &= C_Q T^{(2)}_0 V^{(2)}_0, \\ &= \frac{eQV_{zz}}{4I(2I-1)}(3I_z^2 - I(I+1))\frac{1}{2}[(3\cos^2\Theta - 1) + \eta\sin^2\Theta\cos 2\Psi], \end{aligned} \tag{2.8}$$

where Ψ and Θ are the two Eulerian angles for the first two successive rotations in bringing the principal major axis to laboratory Z axis which is the direction of B_0. Thus

the quadrupole interaction shifts Zeeman energy levels (Fig. 2.1), to first order, by the amount:

$$\Delta E_m = \frac{e^2qQ}{4I(2I-1)}(3m^2 - I(I+1))\frac{1}{2}[(3\cos^2\Theta - 1) + \eta\sin^2\Theta\cos 2\Psi]. \qquad (2.9)$$

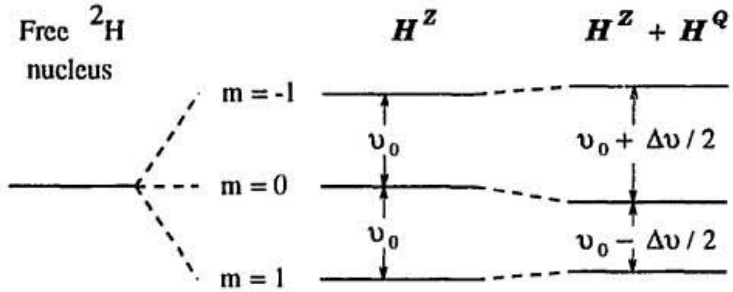

Figure 2.1: Effect of Zeeman and Zeeman plus quadrupole interactions on the energy levels of a deuteron in an external magnetic field.

The selection rule $\Delta m = \pm 1$ makes possible two transitions among the three shifted Zeeman energy levels for the deuteron. The resulting spectrum is a doublet with a splitting $\Delta\nu_Q(\Theta, \Psi)$ [9]:

$$\Delta\nu_Q(\Theta,\Phi) = \frac{3}{2}\left(\frac{e^2qQ}{h}\right)\left(\frac{3\cos^2\Theta - 1}{2} + \frac{1}{2}\eta\sin^2\Theta\cos 2\Psi\right), \qquad (2.10)$$

where $\frac{e^2qQ}{h} = 167$kHz is the quadrupole coupling constant for the deuterium in a C-D bond. In the case of C-D bonds on a fatty acid chain in a lipid bilayer, η is a very small number ($\eta \leq 0.05$), so the term containing the asymmetry parameter in Eq. (2.10) is usually neglected [9]. This leaves

$$\Delta\nu_Q(\Theta) = \frac{3}{2}\left(\frac{e^2qQ}{h}\right)\left(\frac{3\cos^2\Theta - 1}{2}\right). \qquad (2.11)$$

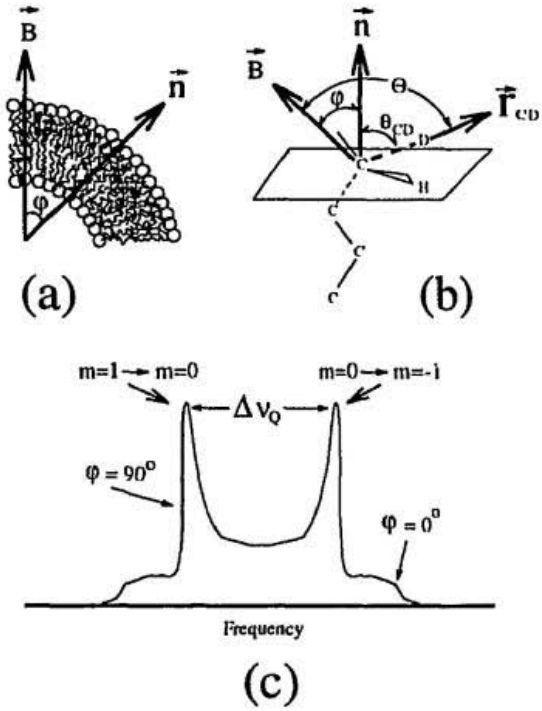

Figure 2.2: Membrane in an external magnetic field with all lipid chains deuterated at a specific site. Local orientation of the bilayer normal (a); specification of various angles in characterizing the motion of a chain (b); and the quadrupole splitting (c).

It is often convenient to distinguish motions which are fast or slow on the NMR time scale. Consider fast reorientation about a slowly varying axis of symmetry. The angle ϕ, varying slowly on the ^{2}H-NMR time scale, is defined to be the angle between the external magnetic field $\vec{B}_0$ and the symmetry axis for motion, i.e., the bilayer normal $\vec{n}$. The angle θ_{CD}, which varies quickly on the ^{2}H-NMR time scale, is the angle between the C-D bond and the bilayer normal $\vec{n}$ (Fig. 2.2(b)). The splitting is then proportional to $P_2(\cos\phi)\langle P_2(\cos\theta_{CD})\rangle$, where P_2 is the rank-2 Legendre polynomial and the average is over the orientations sampled by the fast motion [24]. Thus, if ^{2}H atoms substitute for H atoms at a specific position on every lipid molecule in a sample of randomly oriented

bilayers, we obtain, as mentioned in Chapter 1, the Pake-doublet (Fig. 2.2(c)), in which the two large peaks correspond to ϕ=90°. This splitting of the ϕ=90° edges ($\Delta\nu_Q$) (Fig. 2.2(c)) is now related to θ_{CD} via

$$\Delta\nu_Q = \nu_q \left(\frac{3\langle\cos^2\theta_{CD}\rangle - 1}{2} \right), \tag{2.12}$$

where $\nu_q = \frac{3}{4}(\frac{e^2qQ}{h}) = 125$kHz, and $(3\langle\cos^2\theta_{CD}\rangle - 1)/2$ is defined as the orientational order parameter S_{CD} (see Eq. (1.1) in Chapter 1).

It is interesting to note that S_{CD} can be further expressed as a product of two order parameters [10][59]. One is for the reorientation (wobbling) of the whole chain at the rate of $\sim 10^7 s^{-1}$, the other is for the isomerization of the segments in the chain at the rate of $\sim 10^{10} s^{-1}$ [10]. The NMR experiments, however, can only measure S_{CD}. The relative contributions from chain wobbling and chain isomerization can not be quantified. The true order parameter of the segmental isomerization is thus scaled to a smaller value of S_{CD} by a factor produced by the chain wobbling. Neverthless, measuring the splittings in a bilayer spectrum (and the correspoding S_{CD}) gives us information about molecular motion. In the gel phase, the ^{2}H-NMR spectrum is relatively featureless, because the molecular motion is in the intermediate time scale and asymmetric. In this work, the properties of lipid bilayers in fluid phase are the main concerns.

2.2 Quadrupole Echo

^{2}H-NMR spectra are normally obtained using the quadrupole echo pulse sequence [6]. The decay of the NMR signal, normally due to dephasing of the spins in the xy-plane of the rotating frame, is referred to as a free induction decay (FID). The spectrum is obtained by Fourier transformation of the FID. This section reviews the spin density operator formalism which describes the formation of the quadrupole echo in a pulse

experiment. The FID is obtained from that portion of the echo following the echo maximum.

Spins in a system subjected to a magnetic field $\vec{B}_0$ will precess at angular frequency ω_0 about the Z-axis. It is a convenient to define a system of rotating coordinates x, y, and z. The z-axis of the rotating frame coincides the Z-axis of the laboratory frame, whereas the x- and y-axis are rotating about z (or Z) at angular frequency ω_0 in the same direction as the spins in the system. In the NMR experiment, a time dependent radio frequency pulse along the X axis of the laboratory frame, $H^{RF} = H_X \cos\omega_r t$, can be viewed as the application of a static field H_x along the x axis of the frame rotating about the z (or Z) axis with angular frequency ω_r [57][60].

Following Abragam and Goldman [61], any dynamic observable operator in a system of spin I can be viewed as a vector in a Liouville space, which is spanned by a complete set of $N = (2I+1)^2$ orthonormal basis operators, $(P_i, i = 0, 1, \cdots, N-1, \mathrm{Tr}\{P_i P_j\} = \delta_{ij})$. The spin 1 density operator σ, which contains the complete statistical description of the spin system, can be expressed as [23][30]

$$\sigma(t) = c_0 P_0 + \sum_{i=1}^{8} c_i(t) P_i, \tag{2.13}$$

where P_0 is a unit operator with a normalization factor of $1/\sqrt{3}$ and c_0 is time independent and equals 1. A state of a spin system can then be represented by a vector $C(t) = (1, C_1(t), C_2(t), \cdots)$ in the Liouville space. A convenient choice of the remaining eight basis operators is [23][30]

$$\begin{aligned}
P_1 &= \tfrac{1}{\sqrt{2}} I_x, & P_2 &= \tfrac{1}{\sqrt{2}} I_y, \\
P_3 &= \tfrac{1}{\sqrt{2}} I_z, & P_4 &= \tfrac{1}{\sqrt{6}} (3I_z^2 - 2), \\
P_5 &= \tfrac{1}{\sqrt{2}} (I_x I_z + I_z I_x), & P_6 &= \tfrac{1}{\sqrt{2}} (I_y I_z + I_z I_y), \\
P_7 &= \tfrac{1}{\sqrt{2}} (I_x^2 - I_y^2), & P_8 &= \tfrac{1}{\sqrt{2}} (I_x I_y + I_y I_x).
\end{aligned} \tag{2.14}$$

Here spin operators I_x, I_y and I_z are just 3×3 matrices and may be viewed as being defined in the rotating frame. The evolution of the density operator σ obeys the Liouville-Von Neumann equation

$$\frac{d\sigma}{dt} = \frac{i}{\hbar}[\sigma, \mathcal{H}]. \tag{2.15}$$

Putting Eq. (2.13) into the above equation, we get a set of coupled linear differential equations for the coefficients $c_i(t)$,

$$\frac{dc_i}{dt} = \frac{i}{\hbar}\sum_j Tr\{[P_j, \mathcal{H}]P_i\}c_j, \tag{2.16}$$

which contain all of the information about the time evolution of the system. The ensemble averaged expectation value of an observable, say O, can be calculated from the density matrix by using [30]

$$\overline{\langle O \rangle} = Tr\{O\sigma\} \tag{2.17}$$

The commutators of the spin 1 basis operators which determine the time evolution for the coefficients of the spin 1 density operator have been tabulated [23]. Here the time evolution of c_1 is followed for the purpose of illustrating the quadrupole echo under the assumption that the FID absorption signal appears on the x axis of a frame rotating at the Larmor frequency. Let us examine the quadrupole pulse sequence $(\frac{\pi}{2})_y - \tau - (\frac{\pi}{2})_x - t$. Here $(\frac{\pi}{2})_y$ is a radio frequency (r.f.) pulse which rotates the magnetization by $\frac{\pi}{2}$ about y-axis in the rotating frame. $(\frac{\pi}{2})_x$ is a r.f. pulse which rotates the magnetization by $\frac{\pi}{2}$ about x-axis in the rotating frame. The time separation between the two pulses is τ. The NMR signal, an echo, will appear on the x axis after the second pulse. Assume that the spin system is in a static external field $\vec{B}_0$ (along the Z axis of the laboratory coordinates) for long enough to come to equilibrium. A small excess of spins aligns with the external field, forming a macroscopic magnetization. Assuming no interaction between the spins,

the equilibrium density operator may be written as [30][62]

$$\sigma(0) \approx -\frac{\hbar\omega_0 I_Z}{3kT}, \tag{2.18}$$

in the high temperature approximation. Here k is Boltzman's constant and T is the temperature of the lattice. On the other hand,

$$\sigma(0) = c_3(0)P_3 = c_3(0)\frac{I_Z}{\sqrt{2}}. \tag{2.19}$$

Comparing Eq. (2.19) with Eq. (2.18) and defining $I_0 = -\sqrt{2}\hbar\omega_0/(3kT)$ allow the equilibrium state to be represented by

$$c_1 = 1, \qquad c_3 = I_0, \tag{2.20}$$

and

$$c_2 = c_4 = c_5 = c_6 = c_7 = c_8 = 0. \tag{2.21}$$

The equilibrium state can be expressed as $C = (1,0,0,I_0,0,0,0,0,0)$.

The application of a radio frequency (r.f.) pulse (ω_e) introduces a new field $\vec{B}_1\cos(\omega_e t)$, resulting in an additional contribution to the total Hamiltonian. If the rf field is along the y axis of the rotating frame, then

$$\mathcal{H}^{RF} = \hbar\omega_1 I_y \cos(\omega_e t), \tag{2.22}$$

where $\omega_1 = -\gamma B_1$ is the precession frequency around the magnetic field of the r.f. pulse. In the laboratory axis system, the quadrupole Hamiltonian for the spin 1 system in the absence of an r.f. pulse can be expressed as

$$\mathcal{H}^Q = \frac{\hbar\omega_q}{3}(3I_z^2 - 2), \tag{2.23}$$

and the asymmetry parameter η has been set to zero in the second line, where $\omega_q = \frac{3}{4}\frac{e^2qQ}{\hbar}P_2(\cos\Theta)$ [25][30]. We thus see that the total Hamiltonian for the spin system in

the rotating frame in the presence of an r.f. pulse at $t = 0$ is [57]

$$\mathcal{H} = \hbar(\omega_e - \omega_0)I_z + \hbar\omega_1 I_y + \frac{\hbar\omega_q}{3}(3I_z^2 - 2). \tag{2.24}$$

The first and the third terms on the RHS of the above equation are usually neglected during the pulse because $\omega_e \simeq \omega_0$ and $\omega_1 \gg \omega_q$ [30].

If a r.f. pulse with duration t_1 is applied along the y axis at $t = 0$, the Hamiltonian of the interaction can be expressed as

$$\mathcal{H}_y^{RF} = \sqrt{2}\hbar\omega_1 P_2. \tag{2.25}$$

Putting the $\mathcal{H}^{RF}$ into Eq. (2.16) , we obtain a pair of coupled equations for c_1 and c_3. Solving them, we get

$$c_3 = I_0 \cos(\omega_1 t_1) \tag{2.26}$$

$$c_1 = I_0 \sin(\omega_1 t_1). \tag{2.27}$$

Here the transverse relaxation during the time of the pulse is neglected because $t_1 \ll T_2$, where T_2 is the transverse relaxation time characterizing the dephasing of the spins about the z axis in the xy-plane of the rotating frame. If the rotation of the magnetization during the time t_1 is $\omega_1 t_1 = \pi/2$, then the coefficient c_1 right after the first pulse is $c_1(t_1) = I_0$. This result suggests that the net magnetization in the system, immediately after the first $\pi/2$ pulse, is aligned along the x axis in the rotating frame. For the next period of time τ we solve Eq. (2.16) for c_1 by considering only the quadrupole interaction

$$\mathcal{H}^Q = \sqrt{\frac{2}{3}}\omega_q P_4. \tag{2.28}$$

We thus obtain a pair of coupled equations for c_1 and c_6. By solving the equations, we get

$$c_6 = I_0 \sin(\omega_1 t_1)\sin(\omega_Q t)e^{-\tau/T_2} \tag{2.29}$$

$$c_1 = I_0 \sin(\omega_1 t_1)\cos(\omega_Q t)e^{-\tau/T_2}, \tag{2.30}$$

in which an extra exponential factor is added to take account of transverse relaxation.

For a second pulse with duration t_2, applied along the x axis at the time τ, the Hamiltonian is

$$\mathcal{H}_x^{RF} = \sqrt{2}\hbar\omega_1 P_1. \tag{2.31}$$

This time, by solving Eq. (2.16) again, we obtain

$$c_1 = invariant \tag{2.32}$$

$$c_6 = I_0 \sin(\omega_1 t_1)\sin(\omega_Q \tau)\cos(2\omega_1 t_2)e^{-(\tau+t_2)/T_2}. \tag{2.33}$$

The duration of the second pulse t_2 is very small compared with the pulse separation time τ and can be neglected in the exponential term. After the second pulse the system again relaxes as in the period after the first pulse. We finally get

$$\begin{aligned} c_1 = {} & [-I_0 \sin(\omega_1 t_1)\cos(2\omega_1 t_2)\sin(\omega_Q \tau)\sin(\omega_Q t) \\ & + I_0 \sin(\omega_1 t_1)\cos(\omega_\zeta \tau)\cos(\omega_Q t)]e^{-(\tau+t)/T_2}. \end{aligned} \tag{2.34}$$

If the rotations resulting from the two pulses, $\omega_1 t_1$ and $\omega_1 t_2$, are both $\pi/2$, then we have

$$c_1 = I_0 \cos[\omega_Q(t-\tau)]e^{-(\tau+t)/T_2}. \tag{2.35}$$

Eq. (2.17) may be used to calculate the expectation value of $\langle I_x \rangle$ which is proportional to the transverse magnetization M_x. When $t = \tau$, that is at a time 2τ after the first pulse, spins in the system refocus to give an echo on the x axis of the rotating frame. As was pointed out by Davis et al. [6][26], this pulse sequence shifts the FID signal out of the dead time of the receiver caused by the strong pulse and provides a way to record an undistorted FID signal and to measure relaxation times. The signal picked up from the probe is a time domain signal. Its Fourier transform starting from the top of the echo gives us the spectrum.

2.3 Parameters for Quadrupole Echo Pulse Sequence

The quadrupole echo pulse sequence is $(\frac{\pi}{2})_y - \tau - (\frac{\pi}{2})_x - t-$, as shown in Fig. 2.3. The first pulse was preceeded by a pre-sequence interval of 0.1 s. The two pulses, separated

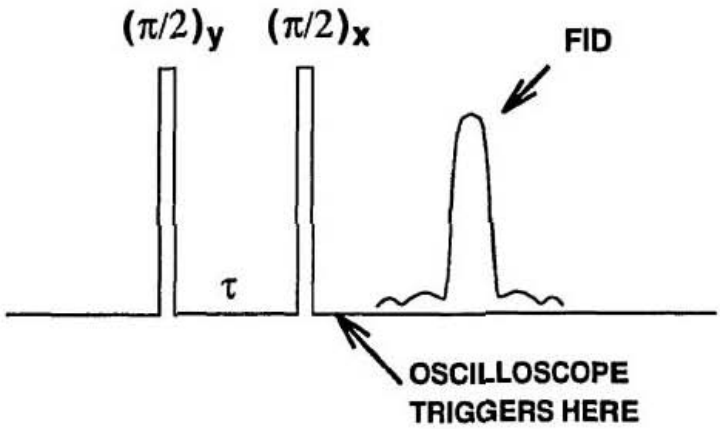

Figure 2.3: Quadrupole pulse sequence.

by a time of τ, were discussed in previous section. The width of these two $\pi/2$ pulses was between 2 and 4 μs. The $\pi/2$ pulse length was determined by maximizing the echo signal before each set of experiments. The subscripts y and x for the $\pi/2$ pulses denote that the magnetic fields generated by the two pulses are along the y axis and the x axis in the rotating frame. In practice, spectra were collected using a phase cycled quadrupole echo pulse sequence to eliminate artifacts and differences between channels in the phase sensitive detector. That is, the two pulses maintain a 90° phase difference but their

effective magnetic fields are along axes $(x,y),(-x,y),(x,-y),(-x,-y)$ in the rotating frame. The pulse separation time τ was normally 35 μs. The digital oscilloscope must be triggered for sampling. This is done 5 μs after the second r.f. pulse. The duration of the trigger pulse was 5 μs. Finally, a time of 0.4 to 0.8 s was used to let the sample relax to its equilibrium state before repeating the sequence.

2.4 The Spectrometer

A standard wide line ^{2}H-NMR spectrometer of local construction was used. Its design was based on instruments used at Guelph and UBC [6]. Its general operation [63][64] is reviewed below. The block diagram of the spectrometer is shown in Fig. 2.4. The frequency synthesizer supplies a local oscillator signal with a frequency of 33.2 MHz and an intermediate frequency of 10.0 MHz. The 10 MHz signal is fed into a switched phase splitter and the 33.2 MHz signal is sent to both the single sideband generator and the receiver The 10 MHz signal is edited into pulses with phases of 0°, 90°, 180°, and 270° in the pulse generator and sent to mixers contained in the single side band generator . The output and the duration (t_p) of these pulses are controlled by a simple pulse programmer adopted from a design by J. Davis (Guelph). The single side band system mixes the 33.2 MHz and 10 MHz signals to generate pulses at the deuteron resonance frequency 23.2 MHz. These pulses are then sent to a home built transmitter via a pulse amplifier. Strong and short r.f. pulses are needed in the solid state ^{2}H-NMR experiment in order to cover the whole range of resonant lines (say, Δ) uniformly. We can see this from the formula for the effective magnetic field:

$$B_{eff} = \frac{1}{\gamma}\sqrt{(\omega_i - \omega_e)^2 + (\gamma B_1)^2}, \tag{2.36}$$

where ω_i is the angular resonant frequency for nucleus i, ω_e and B_1 are the r.f. pulse angular frequency and its magnetic field in the coil. The difference between the angular

resonance frequency ω_i and the r.f. angular frequency ω_e is the width of the spectrum $2\pi\Delta$. If $\gamma B_1 \gg 2\pi\Delta$, then $B_{eff} \approx B_1$, which means that all the magnetization in the range Δ rotates around the direction B_1 (usually set along the x direction of the rotating frame). For a 90° rf pulse, $\gamma B_1 t_p = \pi/2$. Thus $t_p \ll 1/(4\Delta)$ is required [64].

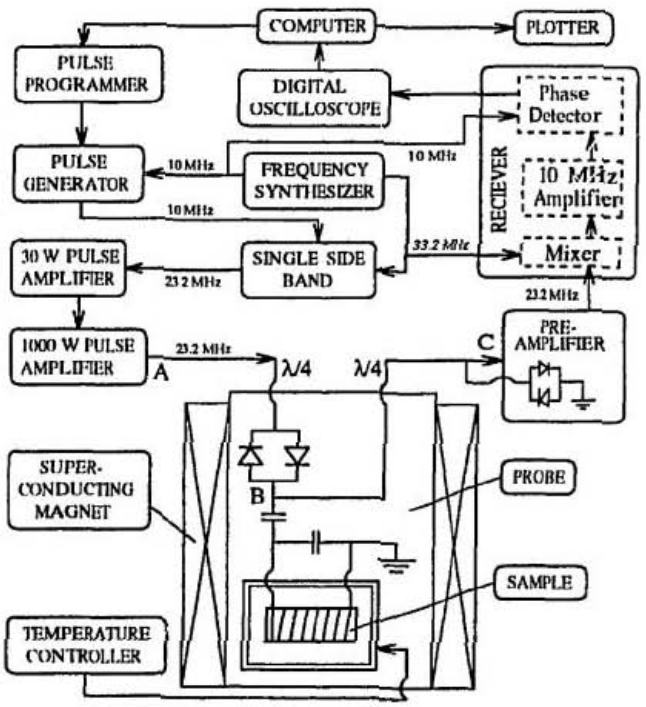

Figure 2.4: Block diagram of a NMR spectrometer.

The home built 1000 W pulse amplifier transmits short pulses at the resonance frequency with an amplitude of about 300 Volts into the probe via crossed diodes which provide a passage for the A.C. current. Another set of crossed diodes at the end of a quarter wave length line is used to protect the pre-amplifier from high voltages generated

by the pulse amplifier. The r.f. coil and the sample are contained in a temperature controlled copper oven in the probe which is inserted into the room temperature bore of a super conducting magnet. The response of the sample spin system to a pair of high power pulses through the coil produces a spin echo as described in last section. The weak spin echo signal needs to be amplified in the pre-amplifier before entering the receiver. The receiver contains a mixer, a 10 MHz amplifier, and a quadrature detector. The mixer mixes the 33.2 MHz local oscillator signal from the frequency synthesizer with the 23.2 MHz carrier wave modulated by FID signal from the pre-amplifier and generates a 10 MHz carrier wave modulated by the FID signal. The 10 MHz wave carrying the FID signal is sent to the quadrature detector. The quadrature detector detects both the real and the imaginary parts of FID signal separately by comparing the FID signal with the reference signal coming from the frequency synthesizer. The FID signals were digitized by a Nicolet 2090A oscilloscope with dwell times of 2 microseconds and 1 microsecond for samples in the liquid crystal state and in the gel state respectively.

To begin the Fourier transform from the top of the echo, it is generally necessary to shift the points in the accumulated signal by some fraction of a dwell time [6]. To improve the signal to noise ratio, even and odd points in the accumulated signal were shifted separately to give two free induction decays with points at the echo maximum. These were added to yield a contracted free induction decay with an effective dwell time twice that of the original signal. For example, although the digitizer dwell time in the gel state is 1 μs, the effective dwell time of the contracted free induction decay is 2 μs. The selection of the dwell time is related to the required spectral width. A dwell time of 1 μs corresponds to a spectral width of 1000 kHz, and 2 μs corresponds to a spectral width of 500 kHz.

To get a good spectrum for a perdeuterated sample with dry weights of 35 mg to 70 mg, usually several thousand scans were used. Where samples contain very little

perdeuterated material, up to 80,000 scans were used in order to improve the signal to noise ratio (S/N). All the signals were accumulated in a Tandy 1200 microcomputer. The free induction decay was Fourier transformed to the frequency spectrum in this computer.

It was important that arcing should not occur in the probe. After being used for long periods, the probe was occasionally observed to have black grains on the inner wall of the capacitors and elsewhere, presumably caused by dust carbonization due to the presence of high voltage. The use of high voltage spray resin was useful for control of arcing in some cases.

2.5 Materials

2.5.1 Diacyl Phosphatidylcholine Samples

Diacy phosphatidylcholines used in this work were kindly provided by Dr. J. H. Davis and were synthesized in his laboratory using the following procedure. Fatty acids were perdeuterated using the method of Hsiao et al. [65] and used in the synthesis of DLPC[d46], DMPC[d54], DPPC[d62], and DSPC[d70] following the method of Gupta et al. [66]. Samples with dry weights between 50 and 90 mg were placed into 8 mm NMR tubes, hydrated with about 250 μl of 50 mM phosphate buffer at a PH of 7.0, and stirred with a fine glass rod. All samples were found to run as a single spot by thin layer chromatography.

2.5.2 DMPC/DSPC Bilayer Mixtures

DMPC[d54] and DSPC[d70] were used to obtain bilayer mixtures of DMPC with DSPC[d70] and DMPC[d54] with DSPC [54]. Ordinary DMPC and DSPC were purchased from Sigma Chemical Co. (St. Louis, MO). The mixtures were dissolved in ethanol. The solvent was then removed by rotary evaporation followed by overnight pumping in a dessicator. Each sample was scraped into 8 mm NMR tubes with the same

hydration and degradation checking described in above paragraph.

2.5.3 Bilayer Mixtures Containing Glycolipids

The perdeuterated glycolipids 24:0 GalCer and 18:0 Galcr were prepared by Dr. C. W. M. Grant and Dr. Dev Singh at the University of Western Ontario. Mixtures of 24:0 GalCer/SOPC, 18:0 GalCer/SOPC, and GalCer/SOPC/Cholesterol were prepared in this laboratory [50, 53]. The procedures for mixing and hydrating were described above.

Chapter 3

Information Obtainable from Model Membrane Acyl Chain Spectra

In NMR experiments, spectra are often obtained for a certain lipid membrane at a series of different temperatures. These spectra contain structural, dynamical, and thermodynamic information about the lipid membrane. This chapter introduces some methods which have been used in our spectral analysis of lipid bilayer membranes. The first section describes the method of obtaining a smoothed order parameter profile from a spectrum. The second section deals with configurational statistics of acyl chain segments and the estimation of chain extension. The third section discusses the use of spectral moments. The last section describes the use of spectral subtraction for construction of a lipid membrane phase diagram.

3.1 Smoothed Order Parameter Profiles

A ^{2}H-NMR powder spectrum is the superposition of signals obtained from all the deuterons on molecules with randomly oriented symmetry axes. The peaks in the powder spectrum correspond to molecules in bilayer regions with the bilayer normal oriented at 90° to the external magnetic field. Bloom and co-workers have developed an algorithm to transform the powder pattern to an oriented spectrum [21][22]. They refer to this process as "de-Pake-ing". The resulting de-Paked spectrum corresponds to that which would be observed in a system in which all the bilayer normals are aligned with the external field.

The de-Paking procedure can be briefly reviewed as follows [21, 22]. Let us denote $F_\phi(\omega)$ as a normalised lineshape function for a C-D bond in a lipid oriented at angle

ϕ, the motionally averaged direction of the lipid relative to the external magnetic field. The observed powder spectrum lineshape $G(\omega)$ is then the superposition of $F_\phi(\omega)$ for orientations from $\phi = 0$ to $\phi = \frac{\pi}{2}$, and is given by

$$G(\omega) = \int_0^{\pi/2} F_\phi(\omega) \sin\phi d\phi. \tag{3.1}$$

Here ω is expressed such that $G(\omega)$ is zero outside of the region $-1 \leq \omega \leq 1$. $\omega = 0$ corresponds to the Larmor freqency. If F_ϕ for $\phi = 0$ is peaked at frequency x, the frequency for other values of ϕ are given by

$$\omega = x[\frac{3\cos^2(\phi) - 1}{2}]. \tag{3.2}$$

Assuming that the area of the lineshape F is independent of the angle ϕ, we have

$$F_0(x) = F_\phi(\omega)\frac{3\cos^2(\phi) - 1}{2}. \tag{3.3}$$

By using Eq. (2) and Eq. (3), Eq. (1) may be recast as

$$G(\omega) = \int dx \frac{F_0(x) I(\omega, x)}{\sqrt{3x(2\omega + x)}}, \tag{3.4}$$

where $I(\omega, x) = 1$ for $-x/2 < \omega < x$ and $I(\omega, x) = 0$, otherwise. De-Paking uses an iteractive procedure to obtain the function F_0(x) which gives rise to the known powder lineshape $G(\omega)$. $F_0(x)$ is then the spectrum which would be observed if the whole sample were oriented with $\phi = 0$.

To make a perdeuterated lipid bilayer sample is much easier than to make samples with sites selectively deuterated. Bloom and co-workers have also introduced a method to obtain a smoothed order parameter profile from the oriented spectrum of a perdeuterated lipid bilayer sample by assuming that the order parameter decreases monotonically along the chain from the interface towards the bilayer middle region [67].

To obtain the smoothed order parameter profile, it is necessary to identify splittings for the methylene groups along the chains in the oriented spectrum. Fig. 3.1 shows half

of the de-paked spectrum for DLPC at 7 °*C*. The left most peak corresponds to two methyls of the DLPC molecules. The right most feature is a superposition of the peaks corresponding to the methylene groups near the DLPC headgroups. The splittings of resolvable doublets, such as the methyl peak and a few methylene peaks next to the methyl peak, can be directly used to obtain the corresponding order parameters. The

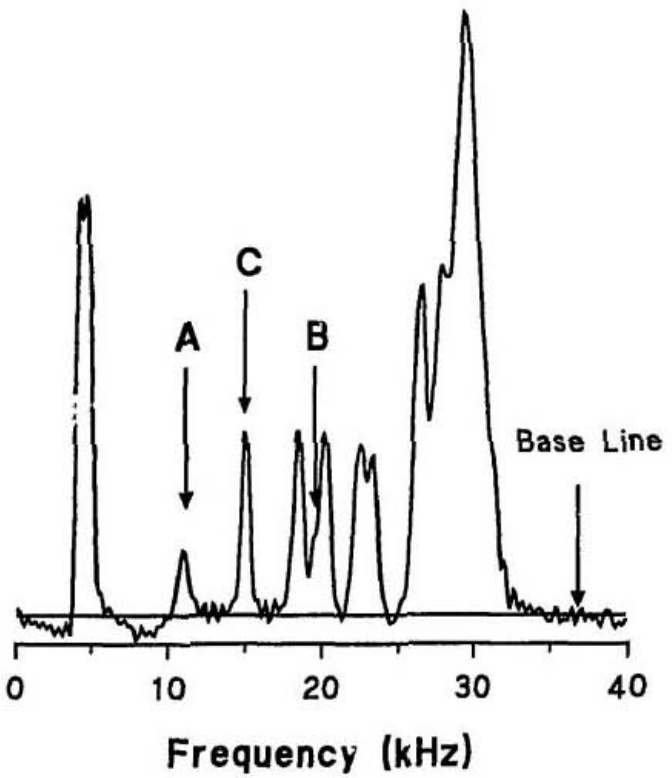

Figure 3.1: Half of the de-Paked spectrum for DLPC at 7 °*C*. The area of peak C provides a reference in the peak resolving process.

method for resolving the remaining methylene peaks is to divide their integrated area equally into an integer number of peaks which equals the total number of unassigned

deuterated methylene groups. In the work described in this thesis, it was often helpful to use the fact that the largest peak close to the methyl peak (peak C in Fig. 3.1) usually encloses an area corresponding to two CD_2 groups. One of them is for a CD_2 group on the *sn*-1 [1] chain, and the other is for one on the *sn*-2 [2] chain. The two groups have similar orientational order. In most cases we cannot distinguish them. Thus the area corresponding to two CD_2 group is judged as an unit area in resolving the oriented spectrum.

The determination of positions for CD_2 groups is somewhat subtle. For example, if the area of a large peak in an oriented spectrum equals 4 unit areas, it means that it has 4 subpeaks corresponding to 4 CD_2 groups on each chain. One may resolve the large peak (or a lump) into 4 subpeaks simply by cutting its total area into 4 strips with 4 identical unit areas. But this method takes no account of the way in which the 4 subpeaks are superposed to form the large peak. It would give rise a smoothed order parameter profile with the length of the plateau slightly shortened relative what would be observed using specifically deuterated samples. Alternatively, we have used a method in which such a large peak is divided by 5 instead of 4. The positions of the subpeaks on the frequency axis are then located at the boundaries of adjacent areas between the two ends of the resolved composite peak. This method may be called a triangular approximation, and is based on an assumption that the subpeaks are Lorentzian lines [68]. The resulting smoothed order parameter profile is consistent with that reported by other researchers [17].

In obtaining smoothed order parameter profiles for diacyl phospholipids, peaks with an area of about a quarter unit area corresponding to a single deuteron can often be identified. These are the peak A and the shoulder B shown in Fig. 3.1. They correspond

[1] *sn* – 1 refers to "stereospecifically numbered" at position 1 of the glycerol backbone.
[2] *sn* – 2 refers to "stereospecifically numbered" at position 2 of the glcerol backbone.

Table 3.1: Positions of deuterons in CD_2 for DLPC

Temperature	*Deuteron Position* (kHz)	
$°C$	D_1	D_2
2	10.651[a]	20.719[a]
17	11.240[a]	18.164[b]
32	11.414[a]	16.921
47	11.463	15.554[b]
52	11.654	15.031
Notes	a: corresponds to	a small peak
	b: corresponds to	a small shoulder

to the deuterons in the CD_2 group nearest the interface (the α position) of the *sn*-2 chain. It is reported that the two phospholipid's peaks are relatively independent of temperature and that their corresponding order parameters do not fit into the smoothed order parameter profiles of the phospholipid under study [9]. However when these two peaks are not clearly apparent in the spectrum, care must be taken to ensure that their locations in spectra for different temperatures are consistent with each other. Table 3.1 shows the positions of the two deuterons in the $\alpha - CD_2$ group of the *sn*-2 chain for DLPC at different temperatures. The labeled values (a and b) correspond to small peaks or lumps visible in spectra. The unlabeled values are determined from area considerations.

It should be noted that the major difference between the true OOPP from selectively deuterated sample [17] and the smoothed OOPP is in the upper half of the OOPP [67]. In that region, the true OOPP does not decay monotonically. The formation of the smoothed OOPP exchanges the order parameters for different carbon numbers. It does not alter the chain extension calculation. Smoothed order parameter profiles are used in Chapter 4 and 5 to examine the accommondation of the excess chain length in chain mismatched bilayers.

3.2 Configurational Statistics of Acyl Chain Segments

3.2.1 Chain Extension

The average chain length projected on the bilayer normal can be expressed as [13, 15, 35, 59]:

$$\langle L \rangle = l_0 \sum_i \langle P_1(\cos\delta_i) \rangle, \tag{3.5}$$

$$= l_0 \sum_i \langle \cos\delta_i \rangle, \tag{3.6}$$

where δ_i is the time-dependent angle between the normal to the D-C-D plane and bilayer normal, i is the carbon number, P_1 is the rank-1 Legendre polynomial, and l_0 is the projection of the C-C bond distance along the all-trans axis [$l_0 = (1.54\mathring{A})\cos 35.3° = 1.25\mathring{A}$]. The order parameter S_{CD} that we obtain from NMR experiments for the ith segment in an acyl chain is defined as

$$S^i_{CD} = \langle P_2(\cos\theta^{(i)}_{CD}) \rangle, \tag{3.7}$$

where $\theta^{(i)}_{CD}$ is the time-dependent angle between the C-D bond and the bilayer normal for the ith segment. P_2 is the rank-2 Legendre polynomial. If it is assumed that the chain disorders by *trans* – *gauche* isomerization, the C-D bonds can assume only a limited number of orientations [15]. It is then possible to express the averages required in terms of sums over accessible conformational states [52].

Fig. 3.2 shows the possible segment conformations for this assumption and the related order parameters. The angle δ may be 0°, 60°, 90°, 120°, and 180°. The angle between bilayer normal and the C-D bond, θ_{CD}, can be 90°, 144.7°, and 35.3°. The probability of a segment having conformation μ is denoted by p_μ. The conformations b to f are degenerate. There are thus twelve conformational patterns for arrangements of a CD_2 segment. Following Schindler and Seelig [15], the abbreviations $S_s = (3\cos^2 s - 1)/2$ is used in Fig. 3.2, in which s denotes an angle under consideration.

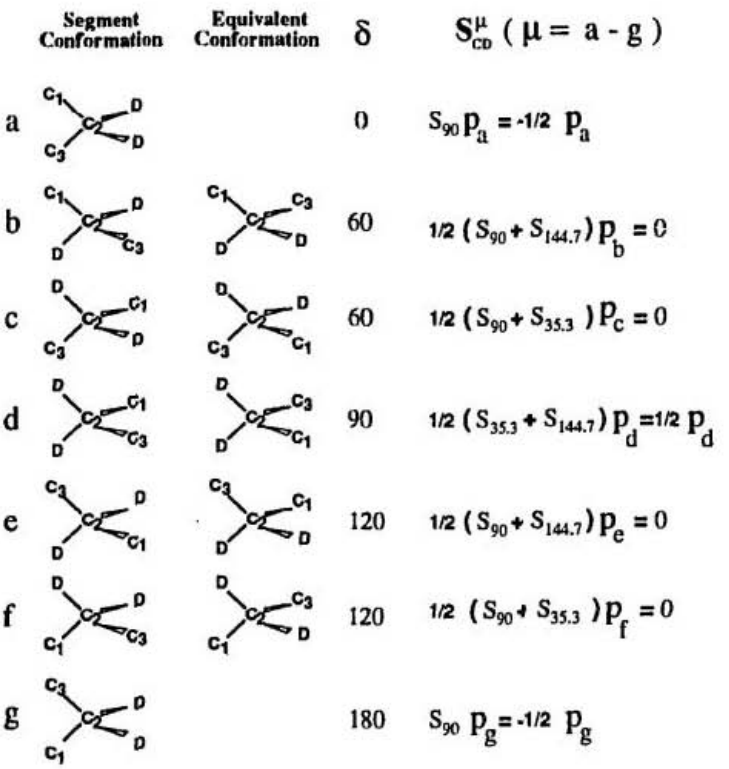

Figure 3.2: The possible segment conformations and the related order parameters. δ is the angle between the bilayer normal and the normal to the plane spanned by the two C-D bonds. The segment order parameter $S_{CD} = \sum_{\mu=a}^{g} S^{\mu}_{CD} = (p_d - p_a - p_g)/2$.

The order parameter for a given segmental conformation, S^{μ}_{CD}, is the average of the order parameters for the two C-D bonds. The order parameter for the chain segment i is then:

$$\langle P_2(\cos\theta_i)\rangle = \sum_{\mu=a}^{g} S^{(i),\mu}_{CD} = \sum_{\mu=a}^{g}\sum_{j=1}^{2} \frac{1}{2} P_2(\cos\theta^{(i)}_{j,\mu}) p^{(i)}_{\mu} = (p^{(i)}_d - p^{(i)}_a - p^{(i)}_g)/2, \qquad (3.8)$$

where j takes account of the two C-D bonds. We also obtain

$$\langle P_1(\cos\delta_i)\rangle = \sum_{\mu=a}^{g} P_1(\cos\delta^{(i)}_{\mu}) p^{(i)}_{\mu} = p^{(i)}_a + \frac{1}{2}(p^{(i)}_b + p^{(i)}_c) - \frac{1}{2}(p^{(i)}_e + p^{(i)}_f) - p^{(i)}_g. \qquad (3.9)$$

At this point we can see that if we identify p_a as $p_{0°}$, $p_b + p_c$ as $p_{60°}$, $p_e + p_f$ as $p_{120°}$, and p_g as $p_{180°}$, Eq. (3.9) reduced to:

$$\langle P_1(\cos\delta_i)\rangle = p^{(i)}_{0°} + \frac{1}{2}p^{(i)}_{60°} - \frac{1}{2}p^{(i)}_{120°} - p^{(i)}_{180°}. \tag{3.10}$$

In the scheme of Schindler and Seelig [15], conformations in which the chain effectively folds back on itself are neglected. These will be referred to as upturning conformations. The neglect of the upturning conformations is equivalent to setting $p_{120°} = p_{180°} = 0$. Eq. (3.4) is then reduced to

$$S^i_{CD} = (p^{(i)}_{90°} - p^{(i)}_{0°})/2,$$

and Eq. (3.6) is reduced to

$$\langle P_1(\cos\delta_i)\rangle = p^{(i)}_{0°} + \frac{1}{2}p^{(i)}_{60°}.$$

Because the total probability for different conformations should equal one,

$$p^{(i)}_{0°} + p^{(i)}_{60°} + p^{(i)}_{90°} = 1,$$

Eq. (3.6) becomes:

$$\langle P_1(\cos\delta_i)\rangle = \frac{1}{2} - S^i_{CD}. \tag{3.11}$$

The chain extension in unit of $\mathring{A}$ is then [15]

$$\langle L\rangle = \sum_{i=2}^{N}\langle l_i\rangle, \tag{3.12}$$

$$= 1.25\left(\frac{N-1}{2} - \sum_{i=2}^{N} S^i_{CD}\right), \tag{3.13}$$

where N is the total number of carbons in the acyl chain under consideration. The formula was further refined by Brown and co-workers [35] to distinguish the difference in the order parameters between the methyl and methylene groups and between the *sn*-1 chain and the *sn*-2 chain to give:

$$\langle L\rangle = 1.25\left(\frac{N-m+1}{2} - \sum_{i=m}^{N-1} S^i_{CD} - 3S^N_{CD}\right), \tag{3.14}$$

where m=2 for *sn*-1 chain and m=3 for *sn*-2 chain. It should be noted that these methods of estimating chain extension from order parameter data neglect the effect of whole molecule reorientation (wobbling) on S_{CD} [10, 59]. In this work, however, the primary concern is with difference in chain extension. The error introduced by neglect of whole molecule reorientation has only a limited effect on the estimates of such differences.

3.2.2 Upturning of the Chain

In the previous discussion of chain extension, chain upturning is neglected, which may result in an overestimate of chain extension. We can not directly obtain upturning probabilities from ^{2}H-NMR spectra but we can estimate the probability that a given C-C bond is perpendicular to the bilayer normal. Considering an acyl chain in a lipid bilayer, the probability that the last C-C bond (methyl rotation axis) is perpendicular to the bilayer normal, $p^m_{90°}$, can be related to the observed methyl order parameter by:

$$p^m_{90°} = 3S^{methyl}_{CD} + 0.5, \tag{3.15}$$

in which it should be noted that the order parameter is generally a negative value. If we assign carbon number along an acyl chain from the α carbon to the methyl, the probabilities for certain sets of conformations on one carbon can be related to those of other sets of conformations on the next. In particular,

$$\underbrace{p_b + p_d + p_f}_{C_n} = \underbrace{p_c + p_d + p_e}_{C_{n+1}}, \tag{3.16}$$

$$\underbrace{p_{bdf} = p_b + p_d + p_f}_{C\text{–}C \text{ bond next to last } C\text{–}C} = \underbrace{p^m_{90°}}_{\text{last } C\text{–}C \text{ bond}}. \tag{3.17}$$

By using $p_a + p_b + p_c + p_d + p_e + p_f + p_g = 1$ (see Fig. 3.2) together with Eq. (3.8) we have

$$p_b + p_c + 2p_d + p_e + p_f = p_{bdf} + p_{cde} = 1 + 2S_{CD}, \tag{3.18}$$

where $p_{cde} = p_c + p_d + p_e$. Using these relations, it is possible to calculate the probability, p_{bdf}, that a given C-C bond in the chain is perpendicular to the bilayer normal from the known order parameter profile. As one can see from Eq. (3.15) to Eq. (3.18) this calculation must start from the methyl end. Chain segments with small order parameters have a relatively large probability of being associated with C-C bonds which are perpendicular to the bilayer normal as we can see from the above formulae. This argument is consistent with theoretical work on the upturning probability for the chains of PC lipids [34].

Obviously, the segments with large values of upturning probability can affect the chain extension calculation of Eq. (3.13). This can be demonstrated by rearranging Eq. (3.9):

$$\langle P_1(\cos\delta_i)\rangle = 2p^{(i)}_{abfg} - \frac{3}{2}p^{(i)}_{bdf} + \frac{1}{2}p^{(i)}_{cde} - 2p^{(i)}_{g} - p^{(i)}_{ef} + 2S^{i}_{CD}, \tag{3.19}$$

$$= (\frac{1}{2} - S^{i}_{CD}) - 2p^{(i)}_{g} - p^{(i)}_{ef}, \tag{3.20}$$

where $p_{ef} = p_e + p_f$ and the terms in the bracket are just the right hand side of Eq. (3.11), in which no account is taken on the upturning probabilities. Thus for a given chain segment i, the decrease of the segmental extension due to the existence of the chain upturning probabilities is:

$$\langle \Delta l_i \rangle = 1.25\mathring{A}(-2p^{(i)}_{g} - p^{(i)}_{ef}). \tag{3.21}$$

This quantity will be discussed in the estimation of chain extension for very long chains in chain mismatched bilayers in Chapter 5.

3.3 Spectral Moments

The nth moment of the ^{2}H-NMR spectrum with normalized lineshape $f(\omega)$ is defined [6][27] by

$$M_n = \int_0^\infty d\omega \omega^n f(\omega), \tag{3.22}$$

where ω=0 corresponds to the Larmor frequency ω_0. Similarily, the nth moment of the quadrupole splittings for the same spectrum in the fluid state with a distribution of quadrupole splittings $P(\delta\nu_Q)$ can be defined as:

$$\langle(\delta\nu_Q)^n\rangle = \int_0^\infty d(\delta\nu_Q)(\delta\nu_Q)^n P(\delta\nu_Q). \tag{3.23}$$

The resulting relationship between the spectral moment and the order parameter is

$$M_n = A_n(2\pi)^n\langle(\delta\nu_Q)^n\rangle = A_n(2\pi\nu_q)^n\langle S_{CD}^n\rangle, \tag{3.24}$$

where [6]

$$A_n = \frac{1}{2^n}\sum_{k=0}^{n}\frac{(-1)^k\binom{n}{k}}{2n-2k+1}3^{n-k} - \frac{1}{\sqrt{3}}[1-(-1)^n]. \tag{3.25}$$

The first moment M_1 has relationship with the mean orientational order parameter given by

$$M_1 = \frac{4\pi}{3\sqrt{3}}\langle\delta\nu_Q\rangle = \frac{4\pi}{3\sqrt{3}}\nu_q\langle S_{CD}\rangle. \tag{3.26}$$

In principle, the moments can provide a complete description of the quadrupole splittings. In this work, the first moment has been used to characterize mean chain order. Plotting moments versus temperature for a membrane can also provide information about membrane phase behavior to some extent [27][40]. The first moment is proportional to the mean orientational order parameter which, in turn is related to chain length extension [see Eq. (3.13)]. The use of this property will be demonstrated in a study of the phase transition behavior for diacyl PC family (see Chapter 4).

3.4 Binary Phase Diagrams - ^{2}H-NMR Spectral Subtraction

The strong distinction between the ^{2}H-NMR spectra for the fluid and gel phases, together with the temperature dependence of the first moment, allows ^{2}H-NMR spectra

to be used to determine phase diagrams for binary lipid mixtures. A preliminary phase diagram can often be derived by inspection and then refined by ^{2}H-NMR spectral subtraction [43][41]. The difference spectroscopy technique for phase diagram determination, as introduced by Vist and Davis and co-workers [43][29], is described below.

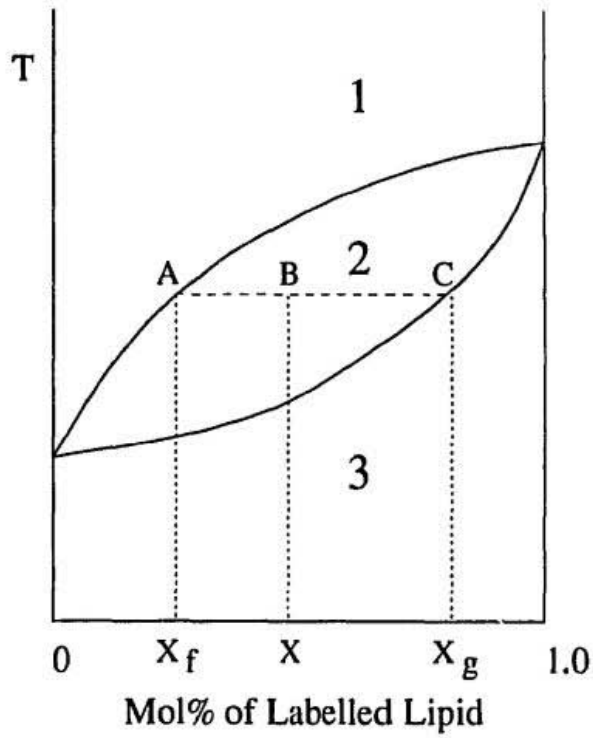

Figure 3.3: A schematic phase diagram for a binary system forming a regular solution. Region 1 corresponds to the fluid phase. Region 2 is the region of gel/fluid two phase coexistence. Region 3 corresponds to the gel phase.

If, within the region of two phase coexistence in the phase diagram (region 2 in Fig. 3.3), there is slow exchange on the ^{2}H-NMR time scale between domains of fluid phase and gel phase, the resulting ^{2}H-NMR spectrum is a simple superposition of gel (g) and fluid (f) state spectra. The spectrum for the binary lipid mixture containing mole fraction x of labelled lipid at a specific temperature T in the two phase coexistence

region (at B in Fig. 3.3) can be expressed mathematically as

$$S(x,T) = f_l S(x_f,T) + (1-f_l)S(x_g,T), \tag{3.27}$$

where S denotes spectrum, x_g and x_f are the concentrations of the labelled lipid at the intersection points of the isothermal tie line and the boundaries of the two-phase coexistence region (C and A in Fig. 3.3 respectively), and f_l is the fraction of the labelled lipid existing in fluid phase. In the above expression the three spectra are all normalized. The fraction f of the sample existing in fluid (include both labelled and unlabelled lipids) is given by the lever rule [3].

$$f = \frac{x_g - x}{x_g - x_f}. \tag{3.28}$$

Because the fractions of f_l and f are related to the mole fraction x of the labelled lipid in the sample, it is possible, by use of the above two equations, to obtain

$$S(x) = \frac{x_f}{x}\left(\frac{x - x_g}{x_f - x_g}\right)S(x_f) + \frac{x_g}{x}\left(\frac{x_f - x}{x_f - x_g}\right)S(x_g). \tag{3.29}$$

It is easy to see from the above equation that by using two spectra on the same tie line within the two phase region, corresponding to the mole fractions of x_A and x_B respectively, the end point spectra $S(x_f)$ or $S(x_g)$ can be identified.

Consider that the mole fractions of labelled lipid for the two measured (and normalized) spectra, S_A and S_B, are x_A and x_B, where $x_A > x_B$. If K is varied such that $S_A - KS_B$ yields an endpoint (gel) spectrum, then the corresponding endpoint composition is given by

$$x_g = \frac{(1-K)x_A x_B}{x_B - Kx_A}. \tag{3.30}$$

[3]The terminology used in the description of binary phase diagrams is presented in many texts dealing with phase equilibrium (see, for example [69]).

If K' is varied such that $S_B - K'S_A$ yields an endpoint (fluid) spectrum, then that endpoint composition is given by

$$x_f = \frac{(1 - K')x_B x_A}{x_A - K'x_B}. \tag{3.31}$$

These expressions ignore differences in transverse relaxation rates between the two phases [41].

An example of a phase diagram obtained in this way appears in Fig. 5.10 in Chapter 5 which shows the phase diagrams for the binary mixtures of glycosphingolipids with SOPC [50][51].

Chapter 4

Experimental Results and Discussion (1): Single Diacyl Phospholipids

4.1 Introduction

In the process of studying the structure and functions of complicated biomembranes, it is often useful to start with simpler model membranes. In studying factors which determine acyl chain order, it is also useful to first consider model membranes containing a single type of acyl chain.

^{2}H-NMR measurements of chain ordering have been done on many single-component phospholipid bilayer systems [6, 9, 12, 13, 17, 27, 35, 70]. One of the interesting things found is that the order parameter profiles and the temperature dependence of first moment, for phospholipids with different chain lengths, look similar for a wide range of systems. Some aspects of chain orientational order for single component bilayers are addressed in this chapter. These include the relationship between order parameter profiles for phospholipids with different chain lengths, the question of which parameters characterize the order parameter profile, and the sensitivity to chain length of the temperature dependence of the first moment (or the mean orientational order parameter) in the vicinity of the liquid crystal to gel transition for phospholipids.

In this project, systematic studies on saturated identical-chain phospholipid bilayer membranes have been carried out. It is found that the order parameter profile is largely determined by the area per lipid molecule or by the order parameter at carbon number 2, and that the order parameter profiles for phospholipid bilayer membranes can be scaled

by the number of carbons in the chain. The dependence of the first moment on chain length in the vicinity of the transition yields the result that the behavior of the bilayer near the transition is largely controlled by the proximity of the spinodal temperature to the transition temperature and that the difference between the spinodal temperature and the transition temperature decreases with decreasing chain length.

The results are reported in the following three sections. In the first section, the chain-length scaling property of orientational order parameter profiles is described. In the second section, the linkage between the scaling property and some related physical parameters is illustrated. In the third section, the chain length dependence of the first moment for the phosphatidylcholine family near the liquid crystal to gel phase transition is discussed.

4.2 Chain-Length Scaling of Orientational Order Parameter Profiles

Lafleur et al. [46] examined smoothed order parameter profiles for the system of 1-palmitoyl-d_{31}-oleoyl-phosphatidylethanoamine (POPE-d_{31}), 1-palmitoyl-d_{31}-oleoyl-phosphatidylcholine (POPC-d_{31}), and POPC-d_{31}:cholesterol. They found that the palmitic acyl chain in the three different bilayers exhibited similar order parameter profiles when the temperatures were selected to give the same mean order (i.e. POPE-d_{31} at 60°C, POPC-d_{31} at 20°C, and POPC-d_{31}:cholesterol 90:10 at 40°C). From these results, they proposed that the order distribution along the lipid acyl chain behaves, to a first approximation, in a universal manner for selected classes of lipids. They concluded that the coupling between the lipid acyl chains results in a correlation length, for changes in orientational order, much greater than one C-C bond length and that local perturbations at specific positions do not produce localized changes in the order parameter, but rather affect the entire order parameter profile.

Table 4.1: Sets of spectra having similar magnitudes of first moment

	DSPC	DPPC	DMPC	DLPC
set 1				
$M_1 \times 10^{-4}(s^{-1})$	3.93	4.00	3.99	3.95
$S_{CD}(2)$	0.202	0.193	0.192	0.193
T ($°C$)	72	62	52	37
set 2				
$M_1 \times 10^{-4}(s^{-1})$	4.36	4.42	4.37	4.29
$S_{CD}(2)$	0.206	0.207	0.206	0.207
T ($°C$)	62	52	42	27
set 3				
$M_1 \times 10^{-4}(s^{-1})$		5.02	4.88	4.76
$S_{CD}(2)$		0.229	0.225	0.225
T ($°C$)	below T_m	42	32	17

We have attempted to extend this observation to systems with the same head group but different chain lengths. The systems are the diacyl phosphatidylcholine (PC) lipids in which the acyl chain lengths are 12, 14, 16, and 18 carbons respectively. We found that the smoothed orientational order parameter profiles for these PC lipids nearly coincide with one another if position along the chain is normalized [49]. The earlier observation that the order parameter profile shape is largely determined by the mean order parameter [46] is thus extended to lipids with different chain lengths. This observation may be called a chain-length scaling property of order parameter profiles. It is illustrated as follows:

Table 4.1 shows three selected sets of data from spectra with each set having a similar magnitude of first moment M_1, or $\langle S_{CD} \rangle$ (see Eq. (3.22) in Chapter 3). The powder spectra, their corresponding de-Paked spectra, and the smoothed order profiles for set 2 in Table 4.1 are shown in Fig. 4.1 and Fig. 4.2, respectively. When the chain position is normalized such that the α deuterons are plotted at position 0 and the terminal methyl deuterons are plotted at position 1 for the four order parameter profiles in Fig. 4.2, the

four scaled order parameter profiles coincide with one another as shown in the middle section of Fig. 4.3. In the same fashion, the scaled order parameter profiles for set 1 and set 3 in Table 4.1 are presented in the left and right sections of Fig. 4.3, respectively.

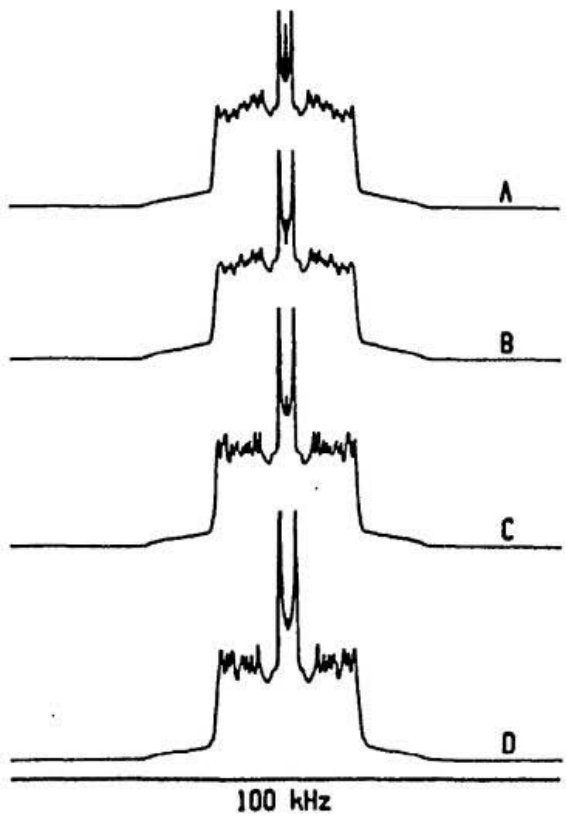

Figure 4.1: ^{2}H-NMR spectra set 2 of table 4.1. (A) DSPC[d_{70}] at 62 °C . (B) DPPC[d_{62}] at 52 °C. (C) DMPC[d_{54}] at 42 °C. (D) DLPC[d_{46}] at 27 °C. These spectra display similar magnitudes of the order parameter in the plateau region of the spectrum.

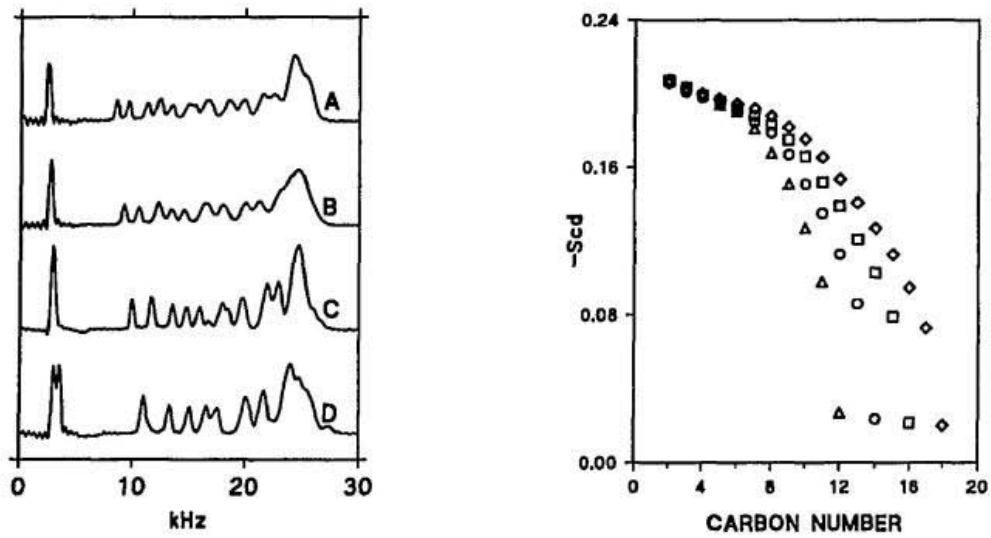

Figure 4.2: De-Paked spectra (left) and their smoothed orientational order parameter profiles (right) for set 2 of table 4.1. (A) DSPC[d_{70}] at 62 °C ($\diamond$); (B) DPPC[d_{62}] at 52 °C ($\square$); (C) DMPC[d_{54}] at 42 °C ($\bigcirc$); and (D) DLPC[d_{46}] at 27 °C ($\triangle$).

4.3 Scaling Property and Mean Molecular Field Theory

The observed scaling property suggests that for a given $\langle S_{CD} \rangle$, the number of carbons over which orientational order decays by a given amount (the correlation length) is proportional to the total number of carbons, N, in chains of the diacyl phospholipids. A number of theories have been used to obtain order parameter profiles [33,70-74] . In general, these theories do not yield a simple relationship between chain length and the shape of the order parameter profile. It can be shown, however, that such a relationship may be implicit in Marcelja's mean field theory [15][71].

Consider the length of the plateau. It should be, in a first approximation, proportional to the number of the segments in the *trans* conformation, $\langle n_{tr} \rangle$. The observed scaling

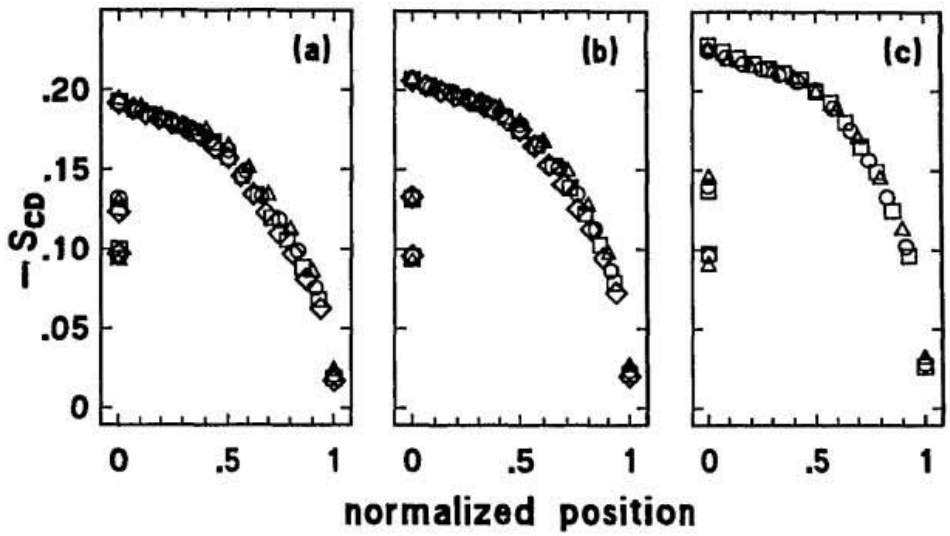

Figure 4.3: Smoothed order parameter profiles for sets of spectra chosen to have similar magnitudes of the order parameter in the plateau region. Chain positions are normalized. Order parameters for *sn*-1 and *sn*-2 chain deuterons (except at the α position) are averaged. (a) Spectra belonging to set 1 of table 4.1. (b) Spectra belonging to set 2 in table 4.1. (c) Spectra belonging to set 3 of table 4.1. For each set of profiles, the symbols indicate (◇) DSPC, (□) DPPC, (○) DMPC, and (△) DLPC.

thus suggests that for a given value of the average order parameter $\langle S_{CD} \rangle$, the ratio $\langle n_{tr}/N \rangle$ should be common.

In mean field theory, the magnitude of the order parameters and the shape of the order parameter profiles can be sensitive to changes in both the lateral pressure and the molecular field Φ in bilayer lipids [33][59]. The molecular field, Φ, describes the strength of the dispersive interaction between the lipid molecules in bilayer. For a given value of lateral pressure, the increase of Φ will increase the chain ordering or reduce the cross

sectional area of the lipid molecule in the lipid bilayer. Similarly, for a given value of Φ, an increase of the lateral pressure will increase the chain ordering, resulting in a decrease of the cross sectional area of the lipid molecule in the bilayer [59].

According to Marcelja [71], the energy of a hydrocarbon chain with the configuration i in a bilayer is given by

$$E^{(i)} = E^{(i)}_{int} + E^{(i)}_{disp} + \pi_c A^{(i)}. \tag{4.1}$$

The first term, E_{int}, represents the *intramolecular* energy of the chain. The second term, E_{disp}, describes the dispersive or Van der Waals interaction between neighboring hydrocarbon chains. The third term, $\pi_c A$, is due to lateral pressure on each chain. π_c is the lateral chain pressure; A is the average cross sectional area of the chain. The *intermolecular* interaction energy has the form

$$E^{(i)}_{disp} = -\Phi(n^{(i)}_{tr}/N)\sum_{j=1}^{N}(1/2)(3\cos^2\delta^{(i)}_j - 1), \tag{4.2}$$

where δ_j denotes the angle between the bilayer normal and the direction of the jth chain segment, which is defined as the normal to the plane spanned by two C-H bond vectors. n_{tr} is the number of segments in the *trans* conformation in the chain. The statistical weight $w^{(i)}$ of the configuration i is:

$$w^{(i)} = exp(-E^{(i)}/RT), \tag{4.3}$$

where R is the universal gas constant and T is temperature. The partition function Z is the summation over all configurations i:

$$Z = \sum_i exp(-E^{(i)}/RT). \tag{4.4}$$

The molecular field is then defined as follows [15]:

$$\Phi = (V/N)\sum_i[(n^{(i)}_{tr}/N)\sum_{j=1}^{N}(1/2)(3\cos^2\delta^{(i)}_j - 1)w^{(i)}]/Z, \tag{4.5}$$

where V is a coupling constant, which is roughly the melting energy per CH_2 group of the appropriate crystalline hydrocarbon [2][15]. This constant models the strength of the van der Waals attraction between the chains. $n_{tr}^{(i)}/N$ is believed to reflect the dependence of the interaction between two chains on the distance between the chains [33][76]. Notice here that the interaction between the chains appears in a scaled form.

The jth segment order parameter, $S_{mol,j}$ is defined [12][15] as

$$S_{mol,j} = (1/2)(3\langle\cos^2\delta_j\rangle - 1), \tag{4.6}$$

and is related to the order parameter for the C-D bond in jth segment, $S_{CD,j}$ as

$$S_{mol,j} \simeq -2S_{CD,j}. \tag{4.7}$$

The molecular field can then be re-written as

$$\begin{aligned}\Phi &= (V/N)\sum_{j=1}^{N}\langle n_{tr}/N\rangle\langle S_{mol,j}\rangle \\ &= -2V\sum_{j=1}^{N}\langle n_{tr}/N\rangle\langle S_{CD,j}/N\rangle \\ &= -2V\langle n_{tr}/N\rangle\langle S_{CD}\rangle. \end{aligned}\tag{4.8}$$

This expression tells us that Marcelja's mean field, Φ, is a function only of the product of $\langle n_{tr}/N\rangle$ and $\langle S_{CD}\rangle$, which are temperature dependent. In other words, different bilayers with the same $\langle n_{tr}/N\rangle$ and $\langle S_{CD}\rangle$ should share a common Φ. In particular, the profiles which can be superimposed by scaling in Fig. 4.3 would share the same values of Φ.

In Fig. 4.2, the shapes of the scaled order parameter profiles are primarily determined by the $S_{CD}(2)$ in the smoothed order parameter profile. These spectra also correspond to nearly the same magnitude of the first moment M_1 (Table 4.1), or the same average order parameter $\langle S_{CD}\rangle$. Chain ordering, reflected by the parameter $S_{CD}(2)$ or $\langle S_{CD}\rangle$, is related to area per lipid. Boden et al. [36][77] presented an empirical expression which

relates $\langle S_{CD} \rangle$ to the average area per chain a_{ch} projected onto the bilayer/water interface:

$$-\langle S_{CD} \rangle = a + b/a_{ch}, \tag{4.9}$$

where a and b are constants. A similar $\langle S_{CD} \rangle$ versus a_{ch} dependence can be derived from the rigid-rod model of Seelig and Seelig [13] for a bilayer lipid [36]. The theory of De Young and Dill [78] predicts that the mean area per molecule, A, is related to the order parameter at the plateau region, say, that of carbon number 2, $S_{CD}(2)$:

$$A = \frac{3A_0}{4S_{CD}(2) + 1}, \tag{4.10}$$

where A_0 is the area per phospholipid molecule in an all-trans conformation state. In general, $\langle S_{CD} \rangle$ and $S_{CD}(2)$ are correlated, so that the shape of the scaled order parameter profile can be taken to be determined by either $\langle S_{CD} \rangle$ or $S_{CD}(2)$. Our experimental data show that the difference between the values of $S_{CD}(2)$ and $\langle S_{CD} \rangle$ is a constant ($= 0.05$) for the members of the PC family over the range of temperatures examined in this work (from just above their phase transition temperatures up to 72 $°C$).

These results suggest that diacyl phospholipids whose order parameter profiles can be scaled have the same mean field, Φ, and the same area per lipid.

It may be that the observed scaling property of order parameter profiles does not hold in binary mixtures. Fig. 4.4 shows sets of smoothed order parameter profiles for mixtures of DSPC[d_{70}] in DMPC, 18:0 GalCer[d_{35}] in SOPC, and 24:0 GalCer[d_{47}] in SOPC, respectively. These profiles correspond to sets of spectra having similar values of the first moment which are shown in Table 4.2. As can be seen, scaling in these systems is not as precise as that in diacyl phospholipids. The shape of the order parameter profile within a given kind of mixture is apparently concentration dependent, although still controlled mainly by the mean orientational order parameter. This observation suggests that scaling may be confined to homogeneous lipid bilayers.

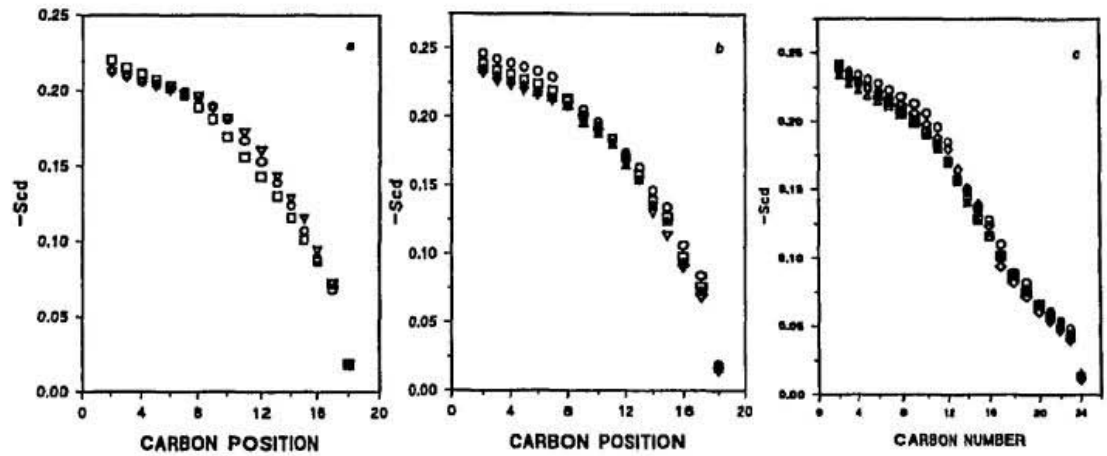

Figure 4.4: Smoothed order parameter profiles for mixtures of spectra chosen to have similar magnitudes of first moment M_1 (see to table 4.2). (a) Spectra belonging to the mixtures of DMPC/DSPC[d_{70}] with DSPC concentrations of 25.2 mol% (○), 50 mol% (□), and 74.8 mol% (△). Order parameters for *sn*-1 and *sn*-2 chain deuterons are averaged. (b) Spectra belonging to the mixtures of 18:0 GalCer/SOPC with 18:0 GalCer concentrations of 10 mol% (○), 20 mol% (□), 29 mol% (△), and 39.4 mol% (▽). (c) Spectra belonging to the mixtures of 24:0 GalCer/SOPC with 24:0 GalCer concentrations of 10.1 mol% (○), 23.9 mol% (□), 34.7 mol% (△), and 53 mol% (▽).

We may thus conclude that diacyl phospholipids with the same scaled order profile have the same mean area per molecule A; the same fraction of trans bond, $\langle n_{tr}/N \rangle$; the same mean value of order parameter $\langle S_{CD} \rangle$; and the same mean molecular field, Φ, in the sense of Marcelja's model. The parameters A, $S_{CD}(2)$, $\langle S_{CD} \rangle$, and $\langle n_{tr}/N \rangle$ may thus be equivalent in terms of describing the chain ordering of the corresponding set of phospholipid bilayers.

Table 4.2: Sets of spectra having similar magnitudes of first moment in binary mixtures

DSPC[d_{70}]/DMPC				
mole% of DSPC[d_{70}]	25.2	50	74.8	
$M_1 x 10^{-4}(s^{-1})$	4.35	4.41	4.47	
T ($°C$)	42	50	54	
18:0 GalCer[d_{35}]/SOPC				
mole% of 18:0 GalCer[d_{35}]	10	20	29	39.4
$M_1 x 10^{-4}(s^{-1})$	5.09	5.02	4.86	4.90
T ($°C$)	40	52	61	67
24:0 GalCer[d_{35}]/SOPC				
mole% of 24:0 GalCer[d_{35}]	10.1	24	30	53
$M_1 x 10^{-4}(s^{-1})$	4.24	4.26	4.21	4.29
T ($°C$)	40	55	64	73

4.4 Phase Transition Behavior for the Diacyl PC Family

The temperature dependence of the first spectral moment M_1 for DLPC, DMPC, DPPC, and DSPC is shown in Fig. 4.5. It can be seen that chain length affects both the jump in M_1 at the main transition and the slope of the M_1 versus T at the transition.

The jump in M_1 indicates the chain melting transition of the PC lipid bilayers [27]. This melting transition has been identified as a first order transition by using mean field theory [71][79], Landau-de Gennes theory [79-84] , and Monte Carlo calculation [85-87]. Many properties of lipid membranes near this phase transition, such as density, lateral compressibility, specific heat and membrane permeability, have been studied theoretically. The work described in this section was an attempt to model the temperature dependence of M_1 near the transition by using a Landau expansion of the free energy.

It is found that the phase behavior of a bilayer near the transition can indeed be modeled in terms of a Landau expansion of the free energy involving a small number of phenomenological parameters. It is also shown that the phase behavior at the transition

is largely controlled by the close proximity of the spinodal temperature to the transition temperature. Unfortunately, the critical temperature, T_c, cannot be determined in this model without making a further assumption. Modeling of the transition by use of Landau theory will be described in section 4.4.1. The analysis of M_1 data using this model is contained in section 4.4.2. Finally, a short summary of the chain-length dependence of lipid bilayer properties near the liquid crystal to gel phase transition is presented in section 4.4.3.

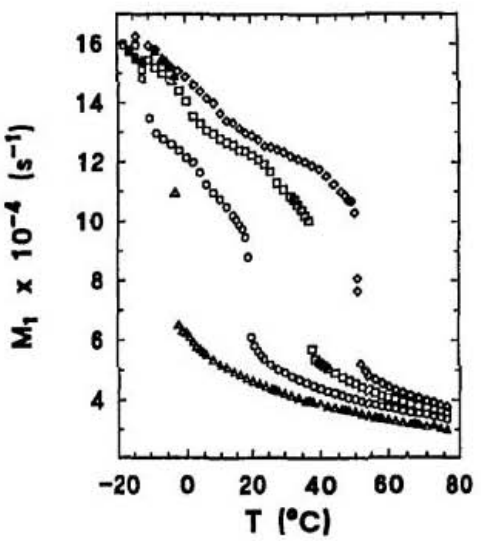

Figure 4.5: First moment M_1 versus T for (△) DLPC[d_{46}], (○) DMPC[d_{54}], (□) DPPC[d_{62}], (◇) DSPC[d_{70}].

4.4.1 Modeling of the Transition

A number of authors have used Landau expansions of the free energy to model lipid bilayer behavior at the transition [80-84] .

The form of the phenomenological free energy we have used is [37]:

$$G = G_0[\frac{s^4}{4} + \alpha(T - T_c)\frac{s^2}{2} + \beta(T_m - T)s], \tag{4.11}$$

where $\alpha(> 0)$ and $\beta(> 0)$ are two parameters, T_m and T_c are the transition temperature and the critical temperature, respectively. s is the order parameter, defined as

$$s = \frac{\langle l\rangle^{-1} - \langle l\rangle_c^{-1}}{\langle l\rangle_c^{-1}}, \tag{4.12}$$

where $\langle l\rangle^{-1}$ and $\langle l\rangle_c^{-1}$ are the reciprocals of the mean extension per acyl chain segment along the bilayer normal at a given temperature and at the critical point respectively. In practice, $\langle l\rangle_c$ is identified as the mean extension at the midpoint of the transition. The mean extension of the acyl chain [15], is obtained from the NMR spectrum through

$$\langle l\rangle = 1.25\left[\frac{1}{2} + \frac{\sqrt{3}}{\pi\sqrt{7}}M_1\right]. \tag{4.13}$$

For DMPC, DPPC, and DSPC, the bilayer volume changes by $\sim 0.07\%$ per degree away from the transition and by ~ 0.04 at the transition [7][89]. If the bilayer volume is treated as a constant, $\langle l\rangle^{-1}$ may be used as an approximation for the area per lipid. Using this argument, the temperature dependence of M_1 can be related to the temperature dependence of area per lipid in the vicinity of the chain melting transition.

Fig. 4.6 shows the dependence of the inverse chain extension $\langle l\rangle^{-1}$ on temperature T. It should be noted that Eq.(4.13) applies to the liquid crystalline state [90]. If, however, it is extended into the gel phase, the ratio for DPPC of $\langle l\rangle^{-1}$ at 20 °C to its value at 50 °C is about 0.72. This agrees well with results from X-ray (about 0.75) [91][92], and neutron diffraction measurements (about 0.72) [93]. Moreover, both experimental and

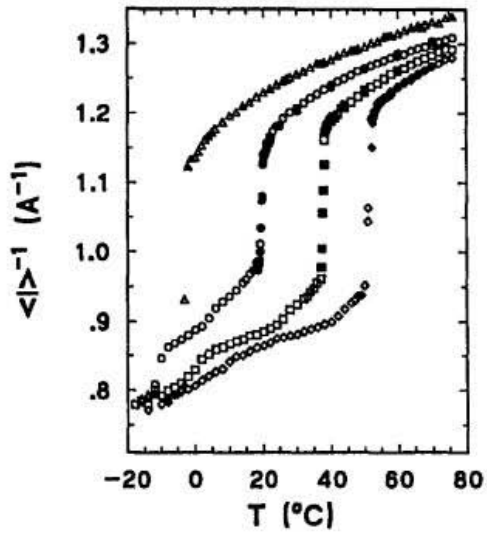

Figure 4.6: Inverse chain extension $\langle l \rangle^{-1}$ versus T. $\langle l \rangle^{-1}$ is obtained from M_1 using the relationship given in Eq. (4.13). (△) DLPC[d_{46}], (○) DMPC[d_{54}], (□) DPPC[d_{62}], (◇) DSPC[d_{70}]. The open symbols are obtained from the data presented in Fig. 4.5. The solid symbols are additional data sets collected from the same samples or samples prepared in the same way from the same stock material in order to better localize the transition.

theoretical work shows that the rotational freedom of the fatty acid chains, which is a characteristic of the liquid crystalline state, first appears at temperatures significantly below that of the main transition [85-87,93] . This suggests that the interpretation of $\langle l \rangle$ and $\langle l \rangle^{-1}$ at temperatures just below the transition temperature is still at least partially meaningful.

The free energy G given by Eq. (4.11) is illustrated schematically by Fig. 4.7. We note that for $T < T_c$ the free energy has two minima, the positions of which may be

determined from the solution of the equation of state [1]

$$\begin{aligned} \frac{dG}{ds} &= G_0[s^3 + \alpha(T - T_c)s + \beta(T_m - T)] \\ &= 0. \end{aligned} \tag{4.14}$$

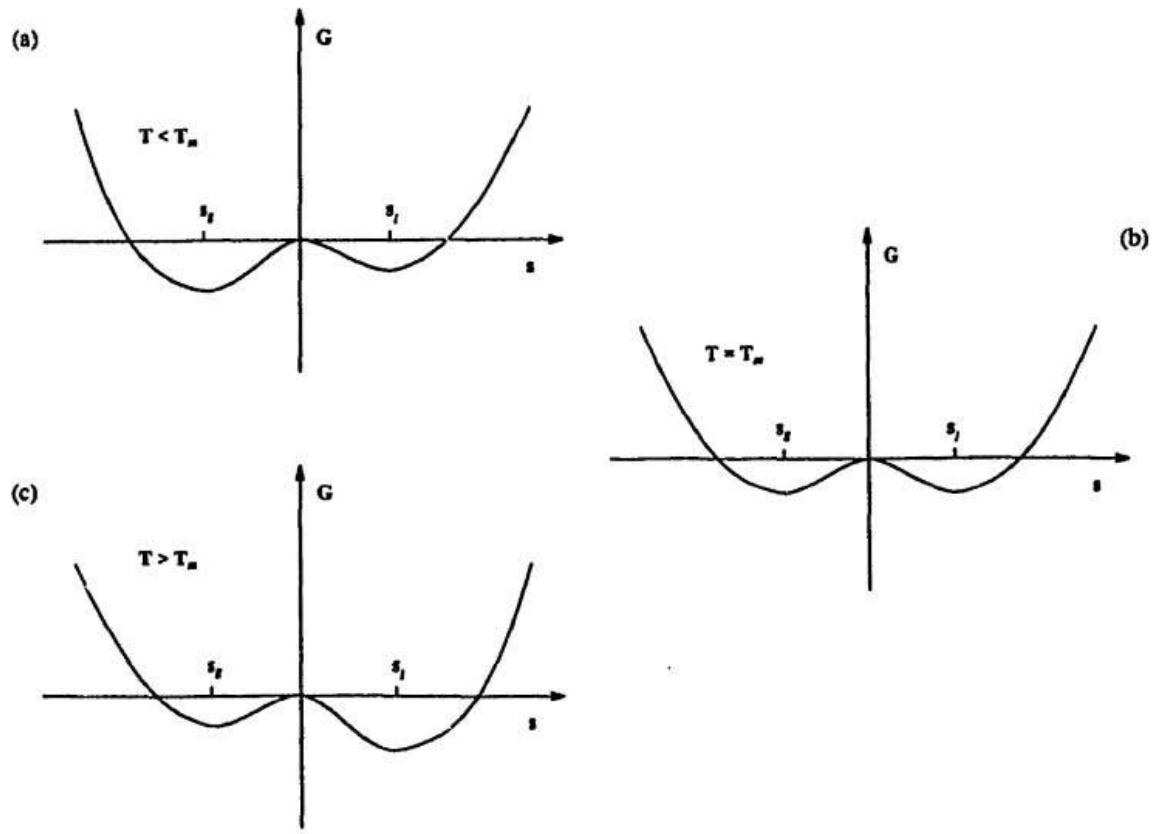

Figure 4.7: A schematic representation of the free energy versus order parameter relationship given by Eq. (4.17) for (a) $T < T_m$, (b) $T = T_m$, and (c) $T > T_m$.

For $T < T_m$ the thermodynamically stable phase, corresponding to the lower free energy

[1]The description of a phase transition in terms of the coexistence curve, an equation of state, and spinodal points at which the system becomes unstable can be found in a number of thermodynamics texts (for example, see [95]).

of the two minima, is the gel phase corresponding to $s < 0$. For $T > T_m$ the thermodynamically stable phase, corresponding to the lower free energy of the two minima, is the liquid crystalline phase corresponding to $s > 0$. For $T = T_m$ the two minima of the free energy have the same value, indicating that at T_m the liquid crystal and the gel phase are both thermodynamically stable. From this we identify T_m as the transition temperature. At $T = T_m$, the two solutions to Eq. (4.14), corresponding to the minima in G are obtained as:

$$s_l = \sqrt{\alpha(T_c - T_m)}, \tag{4.15}$$

$$s_g = -\sqrt{\alpha(T_c - T_m)}, \tag{4.16}$$

where s_l and s_g denote the values of the order parameter at the transition temperature in the liquid crystal and the gel phase respectively. The change in the order parameter s at the phase transition is given by

$$\begin{aligned} \Delta &= s_l - s_g \\ &= 2\sqrt{\alpha(T_c - T_m)}. \end{aligned} \tag{4.17}$$

It is helpful to replace the Landau parameter α in the equation of state by Eq. (4.17). Eq. (4.14) is then rearranged to give

$$s^3 + \frac{\Delta^2}{4}\left(\frac{T - T_c}{T_c - T_m}\right)s + \beta(T_m - T) = 0. \tag{4.18}$$

The solution to Eq. (4.18) is plotted schematically in Fig. 4.8. Any point on the line for the equation of state in the region of $T \geq T_m$ in Fig. 4.8, represents a stable state in the liquid crystalline phase. Similarily, any point on the line for the equation of state in the

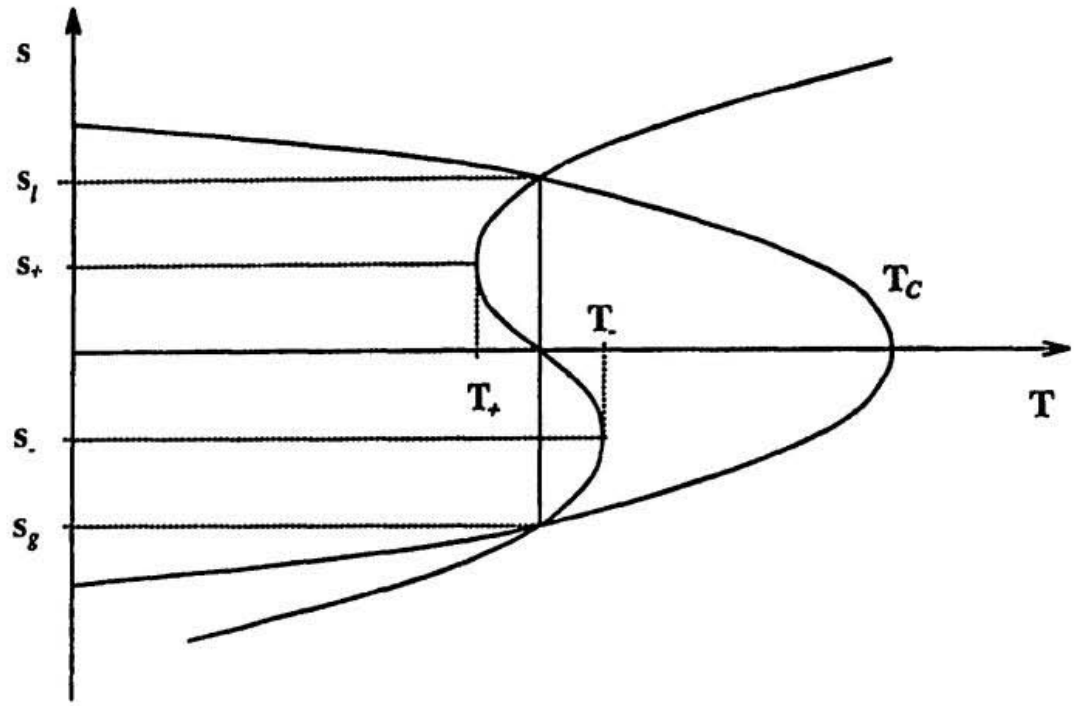

Figure 4.8: A schematic illustration of order parameter versus temperature as given by Eq. (4.14). The points $(T_\pm, s_\pm)$ are spinodals. The coexistence curve crosses $s = 0$ at the critical temperature T_c. The transition occurs at the coexistence temperature T_m (unlabeled) which is indicated by the solid vertical line between T_+ and T_-.

region of $T \leq T_m$ represents a stable ordered state, the gel phase. Spinodals are located at $s_\pm$ and $T_\pm$, and satisfy the relation,

$$\begin{aligned} \frac{d^2G}{ds^2} &= G_0\left[3s_\pm^2 + \frac{\Delta^2}{4}\left(\frac{T_\pm - T_c}{T_c - T_m}\right)\right] \\ &= 0. \end{aligned} \tag{4.19}$$

From Eqs. (4.18) and (4.19) we obtain

$$\left(\frac{s_\pm}{\Delta}\right)^2 = \frac{1}{12}\left(\frac{T_c - T_\pm}{T_c - T_m}\right), \tag{4.20}$$

and

$$s_\pm^3 = \frac{\beta}{2}(T_m - T_\pm). \tag{4.21}$$

If we assume that

$$|T_{\ddagger} - T_m| \ll |T_c - T_m|, \tag{4.22}$$

then the value of the order parameter at the spinodal may be approximated as

$$s_{\pm} \approx \pm \frac{\Delta}{\sqrt{12}}, \tag{4.23}$$

while the spinodal temperatures $T_{\pm}$ would be expressed as

$$T_{\pm} \approx T_m \mp \frac{\Delta^3}{12\sqrt{3}\beta}. \tag{4.24}$$

4.4.2 Analysis of Data

By making use of Eqs. (4.21), (4.22), and (4.23) discarding high order terms, and introducing the quantity

$$\delta = s - s_+, \tag{4.25}$$

Eq. (4.18) can be recast into the following form

$$T = T_+ + \frac{(T_m - T_+)}{2}\left[3\left(\frac{\delta}{s_+}\right)^2 + \left(\frac{\delta}{s_+}\right)^3\right]. \tag{4.26}$$

Eq. (4.26) shows a linear relationship between T and $[3(\frac{\delta}{s_+})^2 + (\frac{\delta}{s_+})^3]$ and provides an opportunity to check the applicability of this model to the transition. The symmetry of the model suggests that $\langle l \rangle_c^{-1}$ should be the value of $\langle l \rangle^{-1}$ at the midpoint of the transition. In practice, this parameter is chosen so that data within a few degrees of the transition are symmetric about the midpoint of the transition. This parameter, however, could not be estimated for DLPC since its transition is not from liquid crystal to gel but to a crystal phase. No fitting was attempted for this lipid. Using the chosen value for $\langle l \rangle_c^{-1}$, the model order parameter s is then determined from $\langle l \rangle^{-1}$ for the liquid crystalline phase according to Eq. (4.12). To plot T versus $[3(\frac{\delta}{s_+})^2 + (\frac{\delta}{s_+})^3]$ an initial value for s_+

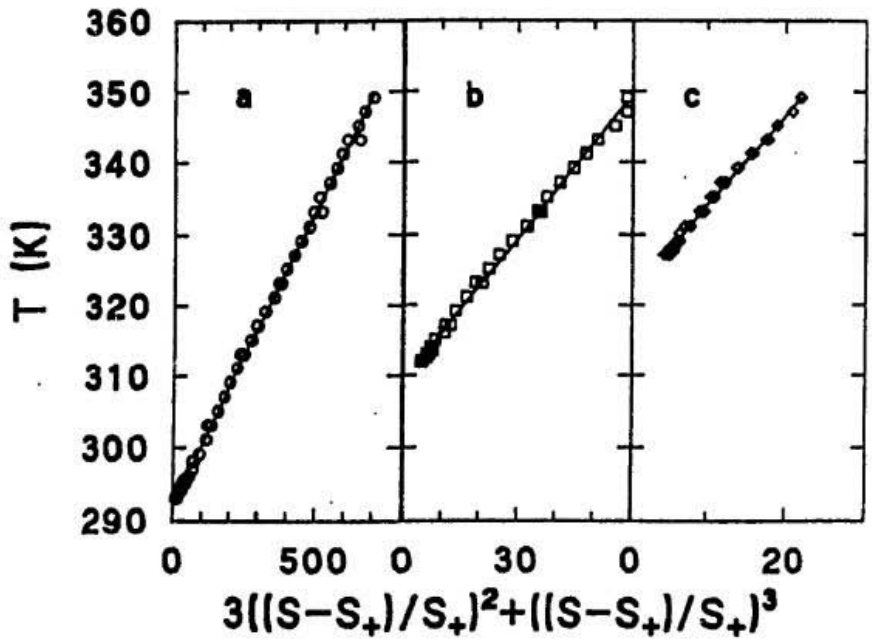

Figure 4.9: Plots of T versus $3[(s - s_+/s_+]^2 + [(s - s_+)/s_+]^3$ in the liquid crystal phase for (a) DMPC[d_{54}] using $\langle l \rangle_+^{-1} = 1.092$ $\AA^{-1}$, (b) DPPC[d_{62}] using $\langle l \rangle_+^{-1} = 1.123$ $\AA^{-1}$, and (c) DSPC[d_{70}] using $\langle l \rangle_+^{-1} = 1.141$ $\AA^{-1}$. The intercept gives the spinodal temperature T_+ and the slope gives $(T_m - T_+)/2$. Values of $s_+ = (\langle l \rangle_+^{-1} - \langle l \rangle_c^{-1})\ /\langle l \rangle_c^{-1}$ were adjusted to obtain consistent values of T_+ from the slope and the intercept. Spectra which contained any gel component were omitted from this analysis.

was chosen by use of Eq. (4.23). The value for s_+ was then adjusted until the slope and intercept of the plot gave the same value for T_+ as required by Eq. (4.26). The final plots for DMPC, DPPC and DSPC are shown in Fig. 4.9. The parameters associated with this fitting are shown in Table 4.3.

The fitting parameters s_+, T_+, and $\langle l \rangle_c^{-1}$, can be used to calculate $\langle l \rangle^{-1}$ versus T for DMPC, DPPC and DSPC by using Eqs. (4.25), (4.26), and Eq. (4.12) as shown in Fig. 4.10. There we see that the model fits the experimental data very well even well below the transition temperature. This suggests that the relationship between mean

Table 4.3: Fitting parameters

	DMPC	DPPC	DSPC
T_m (K)	292.5	310.65	324.15
$\langle l \rangle_c^{-1}$ $(\AA^{-1})$	1.063	1.068	1.074
$\langle l \rangle_+^{-1}$ $(\AA^{-1})$	1.092	1.123	1.141
T_+ (K)	292.3	309.3	321.7
$(T_m - T_+)$ (K)	0.2	1.3	2.4
β x 10^4	2.03	2.10	2.02
$\Delta\langle l \rangle^{-1}$ $(\AA^{-1})$	0.100	0.189	0.232

orientational order and area per lipid retains some validity below the transition temperature. It has been shown [37] that assuming a more restricted temperature dependence of the Landau coefficients yields the relationship $\alpha = \beta$. If this assumption is used, the data in Table 4.3 yield values for $(T_c - T_m)$ of 11 °, 37 °, and 58 ° for DMPC, DPPC and DSPC, respectively. These values are consistent with the assumption described by Eq. (4.22). The value of $(T_c - T_m)$ for DPPC obtained by use of this assumption is roughly comparable with the previous estimate of 39 ° by Doniach [79].

4.4.3 Summary

In this study we have used an explicit form of the Landau free energy. This work provides insight into the nature of the gel/liquid transition and shows that M_1 versus T can be understood in terms of a simple model for phase behavour. One very interesting observation is that the parameter β is found to be independent of chain length within the group of lipids examined. The value $\langle l \rangle_c^{-1}$ is found to depend only weakly on chain length. The separation between the spinodal temperature and the transition temperature $(T_m - T_+)$ decreases with decreasing chain length. This result accounts for the increasing value of the slope with decreasing chain length at the transition. That both the temperature

difference, $T_m - T_+$, and the discontinuity in the area at the transition, $\Delta\langle l\rangle^{-1}$ (or in the first moment M_1) , decrease with decreasing chain length suggests that the latent heat decreases with decreasing chain length and that the system is approaching a critical point as the chain length is reduced.

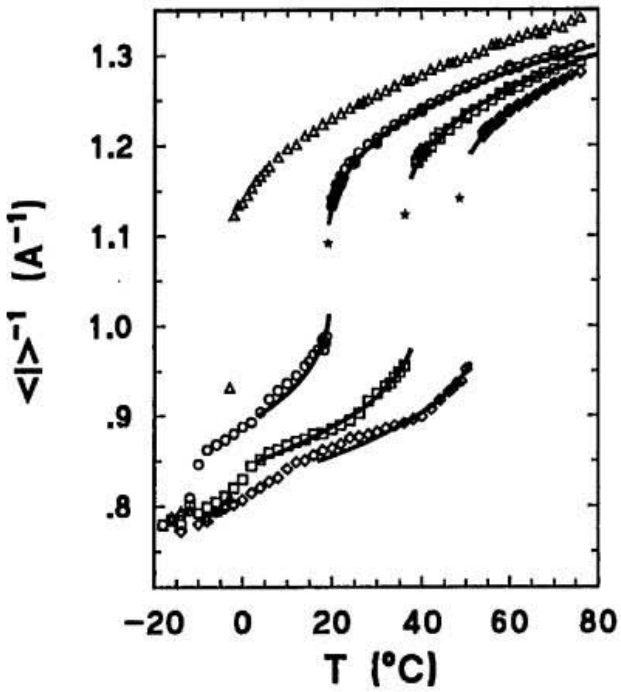

Figure 4.10: Inverse chain extension $\langle l\rangle^{-1}$ versus T. $\langle l\rangle^{-1}$ is obtained from M_1 using the relationship given in Eq. (4.13). (△) DLPC[d_{46}], (○) DMPC[d_{54}], (□) DPPC[d_{62}], (◇) DSPC[d_{70}]. Different samples of a given lipid are not distinguished. Spectra in which gel and liquid crystal components were found to coexist have been omitted for the purposes of clarity near the transition. The solid lines are obtained using parameters found with the procedure illustrated in Fig. 4.9 and listed in Table 4.3. Solid stars mark the spinodal points obtained in this way.

Chapter 5

Experimental Results and Discussion (2): Chain Mismatched Systems

5.1 Introduction

Chain length mismatch has an important influence on phase behaviour and molecular organization in mixed chain systems and in binary systems in which the two kinds of molecules have different chain lengths. Research on the structure and the properties of these systems has been reviewed by Huang and Mason (1986) [96], and Slater and Huang (1988) [97]. One important observation is the occurrence of chain interdigitation in the ordered phase in some of these systems. Interdigitation refers to a situation where chains from opposite monolayers in a lipid bilayer intercalate with each other to some extent.

It is well known that binary mixtures of phospholipids with fatty acids differing significantly in length tend to phase separate and that this effect depends on the difference in length. For binary mixtures of phosphatidylcholines, the empirical rule is that the two components are completely or partially miscible in the gel phase when the absolute difference in the transition temperature (ΔT_m) of the pure components is less than 33 °C, and are immiscible in the gel phase over a large compositional range when the ΔT_m is greater than 33 °C. This general behavior appears to hold irrespective of whether the acyl chains are saturated or unsaturated [98].

For the mixed-chain PC lipid membranes and their binary mixtures, the above mentioned chain mismatch effects have been studied using X-ray diffraction and electron microscopy [99-101] , DSC [102], and both DSC and Raman spectroscopy [96]. The acyl

chain length asymmetry for lipid molecules with unlike chains is defined as $\Delta C/C_L$ [101]. Here

$$\Delta C = \mid n_1 - n_2 + 1.5 \mid$$

is the effective chain-length difference and n_1 and n_2 are the number of carbons in the chains at the *sn*-1 and *sn*-2 position of the glycerol backbone. C_L is the effective length of the longer of the two chains and is defined as

$$C_L = \begin{cases} n_1 - 1, & \text{if } sn\text{-1 is the longer chain;} \\ n_2 - 2.5, & \text{if } sn\text{-2 is the longer chain.} \end{cases}$$

It has been observed that interdigitation will occur in the gel phase if the chain inequivalence parameter $\Delta C/C_L$ has a value close to 0.5 [97]. For lipid bilayers of C(18)C(10)PC ($\Delta C/C_L$=0.527), and C(22)C(12)PC ($\Delta C/C_L$ =0.548), the chains are reported to be interdigitated in both their gel and L_α phases [101, 102, 103]. A binary mixture which has a component with $\Delta C/C_L$ close to 0.5 would have lateral gel phase separation [102][104]. On the other hand, a binary mixture with its two components having similar acyl chain length asymmetry, like C(10)C(22)PC in C(22)C(12)PC or C(18)C(11:1)PC (which contains a double bond at the *sn*-2 chain terminus) in C(18)C(10)PC still exhibits complete miscibility both in the gel and the liquid crystalline phase. This example suggests that the gel phase separation is determined by the mode of chain packing rather than chain mismatch [97].

Another class of system involves binary mixtures of lipids in which only one member has mixed chain lengths (i.e., in which the *sn*−1 and *sn*−2 acyl chains are mismatched). The effective length difference between the two chains in glycosphingolipids can vary by up to six carbons. One interesting observation regarding glycosphingolipids is that the length of their single acyl chain may modulate their membrane receptor properties and intermolecular interactions. As result, there has recently been considerable interest in the

study of binary mixtures containing sphingomyelin and phospholipid [34,40,48,105-117] . It is generally accepted that the long acyl chains are accommodated by interdigitation in the gel phase, but only a few studies have discussed interdigitation in the liquid crystalline phase [109, 111, 113].

In this work we have examined the effect of chain mismatch on the structural properties of bilayer mixtures in two steps. In the first step, single component glycolipid (GalCer) bilayers and mixed bilayers containing glycolipid and phospholipid were used. They were all chain mismatched systems with the long glycolipid acyl chain deuterated. In the second step, mixtures of DMPC/DSPC with either of the two chains deuterated were used to further clarify the mutual interaction between the two components, the accommodation of a long chain in a short chain environment, and the interpretation of ^{2}H-NMR spectra in chain mismatched environments. The acyl chain length of DSPC exceeds that of DMPC by four methylene groups.

Mixtures containing GalCer are of considerable biological interest. An additional reason for using GalCer in this work is the relative insensitivity of its melting transition temperature to acyl chain substitution. 18:0 GalCer and 24:0 GalCer undergo the fluid/gel transition within a few degrees of each other. Hence the results seen can be attributed more directly to consequences of the chain length difference rather than to differences in transition temperature. SOPC has been used as the phospholipid component of the mixture to avoid interference from the ice/water phase transition.

^{2}H-NMR was used to examine the single component bilayer 24:0[d_{47}] GalCer, mixtures of 18:0[d_{35}] GalCer/SOPC, 24:0[d_{47}] GalCer/SOPC, DMPC[d_{54}] /DSPC, and DSPC[d_{70}] /DMPC [50-52]. 24:0[d_7] GalCer, specifically deuterated in the methyl group and the two methylene groups immediately above the methyl, was also examined to confirm that the order parameters on the 24-carbon chain do decrease monotonically toward the methyl end. The "excess segments" of the long chain were generally found to be

very disordered. Their orientational order parameters form a second plateau at the low order end of the order parameter profile. The effect of cholesterol on chain ordering in a chain-mismatched system was examined by comparing results in the ternary systems 18:0 GalCer/SOPC/Cholesterol and 24:0 GalCer/SOPC/Cholesterol. The second plateau in the orientational order parameter profile for the long chain in these system was found to be little affected by the presence of cholesterol.

In the following sections, the ^{2}H-NMR experimental results for GalCer and GalCer/SOPC mixtures will be discussed first. The phase diagrams and the order parameter profiles for 18:0 GalCer/SOPC and 24:0 GalCer/SOPC will be presented and compared. The next section contains the discussion of ^{2}H-NMR experimental results for the systems of DMPC[d_{54}]/DSPC and DMPC/DSPC[d_{70}]. These results include relative chain extension of the two components and the resulting bilayer thickness. The following section deals with the influence on chain ordering of cholesterol present in the GalCer/SOPC mixtures. The final section is devoted to the discussion of the chain arrangement in the bilayer middle region in chain mismatched systems including DMPC/DSPC, 24:0 GalCer/SOPC, and 24:0 GalCer/SOPC/cholesterol.

5.2 GalCer and GalCer/SOPC Mixtures

5.2.1 N-lignoceroylgalactosylceramide (24:0 GalCer)

Glycosphingolipids have a single acyl chain, attached by an amide linkage to a sphingosine backbone (see Fig. 1.6 in Chapter 1). 24:0[d_{47}]GalCer has a 24-carbon acyl chain (lignoceric acid) which was perdeuterated in this work. Thus there is a difference of about 6 to 8 methylene segments between its two chains. Fig. 5.1 shows the temperature dependence of its ^{2}H-NMR spectra. The main transition temperature of 24:0 GalCer dispersed in an excess buffer is 82-85 $^\circ C$. The sample was first warmed to 90 $^\circ C$ for one

hour, then lowered to 75 °C in several steps over a six hour interval, following which it was transferred to the NMR probe which had been preheated to 75 °C. Cooling of this sample from 75 °C to 50 °C proceeded at an effective rate of about 0.6 °C per hour [50].

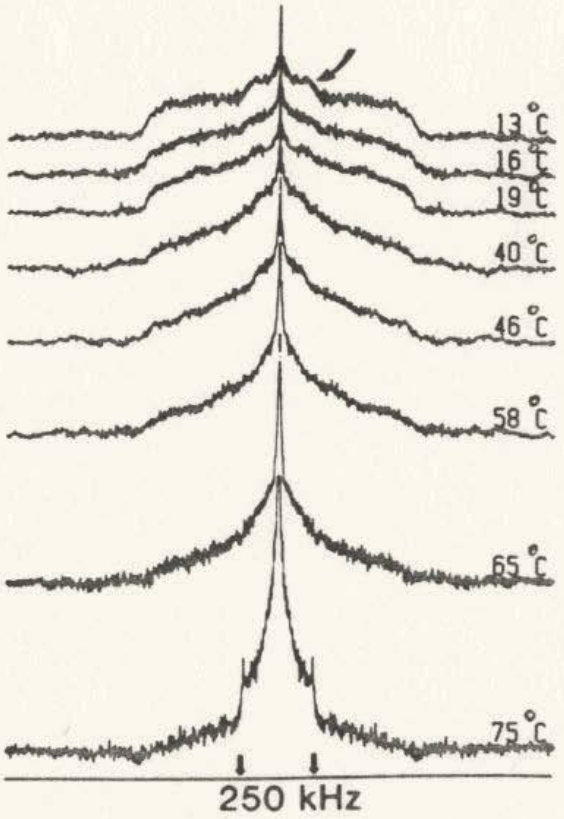

Figure 5.1: Temperature dependence of ^{2}H-NMR spectra for N-lignoceroyl[d_{47}] GalCer in hydrated bilayer form. Vertical arrows indicate ± 17 kHz on the frequency axis. The curved arrow indicate the feature due to the last several segments including the methyl group.

In Fig. 5.1, the vertical arrows indicate ± 17 kHz on the frequency axis. The curved arrow indicates a spectral feature arising from the last several segments including the methyl for the long chain. This feature will be discussed in the next section. The significant disordering near the methyl terminus existing in the gel phase is clearly shown by the

presence of the strong central peak in the spectra. The spectrum for 75 °C displays axially symetric components characteristic of liquid crystalline phase. This is presumably caused by the perdeuteration of the long chain, which is known to reduce the main transition temperature.

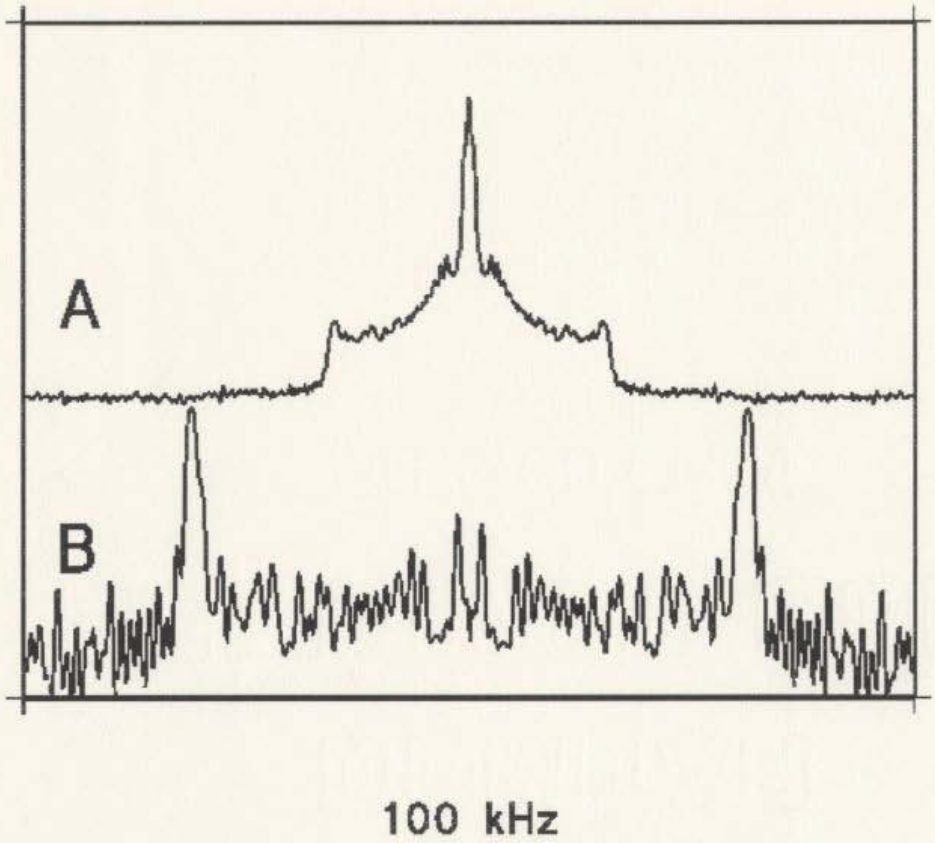

Figure 5.2: Observed (A) and de-Paked (B) ^{2}H NMR spectra for pure fully hydrated 24:0[d_{47}] GalCer at 85 °*C*.

Fig. 5.2 shows observed powder and de-Paked spectra for 24:0[d_{47}]GalCer at 85 °*C*. The central parts of its spectra, either in gel or fluid phase, are clearly different from those in spectra of chain length matched diacylphospholipids shown in Fig. 4.1. Fig. 5.3 shows the smoothed order parameter profile at 85 °C, which is a few degrees above the gel-liquid crystal transition [98][109]. This sample contained 5 mg of 24:0[d_{47}] GalCer. Because of

the low signal to noise ratio, 140,000 scans were accumulated for this spectrum. As can be seen from Fig. 5.3, the order parameter profile of 24:0 GalCer[d_{47}] is different from that of diacyl phospholipids. The slope of the order parameter profile becomes increasingly negative along the chain towards the methyl group for diacyl phospholipids. The order parameter profile of 24:0 GalCer[d_{47}] exhibits a second plateau covering segments from C(19) to C(23), which corresponds to the central part of the spectrum shown in Fig. 5.2. This reflects a significant structural difference between the two chains in the lipid bilayer. The interpretation of profiles displaying a low-order plateau near the bilayer center will be discussed in the last section of this chapter.

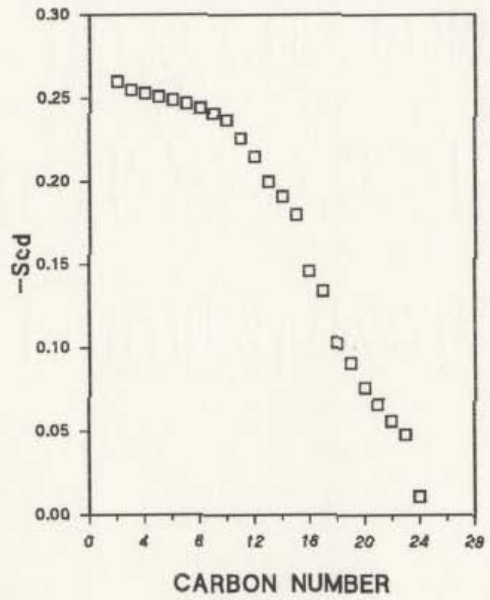

Figure 5.3: *Smoothed order parameter profiles for 24:0 GalCer at 85 °C.*

5.2.2 Mixtures of Glycosphingolipids (GSL) [24:0 GalCer, 18:0 GalCer] with SOPC

A) Phase Behaviour

The molecules of GalCer and SOPC have different head groups. For the mixtures of 18:0[d_{35}] GalCer with SOPC, the two components in the bilayer membrane have similar effective chain length. In the mixtures of 24:0[d_{47}] GalCer with SOPC the two components in the bilayer membrane have an effective chain length difference of about six methylene groups. Fig. 5.4 shows the temperature dependence of the first spectral moment, M_1, for both 18:0[d_{35}] GalCer/SOPC and 24:0[d_{47}] GalCer/SOPC. M_1 is proportional to the weighted average of the spectral splittings [6] and generally increases with chain order

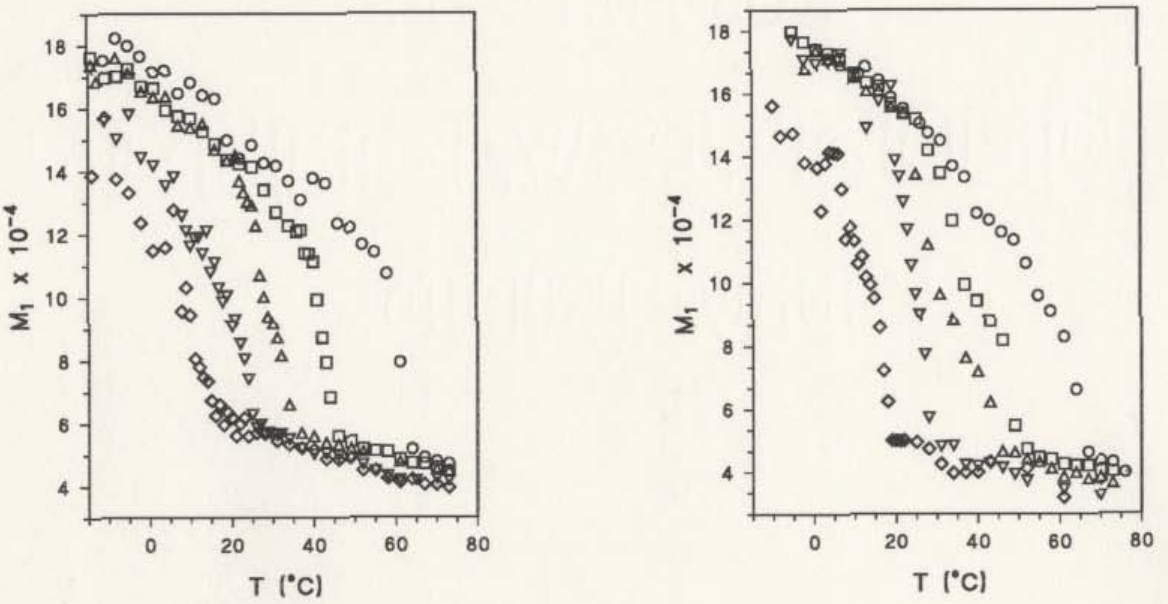

Figure 5.4: Temperature dependence of the first spectral moment, M_1, for N-(C24 GalCer) in SOPC (right) at mole fractions $x = 0.53$ (◯), $x = 0.35$ (□), $x = 0.24$ (△), $x = 0.10$ (▽),and $x = 0.05$ (◇); and for N-(C18 GalCer) in SOPC (left) at mole fractions $x = 0.40$ (◯), $x = 0.29$ (□), $x = 0.20$ (△), $x = 0.10$ (▽),and $x = 0.05$ (◇).

[see Eq. (3.22) in Chapter 3]. It can be seen from Fig. 5.4 that orientational ordering in the gel and liquid-crystal phases is greater for samples with higher glycolipid concentration. The temperature range over which M_1 rises sharply provides a rough estimate of the extent of two-phase coexistence for each sample. This provides a first order approximation to the phase diagram.

The liquidus temperature for each sample can be identified as the temperature at which M_1 departs from its nearly constant high temperature value. In this respect, there is not much difference between the plots for both mixtures of 18:0 GalCer/SOPC and 24:0 GalCer/SOPC. However, the behavior of M_1 at low temperature differs in the two mixtures. The approximate convergence of M_1 between 20 $^\circ C$ and 30 $^\circ C$ for the four samples with highest 24:0 GalCer concentrations, suggests the existence of a horizontal or nearly horizontal boundary (a three phase line) in this temperature range. Low temperature values of M_1 for the four samples are very high and suggest nearly-rigid lattice spectral components. The fact that the lowest concentration sample displays a different behavior suggests that it falls outside the concentration range in which one of the coexisting phases is very highly ordered with a nearly-rigid lattice spectrum.

Fig. 5.5 shows three series of ^{2}H-NMR spectra for five samples of 24:0 GalCer[d_{47}] in SOPC with GalCer mole fraction from 0.05 to 0.53 at 1 $^\circ C$, 16 $^\circ C$, and 70 $^\circ C$ [50]. Each spectrum corresponds to either gel phase, fluid phase, or gel-fluid co-existence. The spectra for the gel and fluid phases differ from the usual spectra observed for phospholipids [6][9], in that there is a greater buildup of intensity near the center of the spectrum. By selective deuteration it was shown that the buildup of intensity in the central region of the spectrum is due to deuterons near the methyl end of the chain. The selectively deuterated sample is *N*-lignoceroyl[d_7] GalCer (24:0[d_7] GalCer), in which the fatty acid terminal methyl group and the two adjacent methylene groups were specifically labeled. The spectral comparison between 24:0[d_7] GalCer and 24:0[d_{47}] GalCer is shown

in Fig. 5.6 [51]. Fig. 5.6 also provides some insight into the nature of the ordered phases as discussed later.

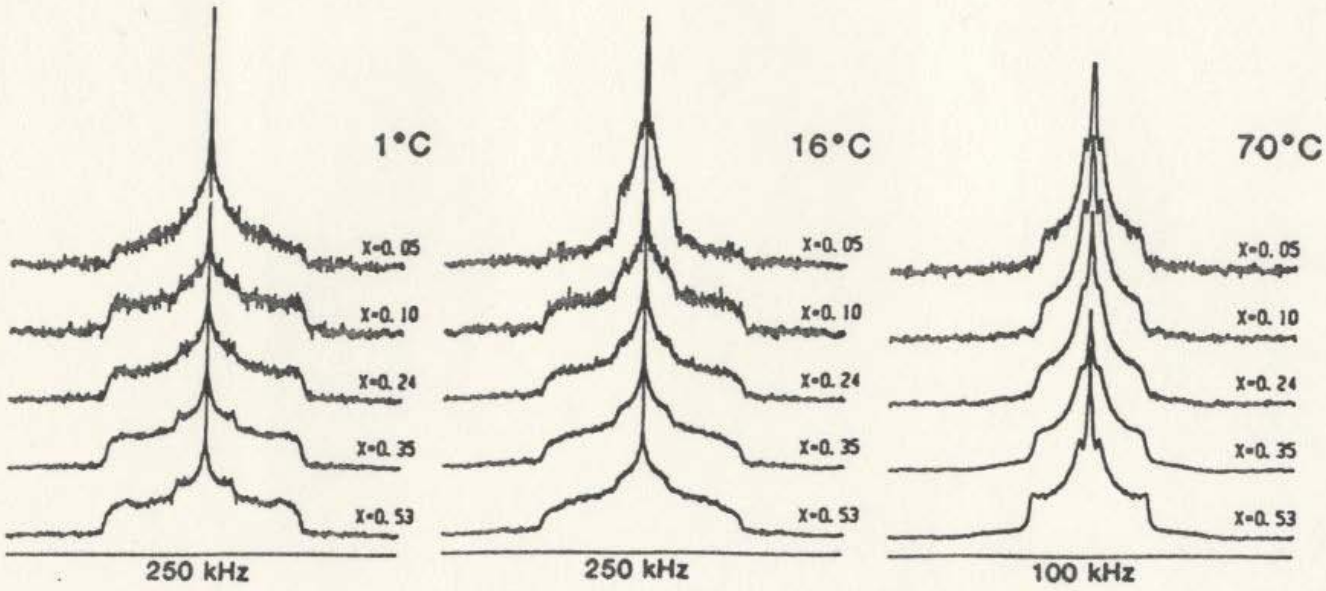

Figure 5.5: Concentration dependence of ^{2}H-NMR spectra for *N*-lignoceroyl[d_{47}] galactosylceramide (24:0[d_{47}] GalCer) in SOPC at temperatures of 1 $°C$, 16 $°C$, and 70 $°C$.

Returning to Fig. 5.5, the spectra in the 1 $°C$ series appear to show two kinds of ordered phase. One kind of ordered phase, seen at a lower concentration of 24:0 GalCer in SOPC, will be referred to as the G1 phase. The G1 phase is characterized by a spectrum such as the one seen for mole fraction 0.05. The distribution of the spectral intensity in this kind of spectrum appears roughly triangular. The other ordered phase, characterized by a spectrum like that seen for $x = 0.53$, will be referred to as the G2 phase. The G2 phase spectrum is nearly identical to the gel phase spectrum of pure 24:0 GalCer (see spectra at low temperatures in Fig. 5.1 for comparison). The spectrum for $x = 0.53$ has some interesting features which distinguish it from the spectrum for mole fraction 0.05. The buildup of intensity at $\pm$ 63 kHz signifies a nearly rigid lattice phase. The sharp step in intensity at $\pm$ 17 kHz, however, indicates a very mobile terminus near

the methyl in the long chain and does not indicate a coexisting liquid crystalline phase. This is shown in Fig. 5.6.

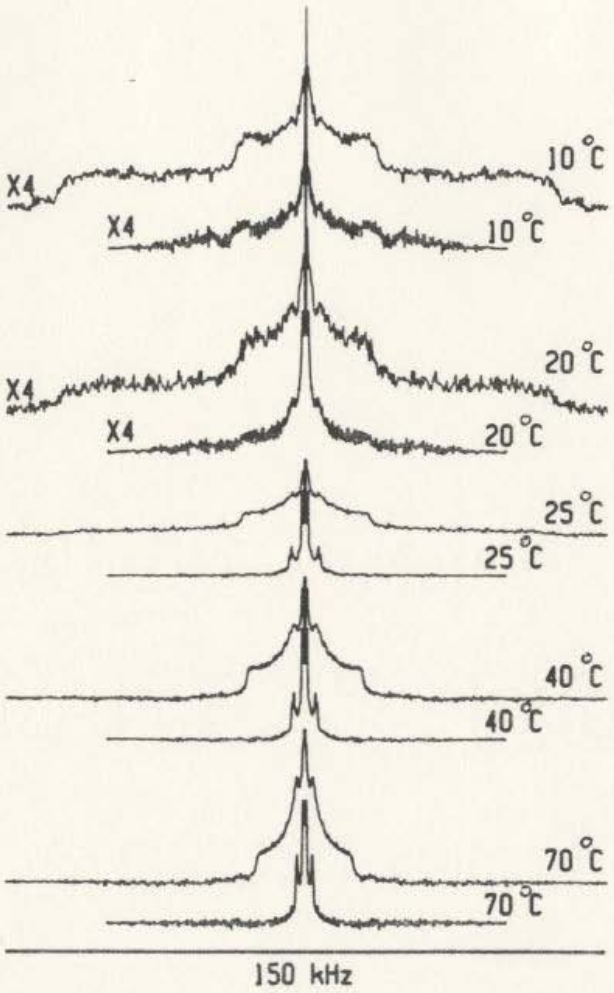

Figure 5.6: Spectra comparison of samples containing 24:0[d_7] GalCer (lower) (i.e., specifically labeled on the terminal methyl group and the two adjacent methylene groups in the acyl chain), with corresponding samples in which the long-chain fatty acid was perdeuterated (i.e., 24:0[d_{47}] GalCer, at low mol% in SOPC)(upper). Spectra shown for 24:0[d_7] GalCer contain 8 mg of deuterated glycolipid. GalCer concentration was 10 mol%.

In Fig. 5.6, spectra at 25, 40, and 70 $°C$ are the liquid crystalline phase spectra for bilayer mixtures of 10 mol% 24:0 GalCer[d_{47}] in SOPC (upper) and of 10 mol% 24:0 GalCer[d_7] in SOPC (lower). The splittings corresponding to the deuterons in the last three segments of the selectively deuterated 24:0 GalCer are much smaller than the largest liquid-crystal splittings for the deuterons near the head group of the perdeuterated 24:0

GalCer. For example, the largest liquid-crystal splittings in the 25 $^{\circ}C$ spectrum are about 34 kHz and 8 kHz for the mixture of 24:0 GalCer[d_{47}] and 24:0 GalCer[d_7] in SOPC, respectively. However, at 10 $^{\circ}C$, spectra for both 24:0 GalCer[d_{47}] in SOPC and 24:0 GalCer[d_7] in SOPC have a similar feature at (and within) $\pm$ 17 kHz (splitting of 34 kHz). It should be noted that there is no evidence of the small splittings which could be associated with a coexisting liquid crystalline phase and that the 34 kHz feature actually remains in the spectra of 24:0 GalCer[d_7] in SOPC down to temperatures at least as low as -10 $^{\circ}C$ [51]. Thus the 34 kHz feature contained in the spectrum for a bilayer mixture of 24:0 GalCer[d_{47}] in SOPC at 10 $^{\circ}C$ cannot be due to coexisting liquid crystalline domains and must arise from the segments near the methyl in the long chain.

The spectra for mole fraction 0.35 and 0.53 in the 1 $^{\circ}C$ series appear to be superpositions of G_1 and G_2 phase spectra. The spectra in the 1 $^{\circ}C$ series show that chain disordering increases as mole fraction of long chain decreases at a given temperature. It can also be seen that even in the ordered phase at 1 $^{\circ}C$ the ends of the long chain in 24:0 GalCer are still very disordered.

Spectra in the 16 $^{\circ}C$ series in Fig. 5.5 show the mixture in different phases. The spectrum for mole fraction 0.05 indicates that the mixture is in the liquid crystalline phase at this temperature and concentration. The spectrum for mole fraction 0.10 may indicate co-existence of the liquid crystalline phase and an ordered phase. The spectra for mole fractions 0.24 to 0.53 suggest an ordered phase.

Spectra in the 70 $^{\circ}C$ series of Fig. 5.5 all indicate a liquid crystalline phase. It can be seen that the build up of intensity near the center of the spectrum increases with decreasing mole fraction, suggesting that disordering of the long chain tail ends increases with decreasing mole fraction in the chain mismatched system.

The above discussion of the temperature dependence of features in the selected sets of spectra may be helpful for constructing a phase diagram for the mixture of 24:0

GalCer[d_{47}] in SOPC. Refinement of the phase diagram using spectral subtraction will be discussed below. First, however, a brief analysis of the spectra for the mixture of 18:0 GalCer[d_{35}] in SOPC will be presented. The comparison between the phase diagram for GalCer[d_{47}] in SOPC and that for 18:0 GalCer[d_{35}] in SOPC will be presented thereafter.

For 18:0 GalCer/SOPC, M_1 increases (see Fig. 5.4) with decreasing temperature and converges at relatively low temperature for all five concentrations of 18:0 GalCer in SOPC. This M_1 versus T behavior suggests that 18:0 GalCer/SOPC has no 3-phase line and that a "cigar-shaped" phase diagram may be expected.

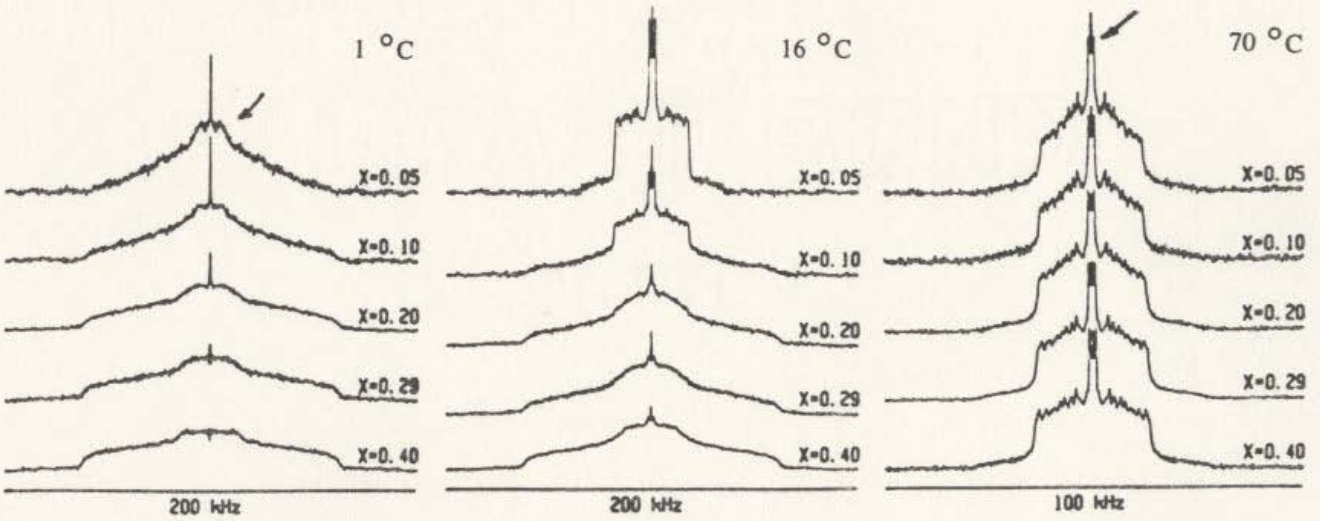

Figure 5.7: Concentration dependence of ^{2}H-NMR spectra for *N*-stearoyl[d_{35}] galactosylceramide (18:0[d_{35} GalCer) in SOPC at temperatures of 1 °*C*, 16 °*C*, and 70 °*C*. Spectra are arranged in vertical groups with glycolipid mole fraction and temperature indicated. Curved arrows for the 1 °*C* (gel phase) and 70 °*C* (fluid phase) 0.05 mole fraction samples indicate features associated with the 18-carbon fatty acid terminal methyl.

Fig. 5.7 shows ^2H-NMR spectra for five samples of 18:0 GalCer[d_{35}] in SOPC with

GalCer mole fractions from 0.05 to 0.40 at temperatures of 1 $°C$, 16 $°C$, and 70 $°C$ [51]. In the 1 $°C$ group, the spectra for all five samples display a broad gel phase spectrum [9][6]. In the 16 $°C$ group, the spectrum for mole fraction 0.05 is in liquid crystalline phase. The spectrum for mole fraction 0.40 is in the gel phase. The spectra for mole fractions 0.10 to 0.29 are superpositions of gel and liquid crystalline phase spectra, indicating fluid and gel coexistence. At 70 $°C$, the spectra indicate a fluid phase for all five samples. The large difference between the spectra for 24:0 GalCer[d_{47}] in SOPC (Fig. 5.5) and 18:0 GalCer[d_{35}] in SOPC (Fig. 5.7) is obviously related to the different accommodation of the molecular chains in the two binary mixtures. The effect of chain mismatch on lipid bilayer properties will be discussed later.

To refine the phase diagrams for both 18:0 GalCer/SOPC and 24:0 GalCer/SOPC, spectral subtraction was used. Fig. 5.8 shows spectral subtractions for mixtures of 24:0 GalCer[d_{47}] with SOPC at 13 $°C$. Spectra A and B are observed spectra at GalCer mole fractions of $x = 0.53$ and $x \approx 0.35$ respectively. Each shows both G_1 and G_2 type spectral features. Spectra E and F are observed spectra at GalCer mole fractions of $x \approx 0.1$ and $x = 0.05$ respectively. These spectra show both liquid crystal and ordered phase features.

Spectrum A ($x = 0.53$) looks similar to spectrum B ($x \approx 0.35$). But spectrum B has slightly more intensity in its central region than spectrum A does. So spectrum A corresponds to a more ordered state than spectrum B. It is much easier to recognize that spectrum F ($x = 0.05$) corresponds to a less ordered state than spectrum E ($x = 0.10$) does, since spectrum F has a prominent 90^0 edge. The factors K and K' (see Chapter 3) used in the spectral subtraction (for example, $K = 0.45$ for obtaining spectrum C) are determined by inspection. In other words, K or K' was adjusted during the spectral subtraction until the end spectrum was judged to be characteristic of a single phase. Spectral subtraction done between spectra A and B yields spectra C and D. Spectrum C is a gel end spectrum ($x = 0.92$) corresponding to G2 phase at 13 $°C$. As can be seen,

this spectrum mimics the gel spectrum at the same temperature for pure 24:0 GalCer (see Fig. 5.1). Spectrum D corresponds to the other end spectrum at 13 $°C$ for the bilayer. Its triangular like intensity profile indicates that it represents the G1 phase. Spectral subtraction done between spectra E and F yields spectra G and H. Spectrum H is a liquid end spectrum ($x = 0.04$).

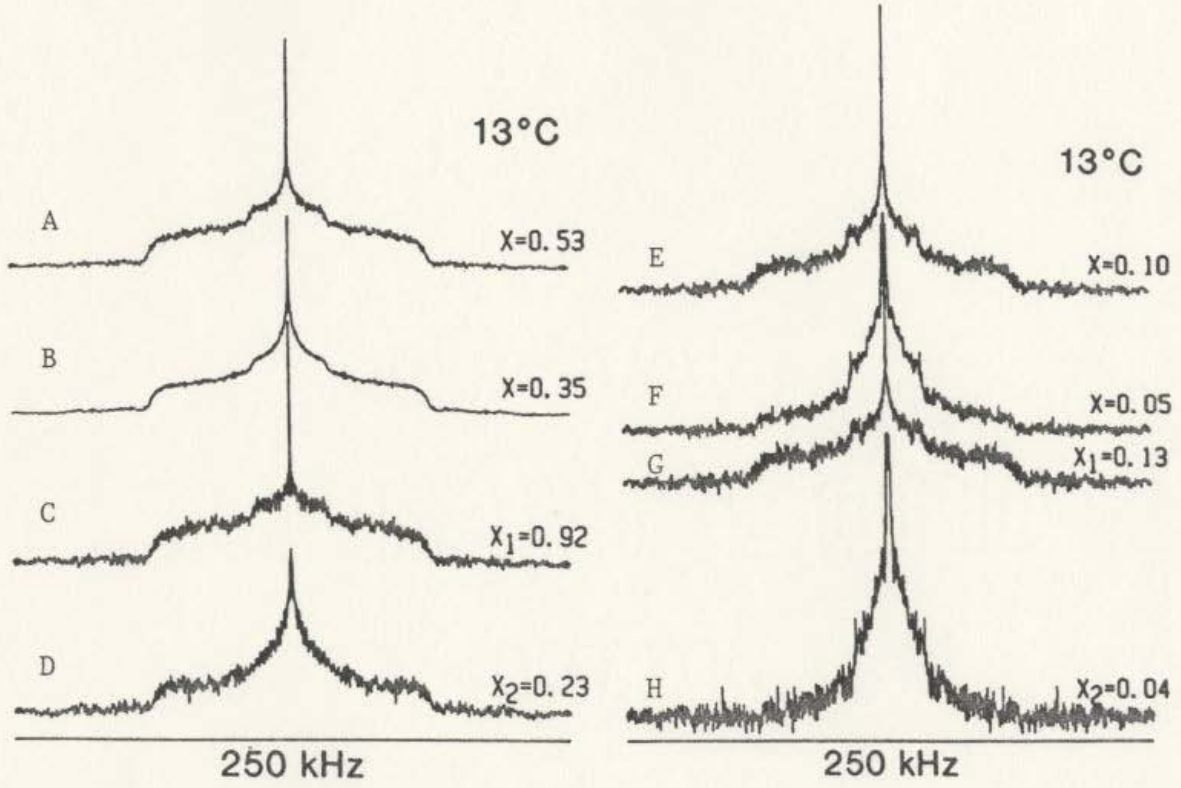

Figure 5.8: Spectra of GalCer[d_{47}] in SOPC at 13 $°C$. x denotes the mole fraction of GalCer[d_{47}] in SOPC for a corresponding spectrum. Spectra A, B, E, and F are observed spectra. C, D, G, and H are end point spectra obtained from spectral subtraction. C = A − 0.45B, D = B − 0.6A, G = E − 0.18F , and H = F − 0.45E. Spectra C and D are assumed to be characteristic of the proposed G_2 and G_1 phases, respectively. The quality of the subtraction for obtaining G is not sufficient to distinguish between G_1 and G_2 but the calculated endpoint composition falls in the G_1 range determined by the subtraction shown in the left plottings.

It differs from spectrum F in that the gel phase feature which appears at the wings of spectrum F cannot be seen. Spectrum G looks like spectrum E. It, however, represents a

more ordered state than spectrum E does, for it has less intensity in the central region. Although the quality of this subtraction is not sufficient to distinguish between G1 and G2, spectrum G probably represents a point at the G1 phase boundary ($x = 0.13$) due to its triangular shape in general. So the phase diagram at 13 $°C$ contains two tie lines with endpoints at $x = 0.04$ and $x = 0.13$, and $x = 0.23$ and $x = 0.92$ (see Fig. 5.10). Similar procedures were carried out at temperatures of 10 $°C$, 7 $°C$, 4 $°C$, and 1 $°C$. A peritectic phase behaviour with a three phase coexistence line between 15 $°C$ and 30 $°C$ was proposed (see Fig. 5.10).

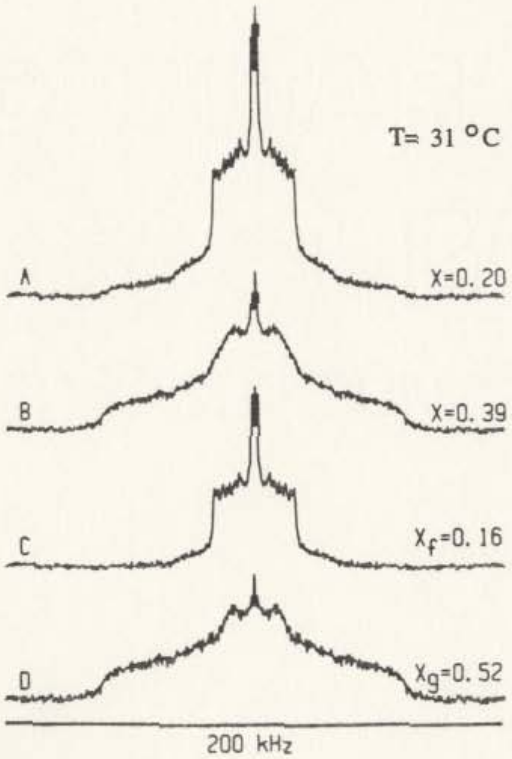

Figure 5.9: Example of spectral subtraction for *N*-stearoyl[d_{35}] galactosylceramide (18:0[d_{35}] GalCer) in SOPC at temperatures of 31 $°C$. Spectra A and B are observed spectra. Spectrum C is A $-$ (0.35)B, giving an endpoint at $x_f = 0.16$ (fluidus point); spectrum D is B $-$ (0.20)A, giving an endpoint at $x_g = 0.52$ (solidus point).

Fig. 5.9 shows an example of a spectral subtraction for mixtures of 18:0 GalCer[d_{35}] with SOPC at 31 $°C$. Spectra A and B are observed spectra at GalCer mole fraction

of 0.20 and 0.39. Both show some coexistence of liquid crystal and gel features. Spectral subtraction done between spectra A and B yields the endpoint spectra C and D. Compared with spectrum A, no gel feature is seen in spectrum C. Spectrum C defines the liquidus point at $x = 0.16$ in the phase diagram (see Fig. 5.10). Spectrum D differs from spectrum B in that the intensity is built up in the wings and reduced in the central region as compared with spectrum B. In particular, the narrow feature due to the methyl group in a fluid phase, which is seen in spectrum B, is largely removed in spectrum D. Spectrum D defines the solidus point at $x = 0.52$ in the phase diagram (see Fig. 5.10).

Fig. 5.10 shows proposed phase diagrams for both 18:0 GalCer/SOPC and 24:0 GalCer/SOPC. The phase behaviors for mixtures of 24:0 GalCer[d_{47}] with SOPC and 18:0 GalCer[d_{35}] with SOPC appear to be alike at low glycolipid concentration. At higher mole fraction ($\geq$ 20 mole%), 24:0 GalCer/SOPC displays a much greater tendency to gel/fluid phase separation and also to gel phase immiscibility than is seen for 18:0 GalCer/SOPC. In the case of 24:0 GalCer in SOPC, there appear to be two types of ordered phase spectra, reflecting solid-phase immiscibility, at intermediate glycolipid concentrations. One of these, which is designated G_1, is relatively enriched in SOPC. The other ordered phase, designated G_2, appears to be nearly pure 24:0 GalCer. It is interesting that the longer chain fatty acid glycolipid stabilized the gel phase phospholipid host matrix more at low glycolipid concentrations than did the shorter chain analogue. The difference in phase behavior between the two mixtures is presumably caused by the different chain lengths of the GalCer components. However, the excess chain length in 24:0 GalCer seems to be accommodated well in fluid phase as reflected in the relative similarity of the 18:0 and 24:0 GalCer phase diagram in fluid region. It should be noticed that the temperature of the three phase line in 24:0 GalCer in SOPC is not well determined.

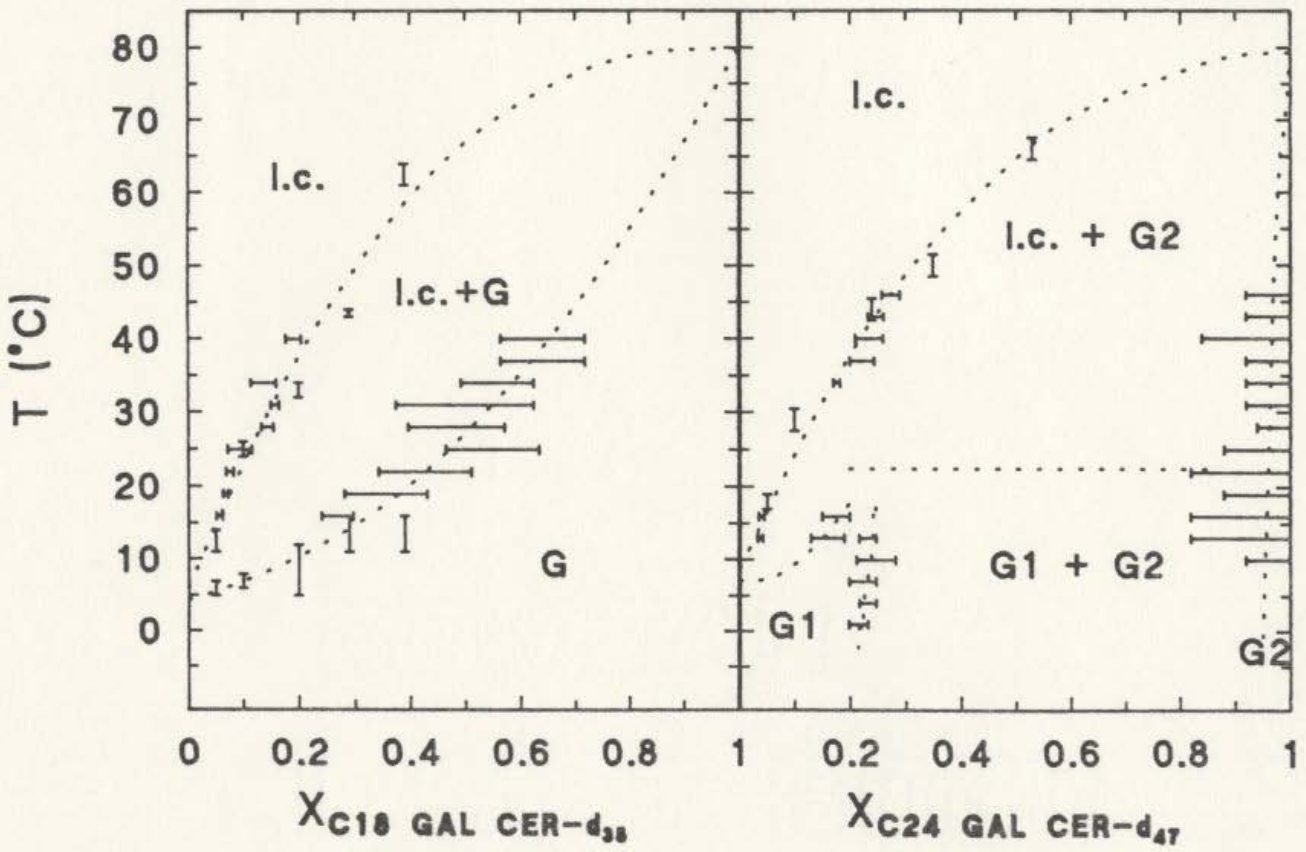

Figure 5.10: Proposed phase diagrams for (left) *N*-stearoylgalactosylceramide (18:0 GalCer) and (right) *N*-lignoceroylgalactosylceramide (24:0 GalCer) in SOPC. Vertical error bars represent estimated range of uncertainty in boundary crossings determined by inspection of spectra and consideration of M_1. Horizontal bars indicate the range of experimental values obtained using spectral subtraction techniques with various spectral combinations.

B) Order Parameter Profiles in Mixtures

Smoothed order parameter profiles can be obtained for binary mixtures of 18:0 GalCer [d_{35}] in SOPC and 24:0 GalCer[d_{47}] in SOPC at different temperatures and component concentrations. Fig. 5.11 shows spectra and their corresponding smoothed order parameter profiles for 10 mole% 18:0 GalCer[d_{35}] in SOPC and 10 mole%24:0 GalCer[d_{47}] in SOPC at 52 °C. The remarkable difference between the two spectra is in the central part, which corresponds to the regions near the methyl ends of the deuterated acyl chains in

the two glycolipids. The order parameters for the two mixtures correspond closely from C(2) to C(15), which indicates that their chains extend, on average, to the same depth at this point. The order parameter profile for 18:0 GalCer/SOPC shows the monotonic change in slope typically seen in bilayers with homogeneous chain lengths. The profile for 24:0 GalCer/SOPC, however, is qualitatively different, having a second plateau in the low order parameter region. It can be seen that the order parameters for the region from C(18) to C(24) on the deuterated chain in 24:0 GalCer are comparable to those of C(17) and C(18) on the deuterated chain in 18:0 GalCer. These segments are very fluid.

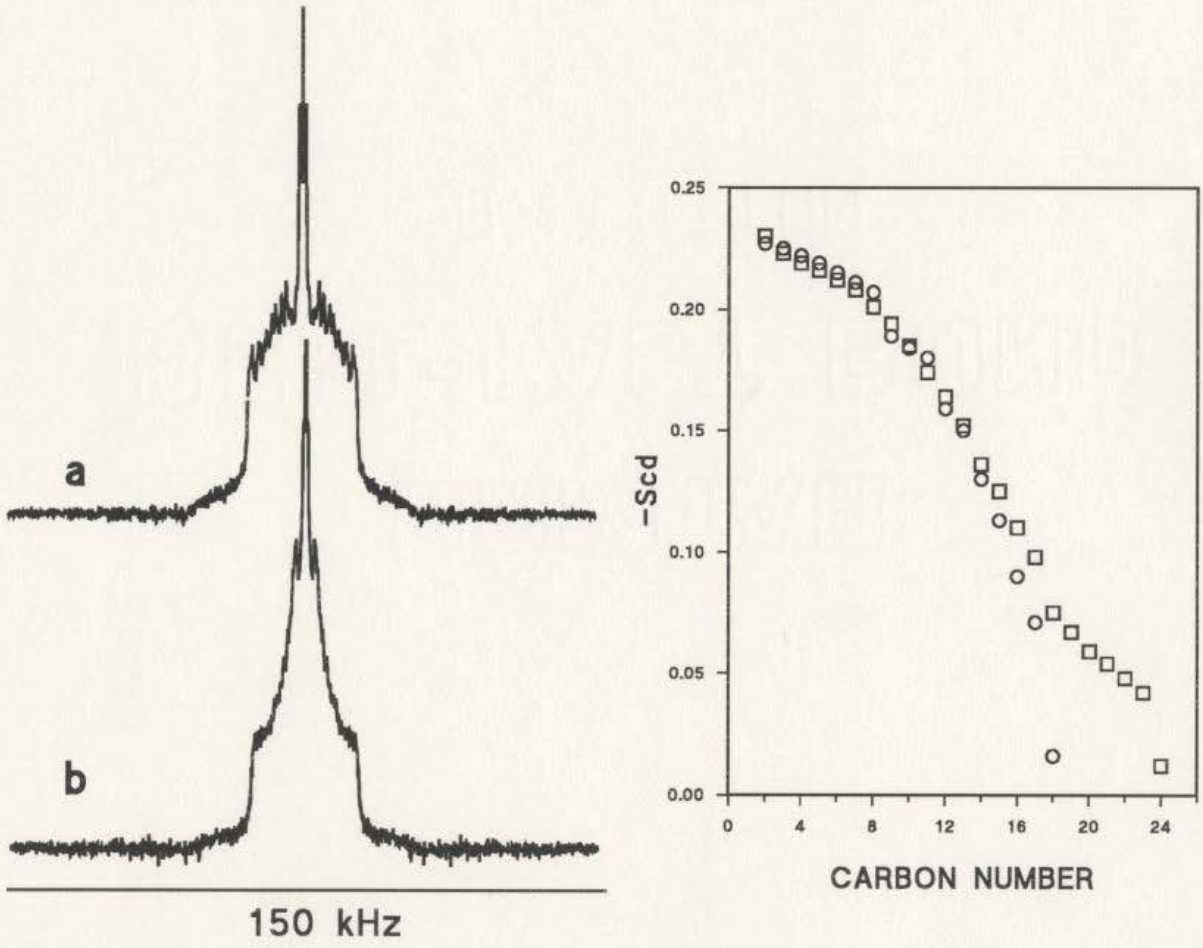

Figure 5.11: Spectra and their smoothed order parameter profiles for *N*-stearoyl[d_{35}] GalCer (a, and ◯) and *N*-lignoceroyl[d_{47}] GalCer (b, and □), dispersed in SOPC at 10 mol% at 52 °*C* .

It may not be straightforward to draw conclusions on the structural properties for the two binary mixtures from the ordering of the glycolipid acyl chains, since we lack information about the SOPC in the bilayers. However, the facts that 18:0 GalCer and SOPC have about the same chain length and that they are miscible in both gel and fluid phase suggest that, to a first approximation, the glycolipid acyl chains of 18:0[d_{35}]GalCer and the SOPC chains order in a similar manner. If we assume that the interactions between the head groups and the acyl chains are localized near the bilayer interface region [118], then the order parameter profile for the small concentration of 18:0 GalCer [d_{35}] in SOPC may be used to approximate the order parameter profiles of the stearoyl chain in SOPC, at least in the region near the methyl end. We can then deduce, for the mixture with a small concentration of 24:0 GalCer in SOPC, (i) that the order parameters for the chains in the mixture correspond closely from C(2) to C(15), (ii) that the order parameters for the segments from C(16) to C(18) on 24:0 GalCer chain are bigger than those for the corresponding segments on the neighbouring short chains, and (iii) that the deuterons of the five methylene groups near the methyl end of the 24:0 GalCer chain all display smaller orientational order parameters than the deuterons on the C(17) methylene of the short chains. It is this latter point which gives rise to the second plateau at low order parameter, similar to what is observed in the pure mixed chain bilayer 24:0 GalCer.

It is generally believed that there is a fluid region in the middle of the bilayer for liquid crystalline phase systems. In the case of a mixture of 18:0 GalCer[d_{35}] and SOPC, this fluid central layer may accommodate C(17) and C(18) segments on the chains of both constituents in the mixture. In the case of mixture of 24:0 GalCer [d_{47}] and SOPC, the central fluid layer may accommodate C(18) to C(24) segments on lignoceroyl chains and C(17) and C(18) segments on SOPC chains. These results reveal that the excess length of the long chain situated at the bilayer middle region is very mobile. If it interdigitates in the bilayer, it would be very transient, given that the conformational motion of the

chain is of large amplitude.

5.3 Mixtures of DMPC/DSPC

In the previous two sections, a second plateau at low order in the smoothed orientational order parameter profile for perdeuterated long chains in chain mismatched systems was discussed. However, the accommodation of the long chain in the short chain host in a binary lipid bilayer remains unclear to some extent, since the ordering behavior of the short chain in the same samples has not been simultaneously examined. It is difficult to make a direct comparison on properties, such as temperature dependence of the orientational order parameter profiles (OOPPs) and concentration dependence of OOPPs, between the two components in the binary mixture. Samples with both components perdeuterated are needed for further investigation of the interaction between long and short chains. For this purpose, mixtures of DSPC/DMPC covering a range of compositions were prepared with either DSPC acyl chains or DMPC acyl chains perdeuterated or, in some special cases, both DSPC and DMPC acyl chains perdeuterated. Using these samples, the effect of chain mismatch in a binary system was examined systematically.

The orientational order parameters in the smoothed order profile of DSPC were found to be slightly higher than those for DMPC at the same carbon positions over a wide range of bilayer compositions. The shape of the smoothed profiles for both components were found to be sensitive to bilayer composition. At low DSPC composition, the order parameter profile for DSPC displays a second plateau at low orientational order like that which appears in the profiles for 24:0 GalCer and the mixture of 24:0 GalCer with SOPC. At high DSPC concentration, the order parameter plateau for DMPC is stretched slightly. The details of this study are presented in the following four sections. The interpretation of spectra which simultaneously show both components in a given mixture is discussed

in section 5.3.1. Chain order in DMPC/DSPC bilayers is described in section 5.3.2. The difference in chain extension between DMPC and DSPC in the mixture is discussed in section 5.3.3. Finally, an estimation of bilayer thickness for DMPC/DSPC mixtures is presented in section 5.3.4.

5.3.1 Selection of Spectra for Comparison of DMPC and DSPC in the Mixture

For the DMPC/DSPC system, with a $\Delta T_m \simeq 32$ °C, gel phase immiscibility is still controversial [41][119]. ^{2}H-NMR experimental data suggest miscibility in the gel phase [40][41]. The phase diagrams constructed from DSPC[d_{70}]/DMPC and DMPC[d_{54}]/DSPC are slightly different [40], presumably because perdeuteration lowers pure lipid transitions by four to five degrees. This raises the question of whether temperature is the appropriate parameter to fix when comparing order parameter profiles for the two components.

One question which arises is whether or not one can assume that the two components, in a given mixture, adjust to have the same area per lipid, a situation sometimes referred to as "lock-in" [40]. For a given class of lipids, such as the PC family, the area per lipid in the liquid crystalline phase is directly related to the value of the order parameter, S_{CD}, at the plateau region of the orientational order parameter profile [34][78]. A comparison of order parameter profiles for the two components (in two mixtures) under conditions that give similar values for the order parameter in the plateau regions of the smoothed order parameter profiles thus corresponds to a comparison under conditions of approximately equal areas per lipid.

Fig. 5.12 shows spectra and their corresponding order parameter profiles for DMPC [d_{54}] at 37 °C, 4.4 mol% DSPC[d_{70}] in DMPC at 42 °C, and DSPC[d_{70}] at 57 °C. The chain melting transition temperature for DMPC[d_{54}] is about 19 °C. The transition temperature of the 4.4 mol% DSPC[d_{70}] in DMPC mixture is found to be 24.5 °C, as

would be expected for nearly pure DMPC with no deuteration. The profiles of DMPC[d_{54}] and for the 4.4 mol% DSPC[d_{70}] in DMPC were thus both obtained about 18 °C above the corresponding bilayer transitions. The 5 °C difference between the temperatures for the DMPC[d_{54}] profile and for the 4.4 mol% DSPC[d_{70}] in DMPC profile is the expected change in transition temperature that accompanies perdeuteration of the DMPC component. Smoothed order parameter profiles for these spectra are shown in Fig. 5.12d.

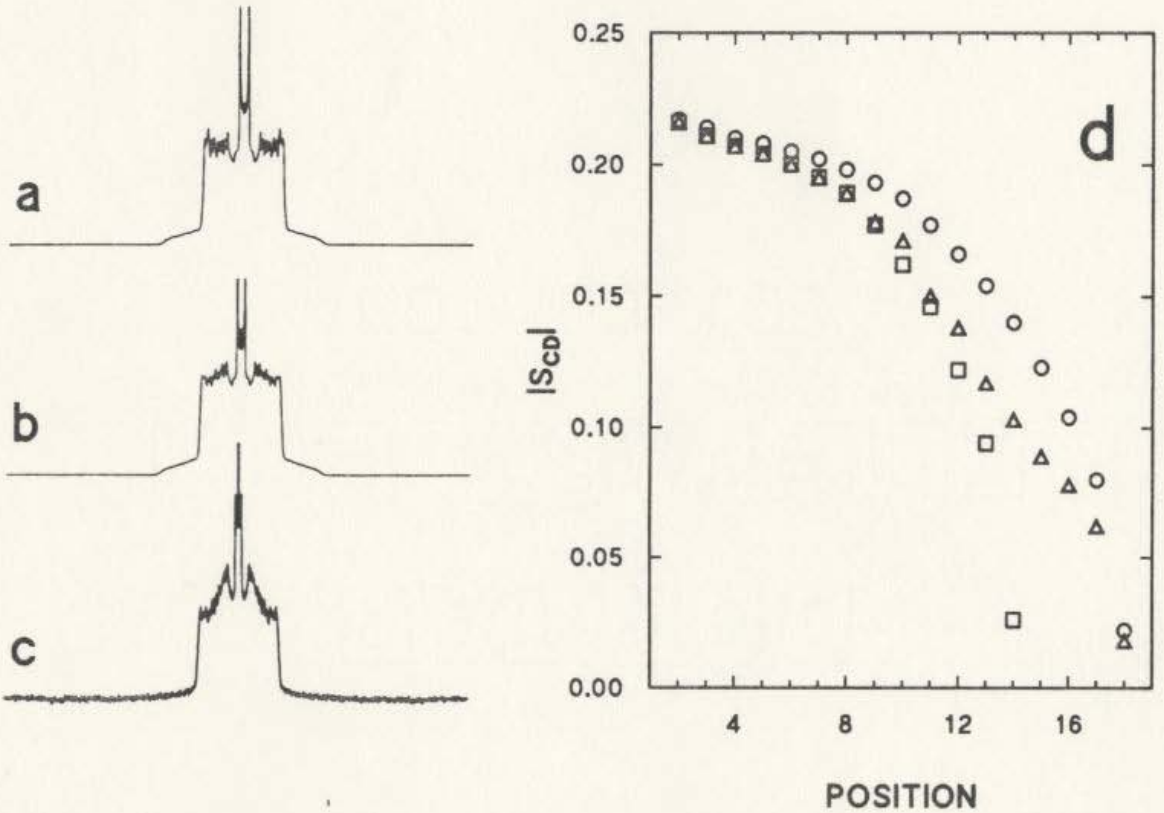

Figure 5.12: (a) ^{2}H-NMR spectrum of DMPC[d_{54}] in excess water at 37 °C. (b) ^2H-NMR spectrum of DSPC[d_{70}] in excess water at 57 °C. (c) ^{2}H-NMR spectrum of 4.4 mol% DSPC[d_{70}] in DMPC at 42 °C. (d) Smoothed orientational order parameter profiles corresponding to the spectra in a (□), b (◯), and c (△).

If it is assumed that the dependence of area per lipid on temperature above the transition is similar for perdeuterated and normal DMPC and if it is assumed that the small

concentration of DSPC has a minor influence on the DMPC order profile, then we can approximate the unknown DMPC profile in the mixture at 42 $^{\circ}C$ by the DMPC[d_{54}] profile at 37 $^{\circ}C$. The comparison in Fig. 5.12d would then suggest that for diacyl phospholipids having the same headgroup, the minor component in a very dilute binary mixture adopts nearly the same area per lipid as the major component.

Fig. 5.12d also shows the smoothed order parameter profile for DSPC[d_{70}] at a temperature (57 $^{\circ}C$) selected to give a corresponding plateau value of the order parameter. It is only 6 $^{\circ}C$ above the transition temperature for DSPC[d_{70}] and is evidence that area per lipid in the fluid phase does not depend only on the separation, in temperature, from the transition. Moreover, for high concentrations of DSPC two phases coexist over a wide temperature range and there is no unique transition temperature [40][49]. It seems from Fig. 5.12d that at very low concentrations in the mixture, the plateau order and, by extension, the area per lipid of the minor component is strongly influenced by the surrounding lipids. The question which arises here is whether the area per lipid for each of the two components is the same for other concentrations.

We are interested in examining profiles for both components corresponding as closely as possible to the profiles they would simultaneously display in a given mixture. Because the phase diagrams for DSPC[d_{70}]/DMPC and DMPC[d_{54}]/DSPC are slightly different [40], it is necessary to determine an appropriate way to select corresponding spectra with one or the other component deuterated. If area per lipid for a given temperature is not altered by deuteration and is insensitive to deuteration-related changes in the binary phase diagram, then comparing spectra obtained at a given temperature should be appropriate. If the two components do share a common area per lipid in the mixture, the appropriate comparison would be between spectra obtained at temperatures for which the plateau values of the orientational order parameters are the same for the two components in mixtures with one or the other component perdeuterated.

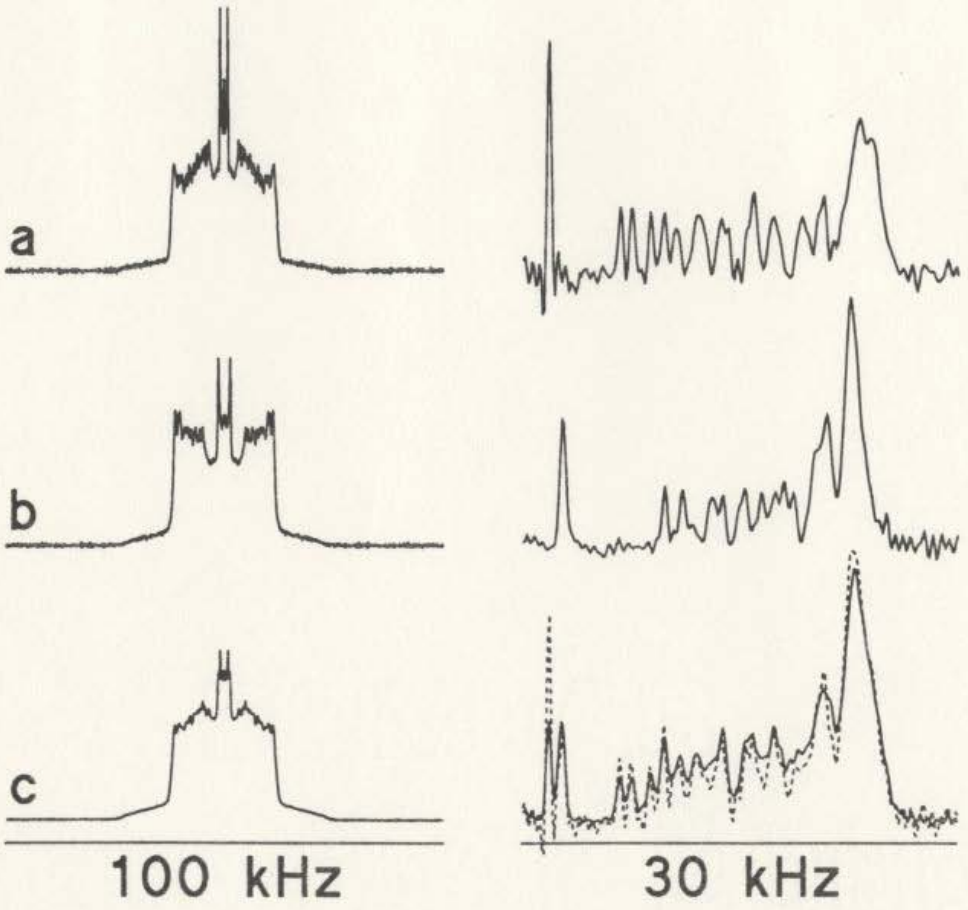

Figure 5.13: ^{2}H-NMR spectra (left) and half of the corresponding de-Paked spectra (right) for DMPC/DSPC mixtures at DSPC concentration of 50 mol% and T=60 °C . (a) DMPC with DSPC[d_{70}]. (b) DMPC[d_{54}] with DSPC. (c) DMPC[d_{54}] with DSPC[d_{70}]. The de-Paked spectrum shown as a solid line corresponds to the observed DMPC[d_{54}] with DSPC[d_{70}] powder pattern. The de-Paked spectrum shown as a dashed line is the weighted sum of de-Paked spectrum for DMPC with DSPC[d_{70}] and DMPC[d_{54}] with DSPC.

To check the first possibility, ^{2}H-NMR experiments on samples of 50 mole% DSPC[d_{70}] in DMPC, 50 mole% DMPC[d_{54}] in DSPC, and 50 mole% DSPC[d_{70}] in DMPC[d_{54}] were conducted. Their spectra at 60 °C are shown on the left of Fig. 5.13. and their corresponding de-Paked spectra are shown on the right of Fig. 5.13. The spectrum of 50 mole% DSPC[d_{70}]/DMPC[d_{54}] (solid line) coincides closely with the weighted sum spectra (broken line) of DSPC[d_{70}]/DMPC and 50 mole% DMPC[d_{54}]/DSPC. This suggests that the

^{2}H-NMR experimental data for DSPC[d_{70}]/DMPC and DMPC[d_{54}]/DSPC are relevant to the situation in DSPC/DMPC at the same temperature in the liquid crystalline phase. The profiles of the deuterated chains in the mixtures with one component deuterated, at a given temperature, show the state of that component in the DMPC/DSPC mixture at the same temperature. It can be seen that at a fixed temperature, there is a small but distinct difference between the maximum quadrupole splittings for the two components in the mixtures with only one component deuterated. This implies a slight difference in plateau values of the orientational order parameter and suggests that they do not share a common value for the area per lipid.

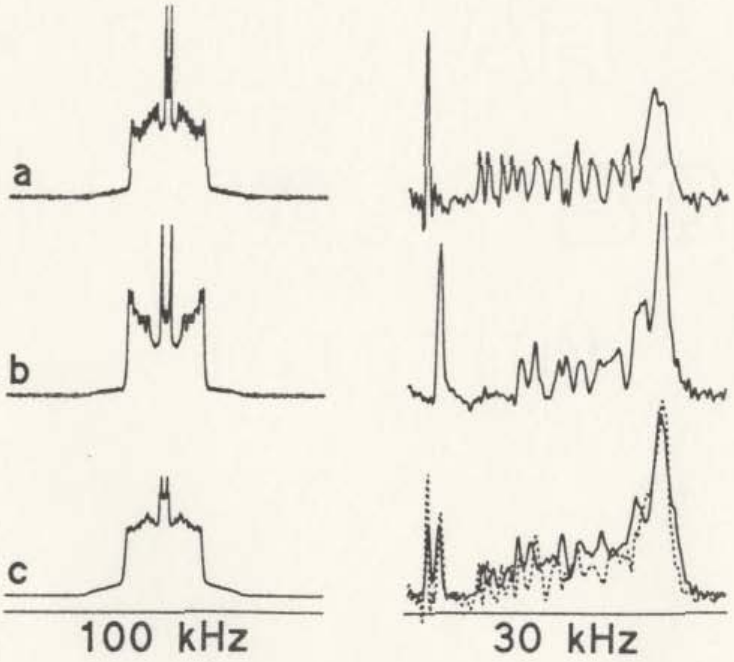

Figure 5.14: ^{2}H-NMR spectra (left) and half of the corresponding de-Paked spectra (right) for DMPC/DSPC mixtures at DSPC concentration of 50 mol% Temperatures were selected to yield powder patterns with the same maximum splitting. (a) DMPC with DSPC[d_{70}] at T=60 °C. (b) DMPC[d_{54}] with DSPC at T=53 °C. (c) DMPC[d_{54}] with DSPC[d_{70}] at T=56 °C. The de-Paked spectrum shown as a solid line corresponds to the observed DMPC[d_{54}] with DSPC[d_{70}] powder pattern. The de-Paked spectrum shown as a dashed line is the weighted sum of de-Paked spectrum for DMPC with DSPC[d_{70}] and DMPC[d_{54}] with DSPC.

The test of the second possibility is shown in Fig. 5.14 in which three spectra share a common quadrupole splitting. The weighted sum of the two spectra obtained with a single component does not correspond to the spectrum observed with both components deuterated. It seems clear that within this mixture, the two lipid components are not constrained to display equal plateau order parameters and thus, by extension, are not constrained to have equal areas per lipid. This observation initially appears to be inconsistent with the comparison illustrated in Fig. 5.12. However, it is interesting to note that, for concentrations between 30 mole% DSPC and 75 mole% DSPC, the average of the liquidus and solidus temperatures for DSPC[d_{70}]/DMPC and DMPC[d_{54}]/DSPC phase diagrams are the same to within about 1° [40]. It may be that over a wide range of concentrations, comparing pairs of spectra at fixed temperature is equivalent to comparing them at the same separation from an effective transition temperature which falls near the center of the two phase region.

5.3.2 Chain Ordering in DMPC/DSPC Bilayers

The comparison presented above provides a reasonable foundation for investigating the mutual influence between the two constituents at a fixed temperature in a binary mixture. Fig. 5.15 shows the smoothed order profiles for both constituents in mixtures with different concentrations of DSPC in DMPC at 60 °C. The order profiles of pure DMPC and pure DSPC have also been presented for comparison. In light of the preceding discussion, the DSPC[d_{70}]/DMPC and DMPC[d_{54}]/DSPC profiles obtained at a given composition and temperature are assumed to represent simultaneously the states of the two components in the particular mixed bilayer. It can be seen that at a given temperature, the order parameter profile is concentration dependent.

The area per lipid for both components tends toward a weighted mean of the two single-component bilayer values. Over the range of DSPC mole fractions between 0.25

and 0.75, the difference between the plateau values of the order parameter for the two components is approximately constant. It would thus appear that the areas per lipid of both components change with concentration in roughly the same way. One simple observation that can be made is that there is little difference between the two lipids in terms of their susceptibility to changes in the average order of the surrounding matrix.

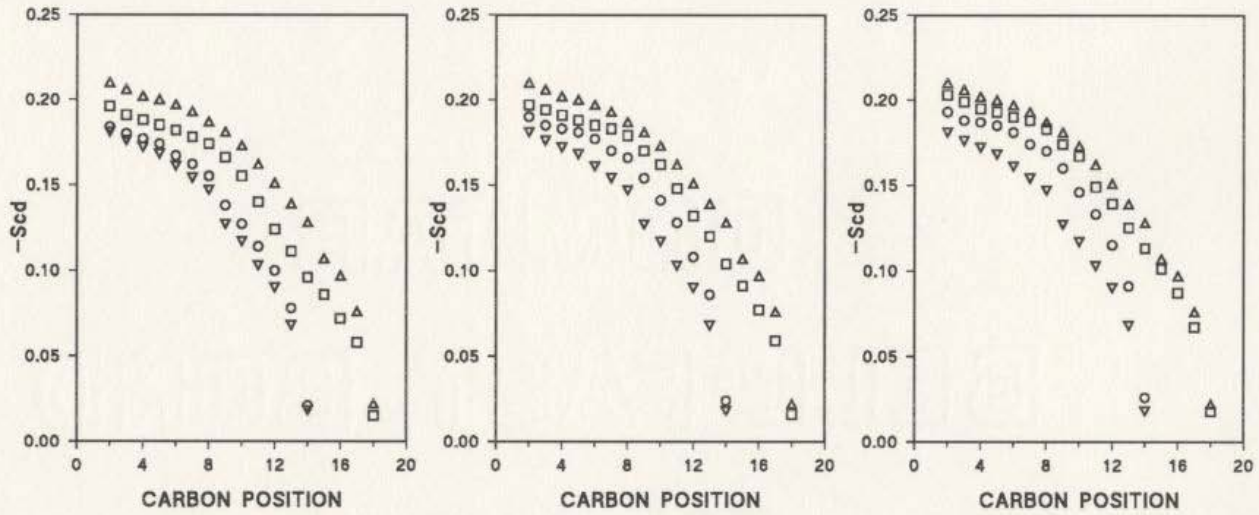

Figure 5.15: Smoothed orientational order parameter profiles at 60 $^{\circ}C$. Profiles for both DMPC/DSPC[d_{70}] (□), and DMPC[d_{54}]/DSPC (◯) with DSPC percentage mole concentration of 25, 50, and 75 are shown at left, middle and right plottings respectively. Profiles for DSPC[d_{70}] (△) and DMPC[d_{54}] (▽) are also shown in the three plottings.

For concentrations below 25 mol% DSPC or above 75 mol% DSPC (see Fig. 5.15), the profiles of the major components in the mixtures are already very close to the corresponding single-component bilayer profiles. It is likely that for higher and lower DSPC concentrations, the profile of the major component becomes insensitive to concentration, whereas that of minor component increasingly approaches the former. This expectation is consistent with the observations illustrated by Fig. 5.12 provided that the effect of

deuteration on the transition temperature is taken into account.

In all of the mixtures, the order parameters of the last two methylene groups near the methyl end of the DSPC[d_{70}] chain [i.e. C(16) and C(17)] are smaller than those of the last methylene group of the DMPC[d_{54}] chain. This observation implies that the steric constraint at the layer where the methylene groups of C(13) in DMPC[d_{54}] reside is greater than that at the layers where methylene groups of C(16), C(17) of DSPC[d_{70}] reside. In this sense, the segments of C(16), C(17), and C(18) on DSPC[d_{70}] which form the second plateau in the order parameter profile for the mixtures, especially at low concentration of DSPC[d_{70}], are situated in a less ordered region than C(13) of DMPC[d_{54}]. This may indicate that the methyl groups of DMPC and the groups of C(16), C(17), and C(18) of DSPC exist in a very fluid region in the middle of the bilayer.

It is evident that the mean order of every segment on the short chain increases from that of the pure short chain lipid as the long chain concentration in the mixture increases. On the other hand, the mean order of every segment on the long chain decreases from that of the pure long chain lipid as the short chain concentration in the mixture increases.

In order to look more closely at the effect of mixture composition on the orientational order parameters, the changes in orientational order parameters from their values for the pure lipids at the same temperature (60 °C), ΔS_{CD} ($= S_{CD}^{mixture} - S_{CD}^{pure\ component}$), are shown in Fig. 5.16. It can be seen that the changes in the orientational order parameter, in response to changes in the surrounding matrix or component concentration, are different for short and long chains and are different for different sections along the chains. For the long chain component, the change in the value of the order parameter for the plateau region is basically constant for the first few segments, whereas the change in the values of the order parameter for the sections beyond the plateau depends on position along the chain, with the biggest change of S_{CD} at carbon number 14. Beyond carbon number 14 the change in the order parameter from its pure lipid value diminishes. The result, for

the long chain, is that the plateau in the order parameter profile shifts to lower values and a second plateau forms at the end of the order parameter profile as the concentration of the short chain is increased. For the short chain component, the change in the order parameter along the chain gets progressively bigger with increasing carbon number until carbon number 9. Beyond this point, the change from pure lipid values decreases with position toward the end of the chain. This results in an expansion of the plateau in the order parameter profile with increasing long chain concentration. The biggest increase of S_{CD} happens at around carbon number 9, which is presumably due to the constraining influence of the middle of the neighboring DSPC chains [120].

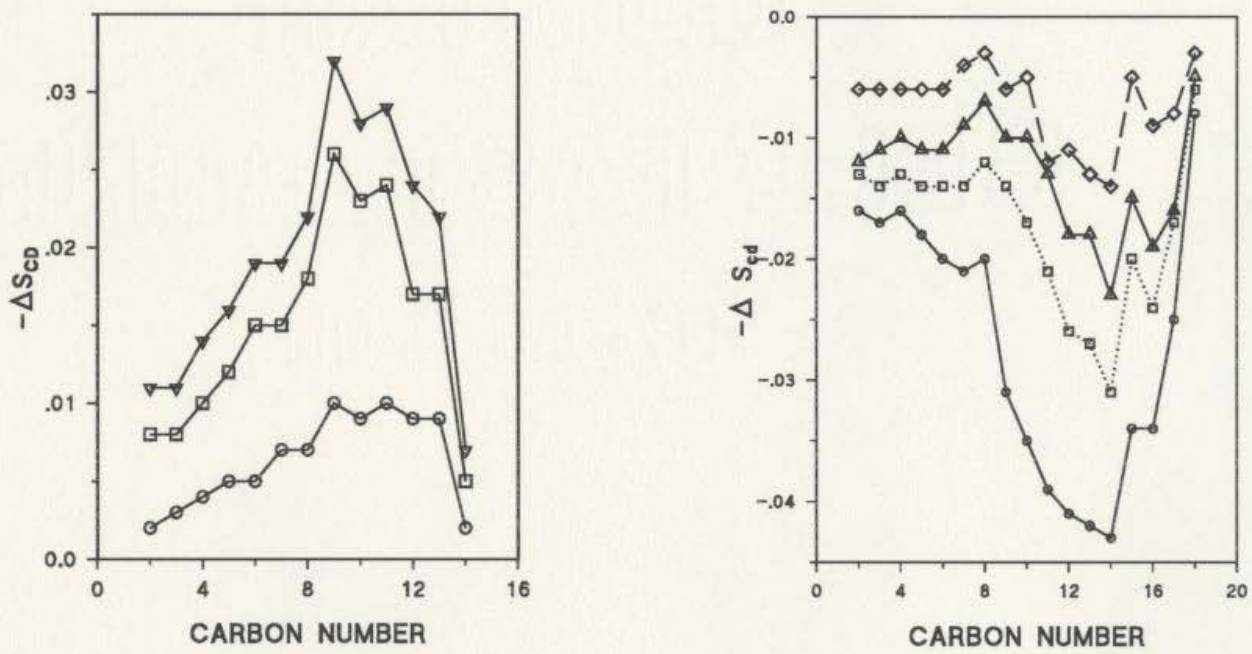

Figure 5.16: Change of order parameter along the chains in the systems of DSPC/DMPC at 60 $°C$ in various constitutional concentrations. ΔS_{CD} $=S_{CD}$(DMPC[d_{54}] in DSPC) $- S_{CD}$(DMPC[d_{54}]) shown in the left graph in which mixtures have DSPC concentrations of 25 mol% (◯), 50 mol% (□), and 75 mol% (▽). ΔS_{CD} $=S_{CD}$(DSPC[d_{70}] in DMPC) $- S_{CD}$(DSPC[d_{70}]) shown in the right graph in which mixtures have DSPC[d_{70}] concentrations of 4.4 mol% (◯), 25 mol% (□), 50 mol% (△), and 75 mol% (◇).

It is interesting to note that order parameters of the methyl groups for both DMPC and DSPC are not much changed as the component concentration changes. The order parameters for the methyl of DSPC in the mixture of DSPC/DMPC are always comparable to or slightly smaller than those in pure DSPC at the same temperature. Disordering for the methyl of DSPC increases with decreasing concentration of DSPC in DMPC. This suggests that the methyl ends of the long acyl chains do not experience any significant ordering influence from short chains on the opposite side of the bilayer and that the dominant interactions are those between molecules on the same side of the bilayer. This also implies that the orientational order near the end of the chain may be determined primarily by intramolecular interactions rather than intermolecular interactions. Similary, the DMPC acyl chain in mixture of DMPC/DSPC also shows no evidence of extra disordering over the last few carbons where interaction with DSPC acyl chains originating from the opposite side of the bilayer might be present. The observation of a limited dependence of the ordering of the methyls of both DMPC and DSPC on the component concentration, as discussed above, suggests that the interaction between the molecules from the two monolayers of the bilayer, if it exists, is weak.

5.3.3 Chain Extension of DMPC and DSPC in Mixtures

Chain extension and bilayer core thickness can be estimated from the orientational order parameters along the acyl chain in the mixtures. However, the formalism available for the estimation of the chain extension [15][35] does not take account of chain upturning probabilities.

In a single component bilayer with two symmetric chains, the chain upturning probabilities are believed to be relatively small for most chain segments [34], since upturning

Table 5.1: Chain Extensions for Mixture DMPC/DSPC at 60°C

DSPC Fraction in DMPC/DSPC	Chain Extension		
	DMPC (l_1)	DSPC (l_2)	$l_2 - l_1$
(Mol %)	($\mathring{A}$)	($\mathring{A}$)	($\mathring{A}$)
0.0	10.24		
4.4		13.32	
25.0	10.34	13.52	3.18
50.0	10.49	13.62	3.13
70.0	10.56		
75.0		13.74	
100		13.89	

would introduce packing difficulties. However, in chain mismatched systems, chain mismatch may create transient voids in the bilayer and facilitate higher upturning probabilities for the mismatched part of the long chain. A higher upturning probability reduces the contribution of the extra part of the chain to the chain extension. Thus the calculated chain extension using the formalism available [15][35] is an overestimate. The systematic error resulting from the neglect of chain upturning in the estimates of chain extension differences will be smaller than that in the chain extension of either component since both chains will typically be affected to some extent.

The chain upturning probability for a given sample varies with position along the chain and with temperature [34]. To date, there is no practical method to extract upturning probability, as presented in Eq. (3.17) (see Chapter 3), from ^{2}H-NMR data. To some extent, this makes the accurate calculation of the bilayer core thickness for the chain mismatched systems difficult, although estimation is still possible.

Table 5.1 presents the mean extensions of the DMPC and DSPC in mixtures with different component concentrations at 60 °C, including those for pure DMPC and DSPC samples. This calculation was based on the Schindler and Seelig [15] formalism.

In the mixture containing DMPC molecules with very small concentration (4.4 mol%) of DSPC, the perturbation of DMPC by DSPC may be neglected. The chain extension of DMPC may then be approximated by that of pure DMPC. The small concentration of DSPC molecules probe the bilayer environment. They are affected by the overwhelming concentration of DMPC molecules, resulting in largest departure of S_{CD} from its value in pure DSPC being at carbon number 14, which coincides to the position of the DMPC methyl (see Fig. 5.16). This suggests that the chain extensions of DMPC and DSPC are similar from carbon number 2 to carbon number 14 in the mixture with a small concentration of DSPC. It should be noted that the biggest S_{CD} departure, relative to pure DSPC, appears at carbon number 14 for all concentrations (see Fig. 5.16).

There are three pieces of significant information in Table 5.1. The first is that the mean chain extensions of both components do not depart very much from those of the corresponding pure lipid bilayer. They are both found to increase by about 0.2 $\AA$ from 25 to 75 mol% DSPC. On the other hand, the half-bilayer core thickness of the pure DSPC is about 3.6 $\AA$ greater than that of pure DMPC at the same temperature. The observation that the change in bilayer thickness with composition is nearly an order of magnitude greater than the change in mean extension of either of the two components can only be understood if the bilayer middle region is disordered to the extend that the ends of different acyl chains can freely interpenetrate the opposite sides of the bilayer, constrained only by a requirement to maintain hydrocarbon density at the value necessary to support the bilayer.

Secondly, both components show a similar increase in mean chain extension with increasing DSPC concentration. This suggests that both molecules have a similar response to changes in mean order of the bilayer.

Thirdly, the chain length differences between DSPC and DMPC at a given temperature, say 60 °C, are nearly independent of DSPC concentration in the mixture and are

around 3.1 $\AA$. This property is obviously helpful in simplifying the formalism for the estimation of the bilayer thickness.

Considering that chain upturning mainly involves the last few segments in the chain, it would appear that, on average, the DSPC chains extend significantly further into the bilayer than the DMPC chains. It also appears that the bilayer thickness for the mixture at the given temperature of 60 $°C$ increases, in a first approximation, linearly with increasing DSPC concentration.

The bilayer core thickness (d) for the mixture of DSPC/DMPC at a given DSPC mole fraction (m) and a given temperature can be approximated by

$$d_m = 2[d^m_{DMPC} + m(d^m_{DSPC} - d^m_{DMPC})] \quad (5.1)$$

$$\simeq 2[d^m_{DMPC} + m(3.1\AA)] \quad (at\ \ 60°C), \quad (5.2)$$

where d^m_{DMPC} and d^m_{DSPC} are the chain lengths in the mixture at the given temperature, and the given DSPC concentration m for DMPC and DSPC respectively. The calculated bilayer core thickness for DMPC/DSPC at 60 $°C$ by using the above formula is comparable to the result of Sankaram and Thompson (1992) [40], where Eq. (3.10) (see Chapter 3) is used for calculation of the chain extension.

5.4 Ternary System of Cholesterol in Glycolipid/SOPC

Cholesterol is known to have a strong influence on membrane thermodynamic and physical properties, such as bilayer thickness, acyl chain ordering, membrane compressibility, and phase behavior in binary cholesterol/lipid mixtures [24, 31, 121]. It is found to increase acyl chain order in the liquid crystalline phase [24, 31, 121]. Similar effects have been found in mixtures of GalCer with cholesterol [122]. In order to obtain further

insight into the nature of the second plateau, the effect of cholesterol on chain ordering for glycosphingolipids in SOPC was examined. In particular, we were interested in whether the cholesterol-induced chain ordering in a predominantly SOPC bilayer would alter the tendency of the long GalCer chain to display a second plateau. Ternary samples were made by adding cholesterol into the binary mixtures containing 10 mol% glycolipid (24:0[d_{47}] GalCer or 18:0[d_{35}] GalCer) in SOPC. The resulting mixture was 7 mol% 24:0[d_{47}] GalCer (or 18:0[d_{35}] GalCer), 23 mol% cholesterol, and 70 mol% SOPC. This allowed a comparison to be made between the order parameter profiles for chain matched and mismatched systems on which cholesterol was exerting an ordering influence [53].

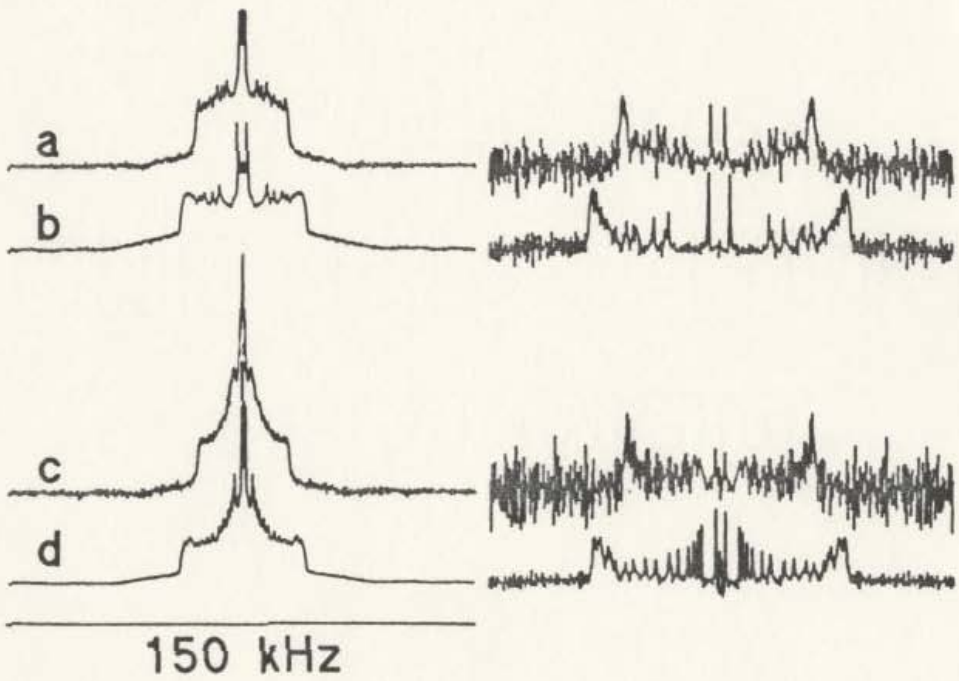

Figure 5.17: Representative ^{2}H-NMR powder spectra (left) and de-Paked spectra (right) for 18:0[d_{35}] GalCer in SOPC (a) and in SOPC/cholesterol (b); and for 24:0[d_{47}] GalCer in SOPC (c) and in SOPC/cholesterol (d). All spectra run on multilamellar vesicles at 40 $^\circ C$.

Fig. 5.17 shows the typical powder spectra and their corresponding de-Paked spectra for 18:0[d_{35}] GalCer (a,b) and 24:0[d_{47}] GalCer (c,d) at 40 $^\circ C$ without cholesterol (a

and c), and with cholesterol (b and d). Corresponding smoothed orientational order parameter profiles are shown in Fig. 5.18.

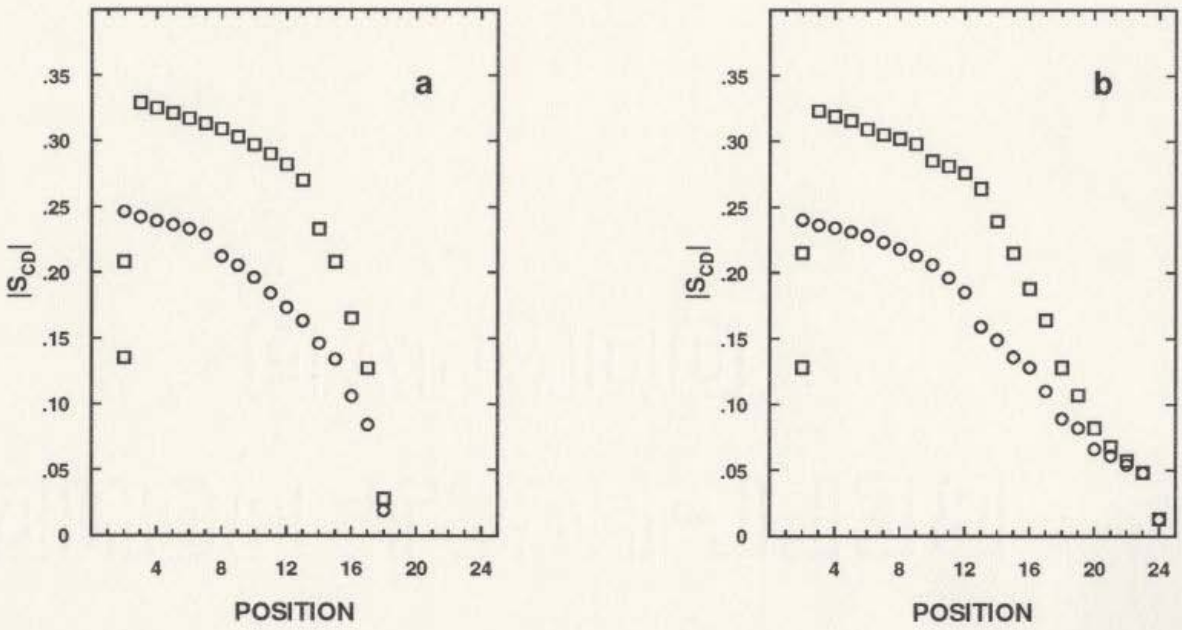

Figure 5.18: Smoothed order parameter profiles for 18:0[d_{35}] GalCer (a), and 24:0[d_{47}] GalCer (b), at 40 $°C$ in bilayer of SOPC (◯), and SOPC/cholesterol (□).

It can be seen from Fig. 5.17 and Fig. 5.18 that the effect of cholesterol on glycolipids in the two mixtures is to increase spectral splitting (Fig. 5.17) or order parameters (Fig. 5.18) along the chain with the greatest absolute effect generally being in the plateau region near the headgroup, and a somewhat larger relative effect immediately below the plateau. The shapes of the order parameter profiles, with and without cholesterol, are similar. It is interesting, though, that cholesterol does not have much effect on the order parameters of the last several segments near the methyl of the acyl chain in 24:0 GalCer

(Fig. 5.18). This seems to indicate that the disorder of the excess length is relatively insensitive to the cholesterol induced increase in order across most of the width of the bilayer. This observation seems to support the the picture of the extra acyl chain length being highly mobile with only transient penetration of the opposite side bilayer.

5.5 The Arrangement of the Excess Chain in Bilayer Mixture

As discussed above, the "extra" lengths of the long chains in low concentrations of DSPC in DMPC, in 24:0 GalCer, 24:0 GalCer in SOPC, and in 24:0 GalCer/SOPC with cholesterol form secondary plateaus in the order parameter profiles. The segments in this extra part of the chains, having small order parameters, are very mobile in the fluid phase. This complicates our analysis of possible arrangement for these chain tails in the binary mixtures.

The mean chain length calculation, [15] without taking account of up-turning probability for the C-C bonds, indicates that the chain length difference in mixtures of DMPC and DSPC is about 3.1 $\AA$. In chain mismatched systems containing GalCer, we are not able to calculate the chain length difference between the long and short chains in the bilayer. However, the analysis of the chain extension for the system of DMPC and DSPC suggests that the extension for segments forming the secondary plateau in the order profile may be used to approximate the chain difference between the long and short chains in the chain mismatched system. Under this assumption, by using the formula of Schindler and Seelig [15], the extra part of the long chain for bilayer 24:0 GalCer/SOPC at around 50 $^{\circ}C$ is calculated to be about 4.3 $\AA$, with effectively no dependence on composition. In the system of 23 mol% cholesterol with 7 mol% 24:0 GalCer in SOPC at 40 $^{\circ}C$, this extra part of the long chain is about 4.4 $\AA$. An important question is how this extra chain length is accommodated in the middle of the bilayer. This question is related to

the motion of the extra part of the long chain.

Considering that for an isotropically reorienting segment, say a methyl group, all conformations (see Fig. 3.1 in Chapter 3) are equally likely, the C-C bond linked to this segment (methyl) would have a probability of 0.5 for orientation perpendicular to the bilayer normal, as discussed in Chapter 3. In the mixture of 24:0 GalCer in SOPC, this probability is about 0.45 for C-C bonds in the region of the second plateau. The motion of the excess chain length in mismatched membranes thus appears to involve very large amplitude, nearly isotropic reorientation. Interdigitation into the opposite bilayer and the occurrence of back folding conformations must both be transient situations.

Thus, the ends, including the extra part of the long chains from both sides of bilayer, are generally intermingled and weakly interacting. They form a very disordered fluid layer in the middle of the bilayer [54]. The midplane, which is used to describe the separation of two opposite monolayer in diacyl single component lipid bilayer, is probably not well defined. The effective bilayer thickness for binary lipid mixtures may be approximated by a weighted mean of the contributions from its two components.

Chapter 6

Summary and Concluding Remarks

^{2}H-NMR spectra, orientational order parameter profiles (OOPP), and the temperature dependence of the spectral first moment M_1 for lipid bilayers contain a wealth of information on physical and thermodynamical properties of the lipid bilayers. In this work the shape of the orientational order parameter profiles and the dependence of M_1 on temperature were studied in some detail. These studies have resulted in the discovery of the scaling relationship between order parameters for single component bilayers of diacyl phospholipids with different chain lengths, and the second plateau at the low order end of the long chain orientational order parameter profiles in chain-mismatched bilayer systems. The effect of chain length on the behaviour of M_1 near the chain melting transition was also examined.

The scaling relationship deduced from a comparison between the shapes of the OOPP for diacyl single component bilayers is summarized in the first section of this chapter. The study of first moment versus temperature is briefly summarized in the second section. Chain mismatch effects in lipid bilayers are reviewed in the third section.

6.1 The Chain-Length Scaling Property of Order Parameter Profiles

It seems that the shape of OOPP for lipid bilayers is in some ways universal. Every smoothed OOPP observed displays a plateau corresponding to a region of the acyl chain near the end of the head of the lipid molecule, with decreasing order toward the methyl terminus. It has recently been demonstrated that for a given lipid component under a

variety of conditions, the shape of the smoothed orientational order parameter profile is largely determined by the mean order parameter and is insensitive to a variety of local perturbations [46]. It has been proposed that the order distribution along the lipid chains behaves in a first approximation in a universal manner and that the order depends on only a few parameters [46].

The relationship between order parameter profiles has been extended to single component diacyl phospholipid bilayers with different chain lengths in this work. Their order parameter profiles have been found to be determined largely by the mean order parameter (or the plateau value of order parameter) if position along the chain is scaled [49]. The area per lipid (equivalently, the mean order parameter, or the order parameter at the plateau region in a order parameter profile) could be one of a few parameters that determine the profile behavior. In the case of binary mixtures (such as DMPC/DSPC, 18:0 GalCer/SOPC, and 24:0 GalCer/SOPC), order parameter profile shapes depend on chain mismatch. They are qualitatively similar for different compositions within a particular kind of bilayer (see Fig. 4.4). However, profiles from bilayers with different degrees of chain-length mismatch cannot be superimposed. It would thus appear that the insensitivity of profile shape to bilayer composition described by Lafleur et. al. [46] and the chain-length scaling reported in this work cannot be extended to all bilayer systems.

6.2 First Moment Versus Temperature Near The Chain Melting Transition

The dependence of first moment on temperature differs for lipid bilayers with different chain lengths. The temperature dependence of first moments for the PC family near the transition was found to be reproduced by a Landau theory. The jump in M_1 indicates the main phase transition. The amplitude of the discontinuity in M_1 and the slope of M_1 versus T at the transition temperature could be linked to the difference between the

spinodal temperature and the transition temperature for a given sample. With decreasing chain length, the decrease in the difference between the spinodal temperature and the transition temperature accounts for both the decrease in the amplitude of the discontinuity in M_1 and the increase in the slope of M_1 versus T at the transition temperature, suggesting that latent heat decreases with decreasing chain length and that the system is approaching a critical point as the chain length is reduced.

6.3 Chain Mismatch Effects in Lipid Bilayer Systems

Both the phase behavior and the molecular chain arrangement in binary mixtures are related to the extent to which the lengths of the acyl chains match or mismatch. The gel phase immiscibility found in 24:0 GalCer/SOPC but not in 18:0 GalCer/SOPC reflects the chain mismatch effect on phase behavior for binary mixtures. The effect of chain mismatch on chain order for bilayer mixtures in the fluid phase has been examined in this work. As shown above, in DMPC/DSPC at small concentration of DSPC [54], in 24:0 GalCer and its mixtures with SOPC [51][52], and in ternary mixture of GalCer, SOPC and cholesterol [53], the bilayer middle region is occupied by both the methyl ends of the short chains and the extra parts of the long chains. In the DMPC/DSPC system , the bilayer thickness may be the weighted mean of the contributions from its two components.

The extra parts of the long chains and the methyl ends of the short chains from the two sides of monolayers of the bilayer are mingled with each other to form a very fluid central layer in the middle of the bilayer. This central layer maintains the hydrocarbon density at the value necessary to support the bilayer. In this case, the bilayer midplane existing in single component diacyl lipid bilayers is poorly defined and is replaced by a central layer. The bilayer thickness is component concentration dependent, and the two

monolayers in the bilayer are partially coupled [97].

It was suggested that the stronger immune function of GalCer in the chain-mismatched systems is due to the protrusion of the headgroup of GalCer, resulting from chain mismatching in the bilayer [47]. This, however, does not match the picture drawn from this work, although the information about the short chain in the bilayer is not available. The stronger immune function of GalCer in the chain-mismatched systems appears to be linked to the presence of the second plateau, corresponding to the central region in the bilayer, in the order parameter profile. At this point, it would be useful to obtain structural information regarding the short chain in regions close to a long chain in the chain-mismatched system.

Real membranes are always mixtures of lipids with differing chain lengths. The accommodation of chain-length mismatch may thus be relevant to a wide variety of real membranes. The very fluid central region observed in chain-mismatched binary mixtures may be a general feature of such membranes. In the bilayer, the central region may be expected to have the largest density fluctuations which may play important roles either in the permeation of ions [123] or in the transmission of information across the bilayer. ^{2}H-NMR provides a way for us to access both structural and dynamical information about a membrane system. It would be a good continuation of this work to study the relaxation of the acyl chain segments in the very fluid central region of the bilayer.

Bibliography

[1] R. B. Gennis. *Biomembranes: Molecular Structure and Function.* Springer-Verlag, Berlin, 1989.

[2] B. L. Silver. *The Physical Chemistry of Membranes.* Allen & Unwin and Solomon Press, New York, 1985.

[3] D. Marsh. *Handbook of Lipid Bilayers.* CRC Press, Inc., Boca Raton, 1990.

[4] D. M. Small. *Handbook of Lipid Research.* Plenum Press, New York, 1986.

[5] D. Chapman. In *Biomembrane Structure and Function.* (ed. D. Chapman) Macmillan Press, London, 1983.

[6] J. H. Davis. *Biochim. Biophys. Acta*, **737**:117, 1983.

[7] G. Cevc and D. Marsh. *Phospholipid Bilayers: Physical Principles and Models.* John Wiley & Sons, Inc., New York, 1987.

[8] G. Govil and R.V. Hosur. In *NMR: Basic Principles and Progress.* (ed. P. Diehl, E. Fluck, and R. Kosfeld) Vol. 20. Springer-Verlag, Berlin, 1982.

[9] J. Seelig. *Q. Rev. Biophys.*, **10**:353, 1977.

[10] N. O. Petersen and S. I. Chan. *Biochemistry*, **16**:2657, 1977.

[11] E. Oldfield, D. Chapman, and W. Derbyshire. *FEBS Lett.*, **16**:102, 1971.

[12] J. Seelig and W. Niederberger. *J. Am. Chem. Soc.*, **96**:2069, 1974.

[13] A. Seelig and J. Seelig. *Biochemistry*, **13**:4839, 1974.

[14] A. Seelig and J. Seelig. *Biochim. Biophys. Acta*, **406**:1, 1975.

[15] H. Schindler and J. Seelig. *Biochemistry*, **14**:2283, 1975.

[16] J. Seelig and N. Waespe-Sarcevic. *J. Phys. Chem.*, **96**:3310, 1978.

[17] J. Seelig and A. Seelig. *Q. Rev. Biophys.*, **13**:19, 1980.

[18] J. Seelig, F. Borl, and T. A. Cross. *Biochim. Biophys. Acta*, **814**:195, 1985.

[19] B. Bechinger and J. Seelig. *Chem. Phys. Lipid*, **58**:1, 1991.

[20] M. Bloom, E. E. Burnell, A. L. MacKay, C. P. Nichol, M. I. Valic, and G. Weeks. *Biochemistry*, **17**:5750, 1978.

[21] M. Bloom, J. H. Davis, and A. L. MacKay. *Chem. Phys. Lett.*, **80**:198, 1981.

[22] E. Sternin, M. Bloom, and A. L. MacKay. *J. Magn. Res.*, **55**:274, 1983.

[23] M. Bloom. In *Proceedings of Enrico Fermi International School on the physics of magnetic resonance in biology and medicine.* (ed. B. Maraviglia) Soc. Italiana di Fisica, Bologna, 1988.

[24] M. Bloom, E. Evans, and O. G. Mouritsen. *Q. Rev. Biophys.*, **24**:293, 1991.

[25] M. Bloom, C. Morrison, E. Sternin, and J. L. Thewalt. In *Pulsed Magnetic Resonance: NMR, ESR, and Optics, A Recognition of E. L. Hahn.* (ed. D. M. S. Bagguley) Oxford University Press, Oxford, 1992.

[26] J. H. Davis, K. R. Jeffrey, M. Bloom, M. Valic, and T. P. Higgs. *Chem. Phys. Lett.*, **42**:390, 1976.

[27] J. H. Davis. *Biophys. J.*, **27**:339, 1979.

[28] J. H. Davis, M. Bloom, K. W. Butler, and I. C.P. Smith. *Biochim. Biophys. Acta*, **597**:477, 1980.

[29] J. H. Davis. In *Adv. Mag. Res.* (ed. W. S. Warren) Vol. 13, 1989.

[30] J. H. Davis. In *Isotopes in the Physical and Biomedical Science.* (ed. E. Buncel and J. R. Jones) Vol. 2. Elsevier Science Publishers B. V., Amsterdam, 1991.

[31] J. H. Davis. In *Cholesterol in Membrane Models.* (ed. L. Finegold) CRC Press, Inc., Boca Raton, 1993.

[32] P. G. de Gennes. *Phys. Lett.*, **47A**:123, 1974.

[33] J.-P. Meraldi and J. Schlitter. *Biochim. Biophys. Acta*, **645**:183, 1981.

[34] J. F. Nagle. *Biophys. J.*, **64**:1476, 1993.

[35] A. Salmon, S. W. Dodd, G. D. Williams, J. M. Beach, and M. F. Brown. *J. Am. Chem. Soc.*, **109**:2600, 1987.

[36] N. Boden, S. A. Jones, and F. Sixl. *Biochemistry*, **30**:2146, 1991.

[37] M. R. Morrow, J. P. Whitehead, and D. L. Lu. *Biophys. J.*, **63**:18, 1992.

[38] D. A. Pink. In *Biomembrane Structure and Function.* (ed. D. Chapman) Macmillan Press, London, 1983.

[39] P. Sheng and E. B. Priestley. In *Introduction to Liquid Crystals.* (ed. E. B. Priestley) Plenum Press, New York, 1974.

[40] M. B. Sankaram and T. E. Thompson. *Biochemistry*, **31**:8258, 1992.

[41] M. R. Morrow, R. Srinivasan, and N. Grandal. *Chem. Phys. Lipid*, **58**:63, 1991.

[42] J. C. Huschilt, R. S. Hodges, and J. H. Davis. *Biochemistry*, **24**:1377, 1985.

[43] M. Vist and J. H. Davis. *Biochemistry*, **29**:451, 1990.

[44] G. E. Pake. *J. Chem. Phys.*, **16**:327, 1948.

[45] G. E. Pake. In *Solid State Physics.* (ed. F. Seitz, D.Turnbull, and H. Ehrenreich) Academic Press, New York, 1956.

[46] M. Lafleur, P. R. Cullis, and M. Bloom. *Eur. Biophys. J.*, **19**:55, 1990.

[47] C. R. Alving, K. A. Urban, and R. L. Richards. *Biochim. Biophys. Acta*, **600**:117, 1980.

[48] C. W. M. Grant. Gangliosides and modulation of neuronal functions. In H. Rahman, editor, *Proceedings of NATO ASI Series Cell Biology* . (ed. H. Rahman) Vol. 7. Springer-Verlag, Berlin, 1987.

[49] M. R. Morrow and D. L. Lu. *Chem. Phys. Lett.*, **182**:435, 1991.

[50] M. R. Morrow, D. Singh, D. L. Lu, and C. W. M. Grant. *Biochim. Biophys. Acta*, **1106**:85, 1992.

[51] D. L. Lu, D. Singh, M. R. Morrow, and C. W. M. Grant. *Biochemistry*, **32**:290, 1993.

[52] M. R. Morrow, D. Singh, D. L. Lu, and C. W. M. Grant. *Biophys. J.*, **64**:654, 1993.

[53] M. R. Morrow, D. Singh, D. L. Lu, and C. W. M. Grant. *Biophys. J.*, **68**:179, 1995.

[54] D. L. Lu, T. Vavasour, and M. R. Morrow. *Biophys. J.*, **68**:574, 1995.

[55] A.-R. Grimmer and B. Blumich. In *NMR: Solid-State NMR 1.* (ed. P. Diehl, E. Fluck, H. Gunther, R. Kosfeld, and J. Seelig) Vol. 30. Springer-Verlag, Berlin, 1994.

[56] D. Freude and J. Haase. In *NMR: Special Applications*, page 1. (ed. P. Diehl, E. Fluck, H. Gunther, R. Kosfeld, and J. Seelig) Vol. 29. Springer-Verlag, Berlin, 1993.

[57] C. P. Slichter. *Priciples of Magnetic Resonance.* Springer-Verlag, Berlin, 1990.

[58] H. W. Spiess. In *NMR: Basic Principles and Progress.* (ed. P. Diehl, E. Fluck, H. Gunther, R. Kosfeld, and J. Seelig) Vol. 15. Springer-Verlag, Berlin, 1978.

[59] M. Jansson, R. L. Thurmond, J. A. Barry, and M. F Brown. *J. Phys. Chem.*, **96**:9532, 1992.

[60] B. C. Gerstein and C. R. Dybowski. *Transient Techniques in NMR of Solids: An Introduction to Theory and Practice.* Academic Press Inc., Orlando, 1985.

[61] A. Abragam and M. Goldman. *Nuclear Magnetism: order and disorder.* Oxford University Press, Oxford, 1982.

[62] J. W. Hennel and J. Klinowski. *Fundamentals of Nuclear Magnetic Resonance.* Longman Scientific & Technical and John Wiley & Sons, New York, 1993.

[63] E. Fukushima and S. B.W. Roeder. *Experimental Pulse NMR: A Nuts and Bolts Approach.* Addison-Wesley Publishing Company, London, 1981.

[64] T. C. Farrar and E. D. Becker. *Pulse and Fourier Transform NMR: Introduction to Theory and Methods.* Academic Press, London, 1971.

[65] C. Y. Y. Hsiao, C. A. Ottaway, and D. B. Wetlaufer. *Lipids*, **9**:813, 1980.

[66] C. M. Gupta, R. Radhakrishnan, and H. G. Khorana. In *Proc. Natl. Acad. Sci. USA*, volume **74**, page 4315, 1977.

[67] M. Lafleur, B. Fine, E. Sternin, P. R. Cullis, and M. Bloom. *Biophys. J.*, **56**:1037, 1989.

[68] A. Abragam. *The Priciples of Nuclear Magnetism.* Oxford University Press, London, 1985.

[69] W. Adamson. *A Textbook of Physical Chemistry.* Academic Press, New York, 1973.

[70] J. Charvolin, P. Manneville, and B. Deloche. *Chem. Phys. Lett.*, **23**:345, 1973.

[71] S. Marcelja. *Biochim. Biophys. Acta*, **367**:165, 1974.

[72] F. Jahnig. *J. Chem. Phys.*, **70**:3279, 1979.

[73] K. A. Dill and P. J. Flory. *Proc. Natl. Acad. Sci. USA*, **77**:3115, 1980.

[74] D. W. R. Gruen. *Biochim. Biophys. Acta*, **595**:161, 1980.

[75] D. W. R. Gruen. *Chem. Phys. Lipid*, **30**:105, 1982.

[76] D. A. Pink. In *Biological Membranes.* (ed. D. Chapman) Vol. 4. Academic Press, London, 1981.

[77] N. Boden, R. J. Bushby, P. F. Knowles, and F. Sixl. *Chem. Phys. Lett.*, **145**:315, 1988.

[78] L. R. De Young and K. A. Dill. *Biochemistry*, **27**:5283, 1988.

[79] S. Doniach. *J. Chem. Phys.*, **68**:4912, 1978.

[80] J. C. Owicki and H. M. McConnel. *Proc. Natl. Acad. Sci. USA*, **75**:1616, 1978.

[81] J. C. Owicki and H. M. McConnel. *Proc. Natl. Acad. Sci. USA*, **76**:4750, 1979.

[82] R. G. Priest. *Mol. Cryst. Liq. Cryst.*, **60**:167, 1980.

[83] F. Jahnig. *Biophys. J.*, **36**:329, 1981.

[84] I. Hatta, S. Imaizum, and Y. Akutsu. *J. Phys. Soc. Jpn.*, **53**:882, 1984.

[85] S. Mitaku, T. Jippo, and R. Kataoka. *Biophys. J.*, **42**:137, 1983.

[86] O. G. Mouritsen. *Biochim. Biophys. Acta*, **731**:217, 1983.

[87] O. G. Mouritsen and M. J. Zuckermann. *Eur. Biophys. J.*, **12**:75, 1985.

[88] J. H. Ipsen, K. Jorgensen, and O. G. Mouritsen. *Biophys. J.*, **58**:1099, 1990.

[89] J. F. Nagle and D. A. Wilkinson. *Biophys. J.*, **23**:159, 1978.

[90] J. H. Ipsen, O. G. Mouritsen, and M. Bloom. *Biophys. J.*, **57**:405, 1990.

[91] M. J. Janiak, D. M. Small, and G. G. Shipley. *J. Biol. Chem.*, **254**:6068, 1979.

[92] L. J. Lis, M. McAlister, N. Fuller, and R. P. Rand. *Biophys. J.*, **37**:657, 1982.

[93] G. Zaccai, G. Buldt, A. Seelig, and J. Seelig. *J. Mol. Biol.*, **134**:693, 1979.

[94] A. G. Lee. *Biochim. Biophys. Acta*, **472**:237, 1977.

[95] D. Chandler. *Introduction to Modern Statistical Mechanics.* Oxford University Press, New York, 1987.

[96] C. H. Huang and J. T. Mason. *Biochim. Biophys. Acta*, **864**:423, 1986.

[97] J. L. Slater and C. H. Huang. *Prog. Lipid Res.*, **27**:325, 1988.

[98] W. Curatolo, B. Sears, and L. J. Neuringer 1985. *Biochim. Biophys. Acta*, **817**:261.

[99] S. W. Hui, J. T. Mason, and C. H. Huang. *Biochemistry*, **23**:5570, 1984.

[100] T. J. McIntosh, S. A. Simon, Jr. J. C. Ellington, and N.A. Porter. *Biochemistry*, **23**:4038, 1984.

[101] T. Zhu and M. Caffrey. *Biophys. J.*, **65**:939, 1993.

[102] J. T. Mason. *Biochemistry*, **27**:4421, 1988.

[103] R. N.A. Lewis, R. N. McElhaney, M. A. Monck, and P. R. Cullis. *Biophys. J.*, **67**:197, 1994.

[104] C. Huang. *Klin Wochenschrift*, **68**:149, 1990.

[105] I. W. Levin. *Biochemistry*, **24**:6282, 1985.

[106] M. J. Ruocco and G. G. Shipley. *Biophys. J.*, **43**:91, 1983.

[107] J. M. Boggs, K. M. Koshy, and G. Rangaraj. *Biochim. Biophys. Acta*, **938**:373, 1988.

[108] J. M. Boggs, K. M. Koshy, and G. Rangaraj. *Bichemistry*, **32**:8908, 1993.

[109] R. A. Reed and G. G. Shipley. *Biochim. Biophys. Acta*, **896**:153, 1987.

[110] R. A. Reed and G. G. Shipley. *Biophys. J.*, **55**:281, 1989.

[111] R. H. Stinson and J. M. Boggs. *Biochim. Biophys. Acta*, **986**:234, 1989.

[112] M. Gardam and J. R. Silvius. *Biochim. Biophys. Acta*, **980**:319, 1989.

[113] P. R. Maulik, D. Atkinson, and G. G. Shipley. *Biophys. J.*, **5**:1071, 1986.

[114] P. R. Maulik, P. K. Sripada, and G. G. Shipley. *Biochim. Biophys. Acta*, **980**:319, 1989.

[115] M. R. Bunow and I. W. Levin. *Biophys. J.*, **32**:1007, 1980.

[116] C. C. Stevenson, N. H. Rich, and J. M. Boggs. *Biochemistry*, **31**:1875, 1992.

[117] K. R. Jeffrey, J. M. Boggs, K. M. Koshy, and A. P. Tulloch. *Biochim. Biophys. Acta*, **986**:241, 1989.

[118] M. Rance, I. C.P. Smith, and H. C. Jarrell. *Chem. Phys. Lipid*, **32**:57, 1983.

[119] G. Schmidt and W. Knoll. *Chem. Phys. Lipid*, **39**:329, 1986.

[120] D. W. R. Gruen and E. H. B. de Lacey. In *Surfactants in Solution.* (ed. K. L. Mittal and B. Lindman) Vol. 1. Plenum Press, New York, 1984.

[121] M. B. Sankaram and T. E. Thompson. *Biochemistry*, **29**:10676, 1991.

[122] W. Curatolo. *Biochim. Biophys. Acta*, **906**:111, 1987.

[123] Y. Lee and S. I. Chan. *Biochemistry*, **16**:1303, 1977.